

## 5. SITE 1073<sup>1</sup>

### Shipboard Scientific Party<sup>2</sup>

#### HOLE 1073A

**Position:** 39°13.5214'N, 72°16.5461'W

**Start hole:** 1710 hr, 13 July 1997

**End hole:** 1535 hr, 17 July 1997

**Time on hole:** 94.42 hr (3.93 days)

**Seafloor (drill pipe measurement from rig floor, mbrf):** 650.9

**Total depth (drill pipe measurement from rig floor, mbrf):** 1314.5

**Distance between rig floor and sea level (m):** 11.5

**Water depth (drill pipe measurement from sea level, m):** 639.4

**Penetration (mbsf):** 663.6

#### Coring totals:

Type: APC

Number: 24

Cored: 215.7 m

Recovered: 228.1 m (105.8%)

Type: XCB

Number: 48

Cored: 447.9 m

Recovered: 434.9 m (97.09%)

#### Lithology:

Unit I: 0–519.8 mbsf; Holocene(?) to Pleistocene

Gray silty clay with minor intervals of sandy mud and rare sand beds and laminae

Unit II: 519.8–654.1 mbsf; Pliocene–Oligocene

Foraminifer-rich clay, silty clay, diatomaceous silty nannofossil clay, and clayey to sandy nannofossil chalk

Unit III: 654.1–663.6 mbsf; late Eocene

Light olive gray, diatom- and clay-rich nannofossil chalk, and olive gray diatom-rich nannofossil clay

**Principal results:** Site 1073 constitutes one of four second-priority sites approved for drilling that were to be undertaken in the event that either time allowed or that operations had to be curtailed at both primary shelf sites. With 5 days remaining on Leg 174A, the decision was made to move to the slope, because it seemed unlikely that at Sites 1071 and 1072 it would be possible to reach objectives deeper than surface m1(s) without unreasonable risk of equipment loss because of unstable hole conditions. Site 1073 was designed to drill as deeply as time would allow into “Icehouse” sediments (Oligocene and younger) at a location where the physical stratigraphy could be related to sequence boundaries traced seaward from the shelf. The objective at Site 1073 is to provide the age and deep-water facies control for surfaces that in shallow water can yield paleobathymetry and facies characterization relevant to determining the history and geologic impact of glacial-eustatic change. Seismic data indicate that an es-

pecially thick and relatively complete Pleistocene succession present at this location can provide information about paleoceanography and depositional and erosional processes on the uppermost slope.

Recovery at Site 1073 was excellent (99.9%). Sediment ranges from upper Eocene to Holocene(?) (<0.4 Ma) and has been subdivided into three major lithostratigraphic units. Unit I is of Pleistocene–Holocene(?) age and extends from 0 to 519.8 mbsf. The dominant lithology is silty clay with minor intervals of sandy mud and rare sand beds. The sediment is strongly bioturbated and hydrotroilite-stained. The lower portion of this unit is characterized by intervals of soft-sediment deformation and by sandy clay with lithic and mud clasts at its base near seismic surface pp4(s) (522–555 mbsf). The “s” designation following the “pp” (provisionally Pliocene–Pleistocene) and “m” (provisionally Miocene) sequence-boundary identifications is meant to distinguish the shelf sequence boundaries, targeted for sampling and logging by Leg 174A, from similarly labeled surfaces calibrated on the slope by Leg 150 (Mountain, Miller, Blum, et al., 1994). Unit II extends from 519.8 to 654.1 mbsf and is Oligocene to Pliocene in age. The sediment is composed of foraminifer-rich clay, silty clay with numerous discrete burrows, diatomaceous silty nannofossil clay, and clayey to sandy nannofossil chalk. Sand and silt laminae are scattered throughout the unit, and thick beds of glauconite are present toward the base. A major unconformity (Oligocene–upper Eocene) and sharp contact separates Units II and III. Unit III extends from 654.1 to 663.6 mbsf and is late Eocene in age. The sediment is composed of clay-rich nannofossil chalk and diatom-rich nannofossil clay that is strongly bioturbated.

Biostratigraphic resolution is excellent throughout most of the Pleistocene through upper Eocene section. Calcareous nannofossils provide detailed zonations for the stratigraphic interval cored, and highlight the various stratigraphic discontinuities at the base of the cored interval (latest Pliocene through late Eocene). Dinocysts are useful for biostratigraphic zonation for the latest Pleistocene through the early Miocene interval. Planktonic foraminifers add to the confidence level of biostratigraphic zonation at Site 1073. Where age calibrations are possible using planktonic foraminifers, they are compatible with the nannofossil zonations. Provenance changes indicated by changes in the benthic foraminifer faunas may be associated with water-depth changes in the Pleistocene. It is inferred that when sea level was relatively low, the source area of inner neritic benthic foraminifers was closest to Site 1073, facilitating transport of shallower water specimens to this location. When sea level was relatively high, these shallower species migrated landward and may not have been transported across the shelf to the slope. Lower Pleistocene to lower Pliocene benthic foraminifer faunas are dominated by *Uvigerina* spp., analogous to present-day faunas from the northeast U.S. continental margin, where the highest abundances of *Uvigerina peregrina* coincide with maxima of organic carbon and silt within slope sediments. The lower Miocene section yields a diverse, in situ bathyal benthic foraminifer assemblage that indicates that the paleodepth may have been comparable to the present water depth (~600 m). Late Eocene assemblages at Site 1073 are comparable to coeval faunas from lower-upper to middle bathyal paleodepths (~500–1000 m) reported from the Leg 150 New Jersey slope sites to the southwest.

Paleomagnetic investigations were conducted on remanent magnetizations after demagnetization at 20 mT. Despite many gas-expansion voids, high-resolution continuous records of inclination and magnetization intensity variations were collected for Pleistocene sediments. Two

<sup>1</sup>Austin, J.A., Jr., Christie-Blick, N., Malone, M.J., et al., 1998. *Proc. ODP, Init. Repts.*, 174A: College Station, TX (Ocean Drilling Program).

<sup>2</sup>Shipboard Scientific Party is given in the list preceding the Table of Contents.

possible short polarity reversals were found within the Brunhes Chron at 15 and 351 mbsf. Magnetic polarity is normal down to 515 mbsf (~pp4[s]), with magnetization intensity fluctuating between 0.1 and 20 mA/m. The Brunhes/Matuyama (B/M) boundary (0.78 Ma) was not found above 515 mbsf. Between 515 and 524 mbsf, the polarity of magnetic inclination shows unstable fluctuations, switching between positive and negative, making it difficult to identify magnetic zones. Below 519 mbsf (~pp4[s]), magnetization intensity is generally low, ranging between 0.05 and 1 mA/m, which again makes it difficult to identify magnetic polarity zones by pass-through measurements on biscuit extended core barrel (XCB) archive-half sections.

Eighty-three interstitial water samples were taken to examine potential "high-resolution" variability in alkalinity,  $\text{NH}_4^+$ , and  $\text{HPO}_4^{2-}$  with depth. Interstitial waters of marine sediments are commonly characterized by broad subsurface maxima in alkalinity,  $\text{NH}_4^+$ , and  $\text{HPO}_4^{2-}$ . The maxima result from bacterial decomposition of organic matter and subsequent diffusion of ions. However, previous work on the New Jersey slope (Leg 150) noted an unusual (if not unique) observation in scientific ocean drilling: at least four peaks in downhole profiles of alkalinity and  $\text{HPO}_4^{2-}$ . Limited sampling of interstitial water at Site 903 precluded a detailed investigation of the observation. Downhole profiles of interstitial water at Site 1073 confirm the observation at Site 903, but at significantly higher resolution. Four well-defined  $\text{HPO}_4^{2-}$  and five alkalinity maxima are observed in interstitial water profiles in the upper 500 mbsf at Site 1073. The maxima appear to exist in interglacial sediment separated by ~90 m and 100 k.y. The maxima indicate that rates of bacterial decomposition of organic matter on the New Jersey slope are highly heterogeneous in time and/or space. The maxima likely are preserved because extreme sedimentation rates on the New Jersey slope (~800 m/m.y.) prevent diffusive homogenization of interstitial water chemistry.

Gaseous hydrocarbons were monitored in all cores by headspace gas and where possible by analysis of gas voids by the syringe/vacutainer technique. Sediments contain abundant gas below 10 mbsf and gaseous voids appear below 34 mbsf. The gas contents in cores decreased below 215 mbsf, probably associated with the switch from advanced hydraulic piston corer (APC) to XCB coring. The composition of gas, as expressed by the  $\text{C}_1/\text{C}_2$  value, shows the expected gradual increase in the relative ethane content with increasing depth and temperature, given the prevailing sedimentation rate and geothermal gradient. Total organic carbon (TOC) content fluctuates between 0.21 and 0.67 wt%, with peaks at 70, 146, 189, and 239 mbsf.

As at other Leg 174A sites, several discontinuities and trends in physical properties measurements coincide with observed lithologic changes, unit boundaries, and with interpreted seismic discontinuities. These are detailed in the "Summary and Conclusions" section, this chapter. Several sharp changes in density correlate with changes in velocity in the same direction (e.g., both increasing downhole); consequently, they reinforce each other in generating acoustic impedance contrasts. The depths of these physical properties changes are generally consistent with previously estimated depths to seismic discontinuities. Natural-gamma radiation measurements include a distinct downward decrease within the lower-middle Miocene Subunit IIC; this is near the predicted level of seismic discontinuity pp4(s). The Pleistocene section contains several increasing upward cycles of natural gamma values that may reflect glacial-interglacial cyclicity. Velocity measurements include a strongly increasing interval from 541 to 561 mbsf, which corresponds to an interval of increasing density. Porosity trends also may reflect overall depositional cycles associated with Pleistocene glacial-interglacial deposition. Resistivity appears to correlate mainly with porosity, as at other Leg 174A sites. Changes in pore-water chemistry appear to have little influence on resistivity values. Resistivity measurements from cores appear to correlate well with those obtained by logging, as do velocities and densities.

An acoustic logging run and a vertical seismic profile (VSP) using the Schlumberger well seismic tool (WST) were successfully conducted to total depth (TD). The data acquired provide critical information for travel-time-depth conversion and for comparing core data with seismic reflection profiles. Much of this work will be conducted postcruise.

## BACKGROUND AND OBJECTIVES

Site 1073 is located at 639-m water depth on the continental slope offshore New Jersey, 39 km east-southeast of Site 1072. This site (Mid-Atlantic Transect [MAT] 13B) constitutes one of four second-priority sites approved for drilling, which were to be undertaken in the event that either time allowed or that operations had to be curtailed at both primary shelf sites (see "Introduction" chapter, this volume). With 5 days remaining in Leg 174A, the decision was made to move to the slope because attempts to core and log at Sites 1071 and 1072 had reached a point of diminishing returns; the potential to reach objectives deeper than surface m1(s) at those sites without unreasonable risk for equipment loss because of unstable hole conditions appeared unlikely.

Site 1073 was designed to drill as deeply as time would allow into "Icehouse" (Oligocene and younger) sediments at a location where the physical stratigraphy could be related to sequence boundaries traced seaward from the shelf. In this manner, the objectives at Site 1073 are consistent with those of Ocean Drilling Program (ODP) Leg 150 (Mountain, Miller, Blum, et al., 1994), where coeval strata were sampled and logged on the slope ~55 km to the southwest. As with Leg 150 sites, the goal at Site 1073 is to provide age and deep-water facies control for potentially correlative surfaces identified beneath the shelf at Sites 1071 and 1072, which yield paleobathymetry and facies characterization relevant to determining the history and geologic impact of glacial-eustatic change. Seismic data also indicate that an especially thick and relatively complete Pleistocene succession present at this location can provide information about paleoceanography and depositional and erosional processes on the slope.

Site 1073 was proposed at the intersection of *Oceanus* 270 Profiles 61 and 32, but concerns expressed by the JOIDES Pollution Prevention and Safety Panel about structural closure and a possible amplitude anomaly led to the relocation of the site 900 m southwest along Profile 32 to cdp 1650. Surfaces pp3(s) and pp4(s) can be traced seaward along Oc270 Profile 51 from where they were sampled at Sites 1071 and 1072. Both features are eroded by unnamed surfaces beneath the outer shelf; these latter surfaces can be followed along Profile 51 and then 9 km northeast along Profile 32 to Site 1073 (see "Downhole Logging" section, this chapter). Based on the assumption of a relatively intact Pleistocene slope section, we anticipated that the ages of pp3(s) and pps(4) could nonetheless be constrained within reasonably narrow ranges (see "Seismic Stratigraphy" section, this chapter). Furthermore, surfaces pp5(s) and m0.5(s), also drilled at Site 1072, were suspected to have nearly age-equivalent strata at Site 1073, despite the difficulty of establishing unambiguous seismic ties. Lastly, surface m1(s), which was reached at only one hole on the shelf (Hole 1071E), was thought to be traceable to the slope, although with uncertainty about the accompanying hiatus that might be present as a result of stratigraphic condensation in deep water.

## OPERATIONS

### Site 1073

The ship steamed 23 nmi from Site 1072 to prospectus site MAT-13B. Hole 1073A was spudded at 1710 hr on 13 July (Table 1). The calculated depth of the seafloor on the basis of recovery of the mudline core is 639.4 mbsl (650.9 mbrf). APC Cores 174A-1073A-1H through 24H were cut from 0 to 215.7 mbsf in soft, gassy sediments. Cores were oriented from Core 3H, and Adara heat-flow measurements were taken at Cores 4H, 6H, and 8H (35°C/km). APC coring was terminated following four partial strokes, 40,000-lb overpull, and a shattered liner. XCB Cores 25X through 72X were recovered from 215.7 to 663.6 mbsf. The hole wall appeared to be stable, but it was suspected that soft clays were extruding into the wellbore even a

**Table 1. Site 1073 coring summary.**

Core	Date (July 1997)	Time (EST)	Depth (mbsf)	Length cored (m)	Length recovered (m)	Recovery (%)
174A-1073A-						
1H	13	1715	0.0-6.6	6.6	6.63	100.5
2H	13	1740	6.6-16.1	9.5	9.70	102.1
3H	13	1825	16.1-25.6	9.5	10.35	108.9
4H	13	1910	25.6-35.1	9.5	10.62	111.8
5H	13	1935	35.1-44.6	9.5	10.29	108.3
6H	13	2020	44.6-54.1	9.5	11.54	121.5
7H	13	2050	54.1-63.6	9.5	10.27	108.1
8H	13	2135	63.6-73.1	9.5	10.75	113.2
9H	13	2200	73.1-82.6	9.5	10.37	109.2
10H	13	2230	82.6-92.1	9.5	10.36	109.1
11H	13	2330	92.1-101.6	9.5	10.31	108.5
12H	14	0005	101.6-111.1	9.5	8.27	87.1
13H	14	0055	111.1-120.6	9.5	10.35	108.9
14H	14	0135	120.6-130.1	9.5	10.83	114.0
15H	14	0215	130.1-139.6	9.5	10.10	106.3
16H	14	0255	139.6-149.1	9.5	10.08	106.1
17H	14	0335	149.1-158.6	9.5	10.28	108.2
18H	14	0415	158.6-168.1	9.5	10.49	110.4
19H	14	0450	168.1-177.6	9.5	10.14	106.7
20H	14	0535	177.6-187.1	7.5	7.14	95.2
21H	14	0605	187.1-196.6	9.5	8.25	86.8
22H	14	0710	196.6-206.1	8.2	8.12	99.0
23H	14	0810	206.1-215.6	9.0	9.02	100.2
24H	14	1005	215.6-225.1	3.9	3.87	99.2
25X	14	1140	225.1-234.6	8.7	5.96	68.5
26X	14	1245	234.6-244.1	9.5	8.47	89.2
27X	14	1335	244.1-253.6	9.6	8.76	91.3
28X	14	1420	253.6-263.1	9.5	7.90	83.2
29X	14	1520	263.1-272.6	9.5	7.61	80.1
30X	14	1610	272.6-282.1	9.5	7.16	75.4
31X	14	1715	282.1-291.6	9.4	7.05	75.0
32X	14	1815	291.6-301.1	9.3	7.78	83.7
33X	14	1910	301.1-310.6	9.4	9.34	99.4
34X	14	2010	310.6-320.1	9.4	8.64	91.9
35X	14	2100	320.1-329.6	8.9	7.72	86.7
36X	14	2205	329.6-339.1	9.4	6.51	69.3
37X	14	2310	339.1-348.6	9.4	5.83	62.0
38X	15	0020	348.6-358.1	9.4	9.49	101.0
39X	15	0135	358.1-367.6	9.4	8.71	92.7
40X	15	0245	367.6-377.1	9.4	8.43	89.7
41X	15	0355	377.1-386.6	9.5	9.92	104.4
42X	15	0510	386.6-396.1	9.4	9.80	104.3
43X	15	0620	396.1-405.6	9.3	8.16	87.7
44X	15	0740	405.6-415.1	8.9	6.93	77.9
45X	15	0845	415.1-424.6	9.4	9.74	103.6
46X	15	1000	424.6-434.1	9.6	9.38	97.7
47X	15	1115	434.1-443.6	9.4	10.00	106.4
48X	15	1245	443.6-453.1	9.5	9.76	102.7
49X	15	1350	453.1-462.6	9.5	9.86	103.8
50X	15	1450	462.6-472.1	9.4	9.99	106.3
51X	15	1630	472.1-481.6	8.9	9.86	110.8
52X	15	1805	481.6-491.1	9.4	10.01	106.5
53X	15	1935	491.1-500.6	9.6	10.00	104.2
54X	15	2055	500.6-510.1	9.4	9.95	105.9
55X	15	2240	510.1-519.6	9.4	10.04	106.8
56X	16	0035	519.6-529.1	9.3	9.98	107.3
57X	16	0255	529.1-538.6	9.5	8.88	93.5
58X	16	0520	538.6-548.1	9.5	9.84	103.6
59X	16	0745	548.1-557.6	7.5	9.84	131.2
60X	16	1025	557.6-567.1	9.4	9.85	104.8
61X	16	1205	567.1-576.6	8.9	9.85	110.7
62X	16	1350	576.6-586.1	9.3	9.86	106.0
63X	16	1510	586.1-595.6	9.4	9.87	105.0
64X	16	1625	595.6-605.1	9.4	9.76	103.8
65X	16	1740	605.1-614.6	9.6	9.80	102.1
66X	16	1910	614.6-624.1	9.4	9.77	103.9
67X	16	2035	624.1-633.6	9.6	9.74	101.5
68X	16	2210	633.6-643.1	9.5	9.93	104.5
69X	16	2335	643.1-652.6	9.5	9.65	101.6
70X	17	0115	652.6-662.1	8.9	9.80	110.1
71X	17	0310	662.1-671.6	9.4	9.81	104.4
72X	17	0510	671.6-681.1	9.5	9.86	103.8
Coring totals:				663.6	662.98	99.91

Notes: An expanded version of this coring summary table that includes lengths and depths of sections, location of whole-round samples, and comments on sample disturbance is included on the CD-ROM in the back pocket of this volume. EST = U.S. Eastern Standard Time.

few hours after wiper trips. Bentonite mud sweeps were circulated roughly every other core to keep the hole clean.

The hole was circulated, and a wiper trip was made in preparation for logging. Soft clay ledges took weight and would not pump off; therefore, five 2- to 5-m-thick intervals from 647 to 568 mbsf had to be reamed. Six meters of fill on bottom was noted, and the hole was circulated; however, the hole was not filled with mud because the sepiolite mud supply had been exhausted by heavy usage during shelf drilling operations and the hole had been stable throughout pre-logging operations. The bit was pulled to 87.4 mbsf for logging.

A Long-Spaced Sonic tool (LSS)/Dual Induction tool (DIT-E)/Natural Gamma-ray Tool (NGT) log was obtained in the upper section of hole when the tool string could not be worked past 287 mbsf. The obstruction was in a section of the hole that had just been reamed through (with rotation) on the conditioning trip to log the hole; therefore, we chose not to employ the Conical Side Entry Sub, in favor of running the bit back down to maintain the ability to rotate. The bit was placed at 359.5 mbsf and the LSS/DIT-E/NGT log was rerun to 651 mbsf (12 m off bottom) in 3.5 hr.

It appeared that the hole was rapidly closing because of swelling clays, and the WST tool could only be worked down to 424 mbsf. Three VSP stations were obtained. The DIT-E/Hostile-environment Litho-Density Tool (HLDT)/Accelerator Porosity Sonde (APS)/Hostile-Environment Gamma-ray Spectrometry tool (HNGS) log was run to 650 mbsf (13 m off bottom) in 2.75 hr. The bottom of the hole seemed to be closing in again; therefore, the pipe was pulled to 247.4 mbsf. The LSS/DIT-E/NGT log was run from 384 mbsf in 2 hr, completing that log in the middle section of the hole. The pipe was pulled to 87.4 mbsf, and nine VSP stations were completed in the upper hole from 285 mbsf. Operations were terminated as available time was depleted. The pipe was pulled, and the bit cleared the rotary at 1535 hr on 17 July, ending Hole 1073A.

## Sea Voyage to New York

The 120-nmi sea voyage to New York was completed in 11.25 hr at an average speed of 10.7 kt. The A-frame at the top of the derrick was laid down for the transit under the Verrazano Narrows bridge in New York. The first line was ashore at Passenger Terminal Pier 88, Berth 5 at 0801 hr on 18 July, officially ending Leg 174A.

## LITHOSTRATIGRAPHY

### Introduction

Site 1073 was drilled on the upper slope to recover a thick Pleistocene section and to sample a relatively condensed Pliocene and older downdip section thought to be partially age-equivalent to the strata recovered in the updip shelf settings at Sites 1071 and 1072 (see "Background and Objectives" section, this chapter). The succession in Hole 1073A also provides a link between the shelf sites drilled for Leg 174A and the deeper water sites of Leg 150 (Mountain, Miller, Blum, et al., 1994) and Deep Sea Drilling Project (DSDP) Leg 93 (van Hinte, Wise, et al., 1987). Compared to these previous sites, Site 1073 is most similar in lithology to Site 903 of Leg 150 (Shipboard Scientific Party, 1994); however, the successions in Hole 1073A are sufficiently different in character to justify an independent lithostratigraphic subdivision. Intervals of Hole 1073A that may be lithostratigraphically correlated to Site 903 (e.g., through the middle Miocene-Eocene section) are described below. The succession at Hole 1073A is predominantly clay and silt with glauconite becoming increasingly abundant downhole (Fig. 1; Table 2). Lithostratigraphic units are defined principally from the recognition of discontinuities and/or assemblages of lithofacies. Units bounded by major discontinuities are expressed as abrupt changes in sedimentologic character; subunits are defined by less prominent transitions.

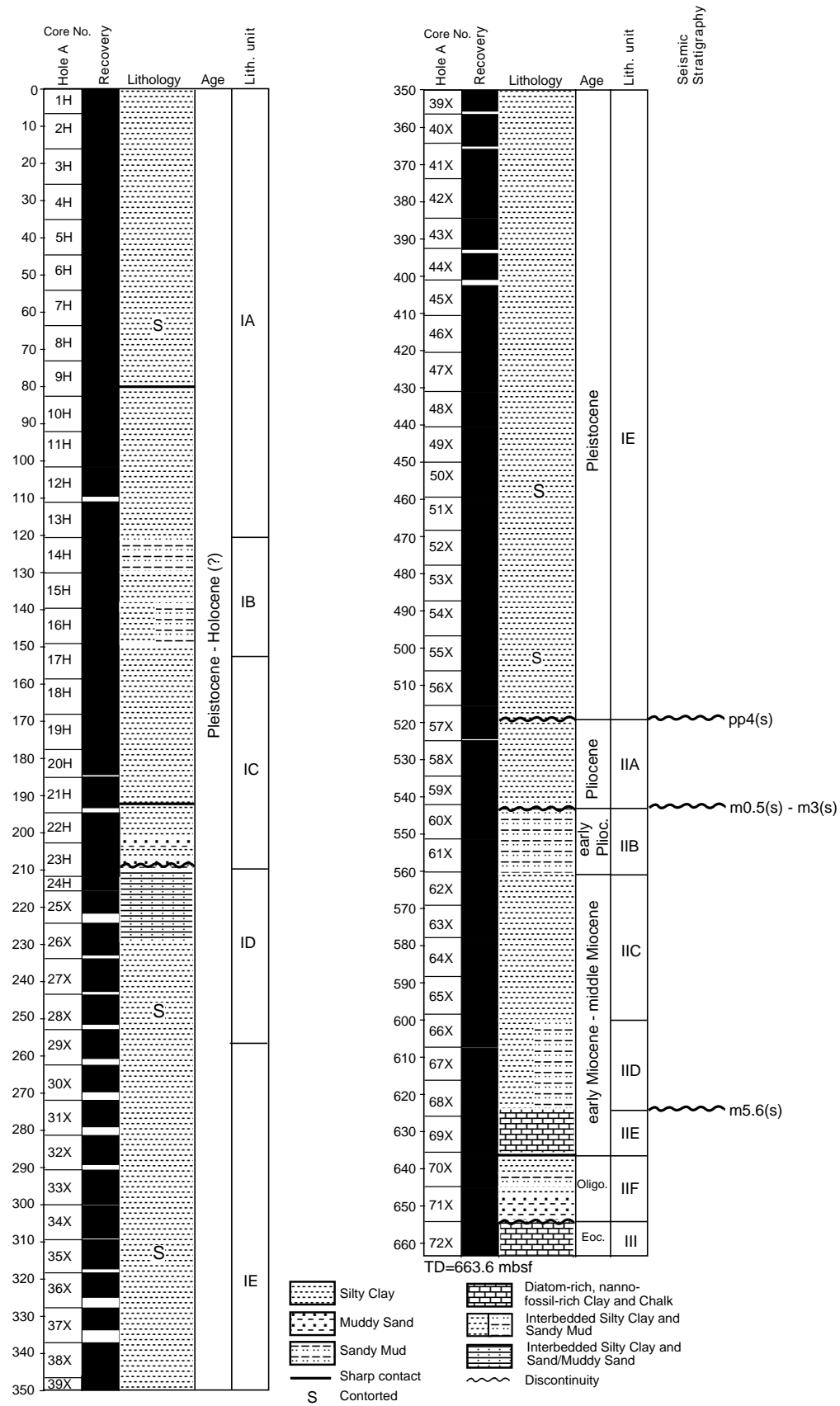


Figure 1. Generalized summary for Hole 1073A showing core recovery, lithology, age, and lithologic units and subunits. Correlations (approximate) to identified seismic discontinuities are also shown (far right).

**Table 2. Lithostratigraphic summary of Hole 1073A.**

Unit and subunit	Series	Interval (mbsf)	Lithology
IA	Holocene(?)–Pleistocene	174A-1073A-1H-1, 0 cm, to 14H-1, 129 cm (0-121.9)	Clay, silty clay, and thinly to thickly interbedded silty clays and sandy clays, thoroughly bioturbated and hydrotroilite stained.
IB	Pleistocene	14H-1, 129 cm, to 17H-3, 104 cm (121.9-153.1)	Micaceous silty clay and sandy mud, heavily bioturbated and locally stained by hydrotroilite.
IC	Pleistocene	17H-3, 104 cm, to 23H-5, 65 cm (153.1-209.5)	Micaceous silty clay and clay, heavily bioturbated and locally stained by hydrotroilite.
ID	Pleistocene	23H-5, 65 cm, to 29X-3, 150 cm (209.5-257.5)	Silty clay and clay, interbedded with thin beds of sandy mud, muddy sand, and sand. Sand layers commonly have sharp bases. Soft-sediment deformation features are present locally.
IE	Pleistocene	29X-3, 150 cm, to 57X-3, 150 cm (257.5-519.8)	Micaceous silty clay and clay with intervals of soft-sediment deformation and very fine to thick sand beds. Discrete burrows. Sandy clay with lithic and mud clasts at base near seismic surface pp4(s).
IIA	Pliocene	57X-4, 0 cm, to 60X-1, 70 cm (519.8-542.5)	Foraminifer-rich clay and silty clay with scattered silt- and fine-grained sand laminae. Discrete burrows.
IIB	lower Pliocene	60X-1, 70 cm, to 61X-CC, 45 cm (542.5-560.1)	Thick beds of glauconitic, sandy mud and silty clay. The subunit base is near seismic surfaces m0.5(s)-m3(s).
IIC	middle Miocene	62X-1, 0 cm, to 65X-CC, 4 cm (560.1-597.8)	Locally glauconitic, silty clay with discrete burrows.
IID	lower Miocene-middle Miocene	66X-1, 0 cm, to 69X-2, 100 cm (597.8-628.8)	Interbedded sandy mud and silty clay with small-scale cross-lamination and color variations. Discrete burrows. The base is near seismic surface m5.6(s).
IIE	lower Miocene	69X-2, 100 cm, to 69X-CC, 33 cm (628.8-635.8)	Locally glauconitic and diatomaceous, silty nannofossil clay and clayey to sandy nannofossil chalk with discrete burrows.
IIF	Oligocene	70X-1, 0 cm, to 71X-CC, 37 cm (635.8-654.1)	Interbedded glauconitic, silty clay and sandy mud. Discrete burrows. Base is coarser grained glauconitic sand and forms a sharp contact with the chalks below.
III	upper Eocene	71X-CC, 37 cm, to 72X-CC, 48 cm (654.1-663.6)	Clay-rich nannofossil chalk and diatom-rich nannofossil clay that is strongly bioturbated.

## Description of Lithologic Units

### Unit I

Interval: 174A-1073A-1H-0, 0 cm, to 57X-3, 150 cm  
 Depth: 0–519.8 mbsf  
 Age: Holocene(?) to Pleistocene

Unit I is predominantly gray silty clay with minor intervals of sandy mud and rare sand beds and laminae (Fig. 1). Five subunits are recognized based primarily on the presence or absence of sand.

#### Subunit IA

Interval: 174A-1073A-1H-0, 0 cm, to 14H-1, 129 cm  
 Depth: 0–121.9 mbsf

Subunit IA is dominated by mud. The upper part of the subunit (interval 174A-1073A-1H-1, 0 cm, to 4H-5, 48 cm) is composed of slightly micaceous, olive gray (5Y4/2) clay (Fig. 1). The clay is thoroughly bioturbated and typically exhibits black hydrotroilite staining, which commonly accentuates burrows or burrow mottles.

The middle part of the subunit (interval 174A-1073A-4H-5, 48 cm, to 10H-2, 115 cm) is generally coarser and contains thinly to thickly interbedded silty clays and sandy clays. These sediments are gray (5Y5/1) to dark gray (5Y4/1), micaceous, and stained by hydrotroilite. Most of the sediment is thoroughly bioturbated and burrows are usually manifested by their silty or stained fills. Despite heavy bioturbation, rare fine sand and silt laminae are locally observed in both silty and sandy clays. Thin intervals of soft-sediment deformation are present locally (e.g., intervals 174A-1073A-4H-5, 48–103 cm, 5H-4, 130–140 cm, and 7H-7, 74–82 cm) and appear to be slump folds. The middle part of the subunit also includes some bioturbated sandy mud, muddy sand, and sand containing scattered pebbles and wood fragments (i.e., interval 174A-1073A-9H-4, 72 cm, to 9H-5, 93 cm). The base of this coarser interval (at 80.03 mbsf) is a very sharp contact, which is highly burrowed by a firmground trace-fossil assemblage (Fig. 2). This discontinuity is located close to seismic surface pp1(s) at ~75 mbsf (see “Seismic Stratigraphy” section, this chapter).

The lower part of Subunit IA (interval 174A-1073-10H-2, 115 cm, to 14H-1, 129 cm) is gray (5Y5/1), micaceous, burrow-mottled silty clay with hydrotroilite staining and rare thin beds or laminae of

silt and fine sand. The contact at the base of this subunit is somewhat gradational.

#### Subunit IB

Interval: 174A-1073A-14H-1, 129 cm, to 17H-3, 104 cm  
 Depth: 121.9–153.1 mbsf

Subunit IB consists primarily of thickly interbedded olive gray (10YR4/1) silty clay and dark gray (5Y4/1), very fine sandy mud. These sediments are micaceous, locally hydrotroilite-stained, and generally completely bioturbated. Burrows are typically visible because they are filled with silt to fine sand and/or are preferentially stained. Interbeds of clayey silt are present in the lower part of the subunit (interval 174A-1073A-17H-2, 97 cm, to 17H-3, 104 cm).

#### Subunit IC

Interval: 174A-1073A-17H-3, 104 cm, to 23H-5, 65 cm  
 Depth: 153.1–209.5 mbsf

Subunit IC, like Subunit IA, is dominated by mud. The upper part of the subunit (interval 174A-1073A-17H-3, 104 cm, to 20H-CC, 26 cm) is characterized by gray (5Y5/1) to very dark gray (5Y3/1), slightly micaceous silty clay and clay with locally extensive hydrotroilite staining. These sediments are generally completely bioturbated, but discrete burrows are rare. Burrows with clay cores and very clean sand mantles are common in some intervals (e.g., interval 174A-1073A-20H-1, 0 cm, to CC, 26 cm). Pebbles, which may represent glacial dropstones, are rare (Fig. 3).

The lower part of Subunit IC (interval 174A-1073A-21H-1, 0 cm, to 23H-5, 65 cm) is characterized by interbedded silty clay, clay, and muddy sand. The silty clay and clay intervals are generally dark greenish gray (5GY4/1), micaceous, and locally contain rare silt or fine-sand laminae. The clay intervals are thoroughly bioturbated with discrete burrows generally restricted to rare *Chondrites* and unidentified sand-filled burrows. Muddy sand intervals (intervals 174A-1073A-21H-4, 64–94 cm; 22H-5, 40–94 cm; and 23H-4, 0 cm, to 23H-5, 65 cm) are dark gray (5Y4/1), locally pebbly, and typically exhibit sharp, burrowed bases. The lower portion of Subunit IC is characterized by muddy sand and sandy mud interbeds, and the base of the subunit is marked by a sharp erosional contact at the base of this sandy interval (Fig. 4). This contact appears to correspond to a

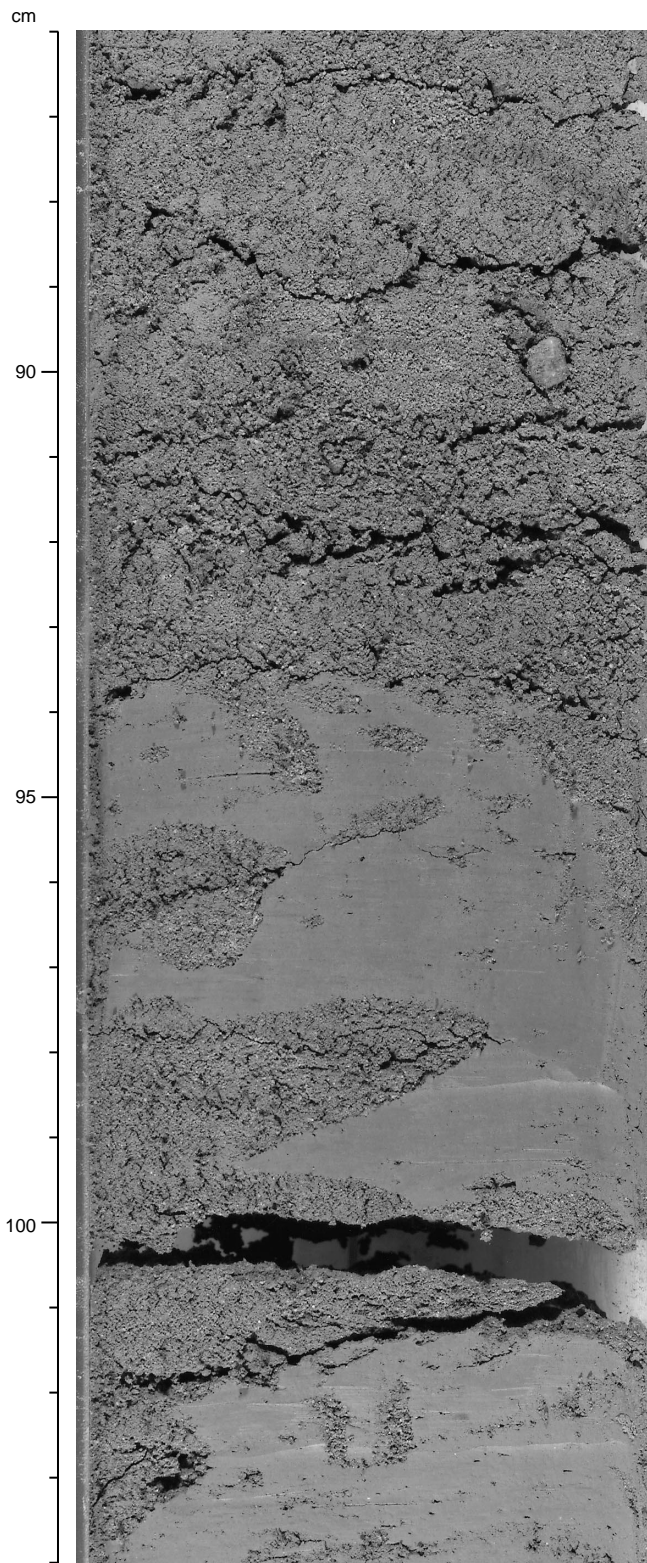


Figure 2. Highly burrowed clay at the base of a coarse-grained interval close to seismic surface pp1(s) (interval 174A-1073A-9H-5, 86–104 cm). Note the sharp, irregular contact at 94 cm and pebble at 90 cm.

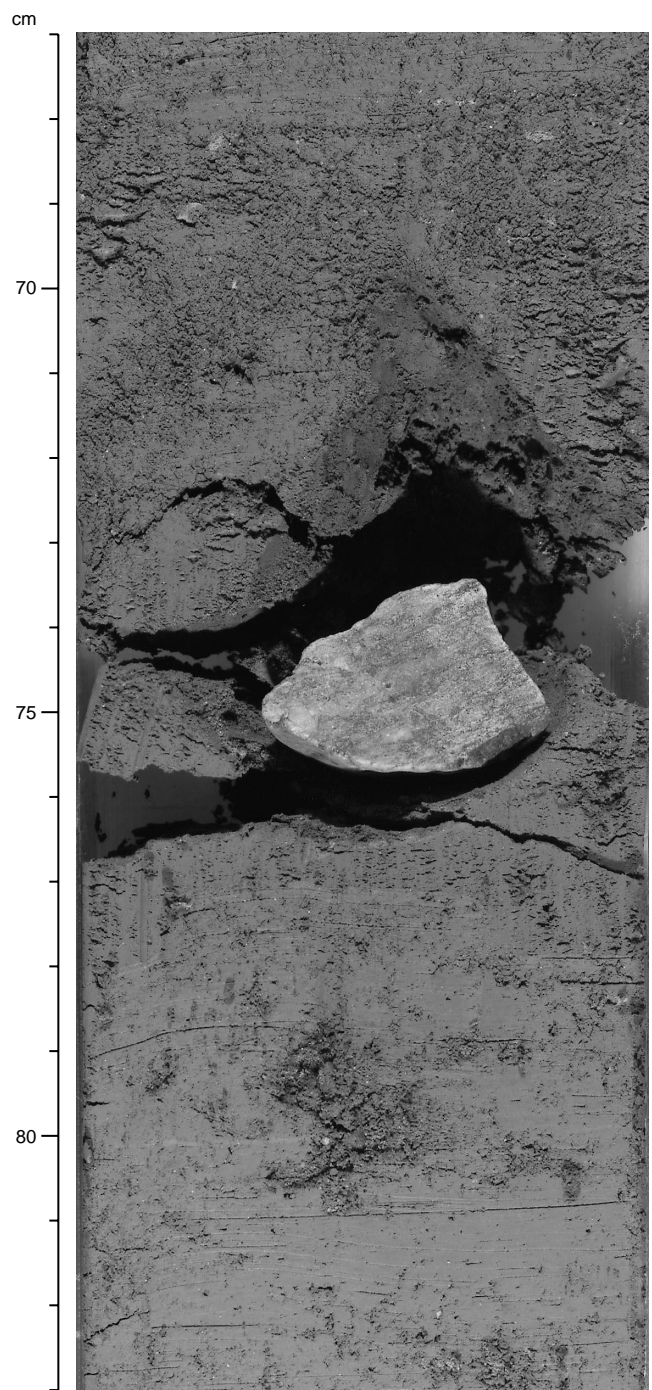


Figure 3. Possible glacial dropstone marks the surface between dusky yellow green silty clay above 75 cm and the dark gray silty clay below (interval 174A-1073A-17H-5, 67–83 cm).

distinct boundary between seismic facies units (see “Seismic Stratigraphy” section, this chapter).

**Subunit ID**

Interval: 174A-1073A-23H-5, 65 cm, to 29X-3, 150 cm  
 Depth: 209.5–257.5 mbsf

Subunit ID is characterized by dark greenish gray (5GY4/1) to grayish brown (5YR4/2) silty clay or clay with laminae and thin beds of silt and very fine sand, sandy mud, or muddy sand (Fig. 5). Some

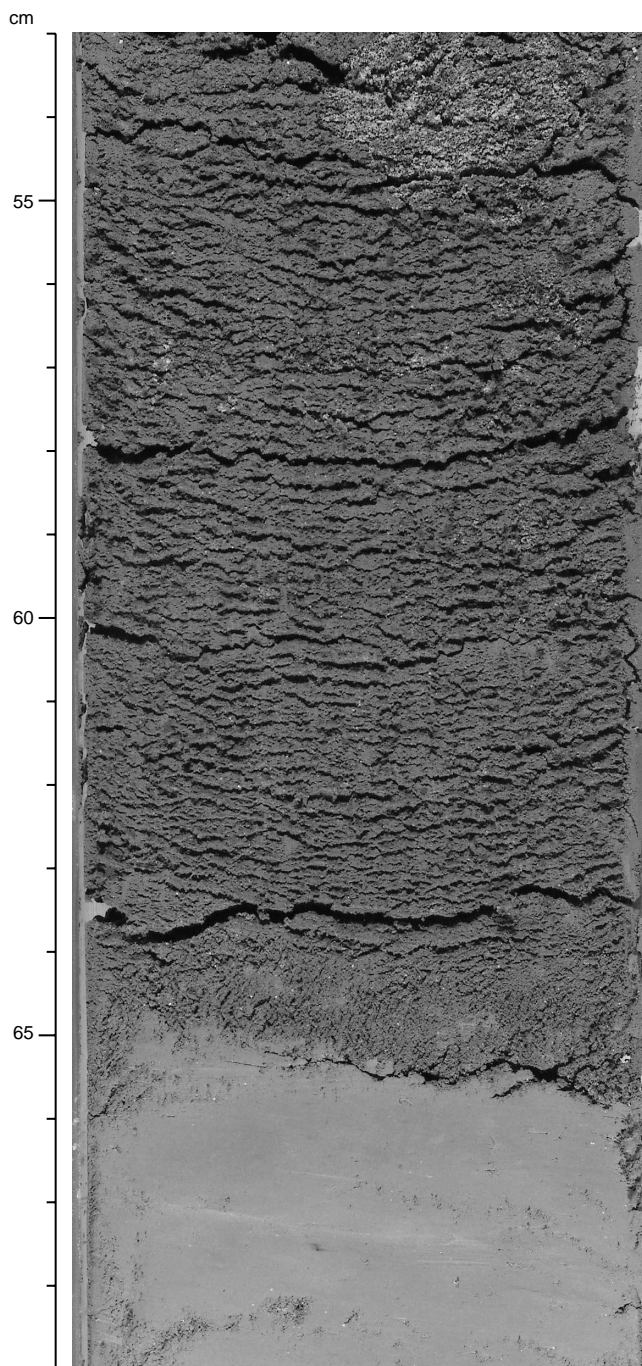


Figure 4. Sharp erosional contact at the base of the muddy sand interval that marks the base of Subunit IC. This contact appears to correspond to a distinct boundary between seismic facies units (interval 174A-1073A-23H-5, 53–69 cm; see “Seismic Stratigraphy” section, this chapter).

intervals of silty clay are horizontally color-banded, commonly by hydrotroilite. The silty clay and clay are generally bioturbated, but discrete traces are generally limited to *Chondrites* and *Planolites*(?). The laminae and thin silt/sand layers commonly exhibit sharp bases and subtle normal grading (Fig. 5). This portion of Subunit ID appears to correspond with seismic facies returned from the side wall or overbank portion of a submarine canyon/channel (see “Seismic Stratigraphy” section, this chapter). The sediment facies in the cores (color-banded mud, silt/fine sand laminae) suggest that at least this upper part of the subunit represents overbank deposits associated

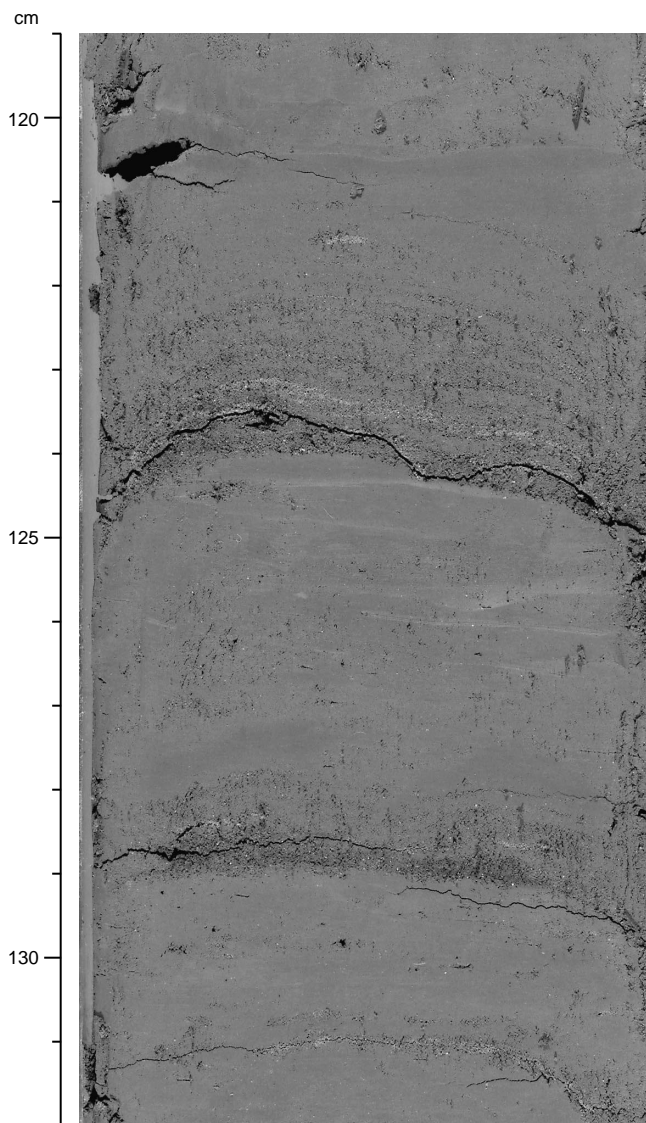


Figure 5. Thin silt and very fine sand laminae in silty clay interpreted as overbank deposits associated with a buried submarine canyon/channel (interval 174A-1073A-23H-5, 119–132 cm).

with this canyon/channel. Short intervals of soft-sediment deformation, presumably associated with slumping, are present within the lower portion of the subunit (interval 174A-1073A-28H-1, 81 cm, to 28H-5, 130 cm).

#### Subunit IE

Interval: 174A-1073A-29X-3, 150 cm, to 57X-3, 150 cm  
Depth: 257.5–519.8 mbsf

Subunit IE is predominantly dark gray (5Y4/1) to very dark gray (5GY4/1), grayish green (5GY4/1), or dark greenish gray (5GY5/1), slightly micaceous silty clay and clay. Sediments are generally diffusely burrow mottled and are commonly accentuated by hydrotroilite staining. Discrete burrows similar to *Chondrites*, *Helminthopsis*, *Palaeophycus*, *Planolites*, *Teichichnus*, *Thalassinoides*, and *Zoophycos* are observed locally. Soft-sediment deformational features indicative of slumping are observed in several scattered intervals (174A-1073-30X-4, 71 cm, to 30X-CC, 60 cm; 35X-4, 10 cm, to 36X-2, 150 cm; 39X-2, 15 cm, to 40X-3, 50 cm; 41X-4, 0–100 cm; 42X-1, 67–87 cm; 50X-5, 30 cm, to 50X-7, 120 cm; and 51X-2, 0 cm, to 51X-4,

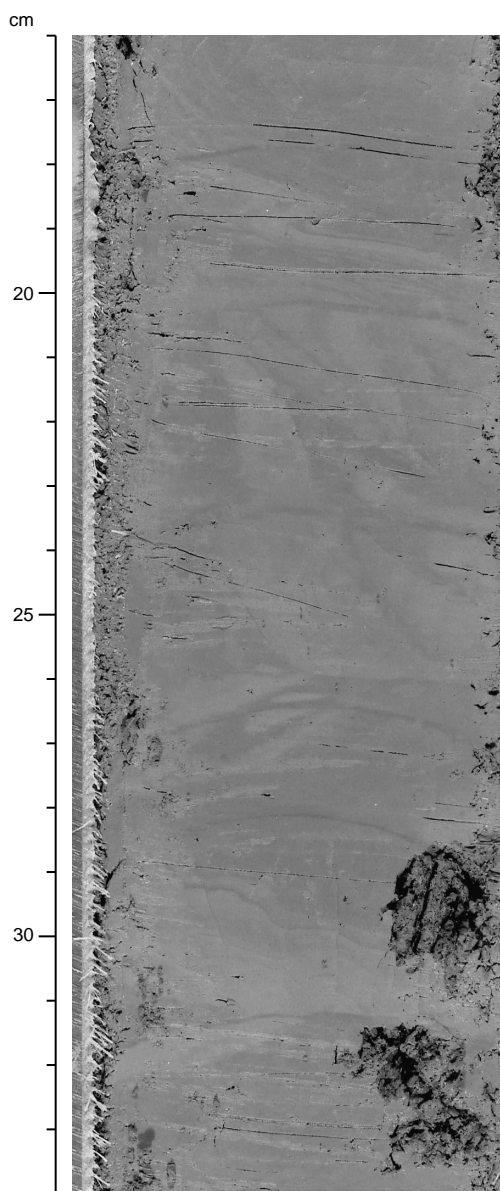


Figure 6. Subtle, deformed, and folded bedding interpreted as slumping, Subunit IE (interval 174A-1073A-35X-4, 16–34 cm). Note that formation of drilling biscuits has further disrupted these layers.

150 cm; Fig. 6). Thin beds and laminae of fine to very fine sand are also observed throughout the subunit and are locally abundant in some intervals (e.g., interval 174A-1073A-44X-4, 0 cm, to 44X-CC, 36 cm). Thicker sandy mud beds are restricted to an interval <5 m thick (interval 174A-1073A-47X-4, 0 cm, to 47X-6, 150 cm). Seismic surface pp3(s) is located at ~243–325 mbsf; it may correlate with the base of an interval characterized by intermittent soft-sediment deformation features. The lowermost interval of Subunit IE is characterized by pebbly sandy clay (Fig. 7) with some exotic reddish brown (5YR5/3) mud clasts (Fig. 7). This basal interval appears to correlate with seismic surface pp4(s), which is located at ~522–555 mbsf (see “Seismic Stratigraphy” section, this chapter).

## Unit II

Interval: 174A-1073A-57X-4, 0 cm, to 71X-CC, 37 cm  
Depth: 519.8–654.1 mbsf  
Age: Pliocene–Oligocene

### Subunit IIA

Interval: 174A-1073A-57X-4, 0 cm, to 60X-1, 70 cm  
Depth: 519.8–542.5 mbsf

Subunit IIA is apparently Pliocene in age (see “Biostratigraphy” section, this chapter) and is composed predominantly of foraminifer-rich silty clay, although the uppermost part (interval 174A-1073A-57X-4, 0 cm, to 57X-CC, 33 cm) is less silty. Both the silty clay and clay intervals are dark greenish gray (5GY4/1) to olive grayish green (5GY3/2). The silty clay lithofacies locally contains scattered, thin silt- or fine-sand laminae. This subunit is completely bioturbated and contains biogenic structures that are allied with *Chondrites*, *Palaeophycus*, *Planolites*, *Teichichnus*, *Terebellina*, *Thalassinoides*, and *Zoophycos*.

### Subunit IIB

Interval: 174A-1073A-60X-1, 70 cm, to 61X-CC, 45 cm  
Depth: 542.5–560.1 mbsf

Subunit IIB (apparently lower Pliocene) is characterized by thick beds (1–3 m) of sandy mud and silty clay, which are typically dark gray (5Y4/1) to dark olive gray (5Y3/2), glauconitic, and thoroughly bioturbated. Identifiable trace fossils include *Zoophycos*, *Thalassinoides*, *Planolites*, and *Palaeophycus*. A slightly coarser muddy sand, with localized, poorly defined cross-lamination, is present near the top of the subunit (interval 174A-1073A-60X-2, 25–78 cm). Subunit IIB may be approximately equivalent to lithostratigraphic Unit III delineated within sediments of the nearby continental slope during Leg 150 (Mountain, Miller, Blum, et al., 1994). The base of Subunit IIB corresponds approximately with seismic surfaces m0.5(s)–m3(s) (see “Seismic Stratigraphy” section, this chapter).

### Subunit IIC

Interval: 174A-1073A-62X-1, 0 cm, to 65X-CC, 4 cm  
Depth: 560.1–597.8 mbsf

Subunit IIC comprises middle Miocene sediments that are generally finer grained than those of Subunits IIB and IID, consisting entirely of silty clays. These silty clays are dark olive gray (5Y4/1) to very dark gray (5Y3/2), variably glauconitic, and thoroughly bioturbated. Fabrics are dominated by relatively large, predominately horizontal burrows (e.g., *Thalassinoides*, *Planolites*, *Taenidium*), although more vertically extensive burrows (e.g., *Teichichnus*) are seemingly more abundant in the lower part (e.g., Core 174A-1073A-65X). Subunit IIC is perhaps equivalent to Unit IV delineated in slope sequences during Leg 150 (Mountain, Miller, Blum, et al., 1994).

### Subunit IID

Interval: 174A-1073A-66X-1, 0 cm, to 69X-2, 100 cm  
Depth: 597.8–628.8 mbsf

Subunit IID is characterized by lower to middle Miocene very fine sandy mud and silty clay that are either interbedded or, more commonly, thoroughly admixed by bioturbation. Color ranges from dark gray (5Y4/1) and dark grayish brown (2.5Y3/2) to dusky green (10G3/2) and dark green (10G2.5/1). In addition, reddish brown (2.5YR 3/1) and dusky red (2.5Y3/2) layers are observed within Core 174A-1073A-67X. Cross-stratification was observed in interval 174A-1073A-68X-1, 0–12 cm (Fig. 8). Sediment color varies considerably (various shades of dark gray, green, and brown), primarily reflecting variations in glauconite content. Trace fossils in this subunit resemble *Chondrites*, *Planolites*, *Skolithos*, *Taenidium*, *Teichichnus*, *Thalassinoides*, and *Zoophycos*. Subunit IID is roughly equivalent to Unit V delineated during Leg 150 (Mountain, Miller, Blum, et al., 1994). The base of Subunit IID is at about the depth of seismic surface m5.6(s) (see “Seismic Stratigraphy” section, this chapter).

### Subunit IIE

Interval: 174A-1073A-69X-2, 100 cm, to 69X-CC, 33 cm  
Depth: 628.8–635.8 mbsf

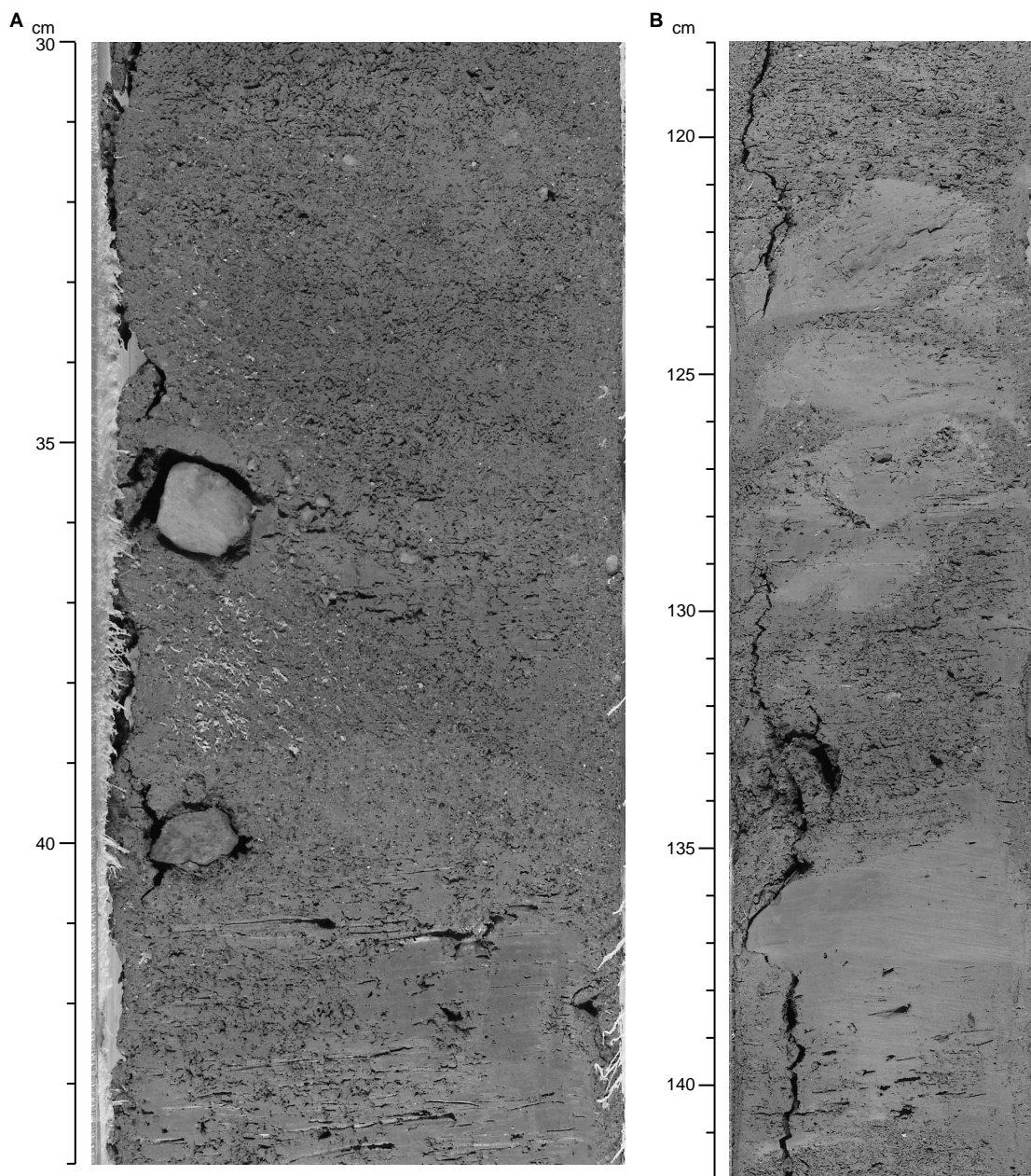


Figure 7. Pebbly sandy clay near the base of Subunit IE. This interval may correlate approximately with seismic surface pp4(s). **A.** Sandy mud with pebbles up to 1 cm (interval 174A-1073A-57X-1, 30–44 cm). **B.** Large, reddish brown exotic mud clasts (121–130 cm) in the same unit, and a large gray mud clast at 135–141 cm (interval 174A-1073A-57X-2, 118–142 cm).

Subunit IIE is predominantly bioturbated, gray (2.5Y5/1) to grayish brown (2.5Y3/2), silty nannofossil clay and clayey to sandy nannofossil chalk of early Miocene age. The boundary with the overlying subunit is abrupt and bioturbated. These sediments are generally glauconitic and, according to smear-slide analyses (see below), are diatomaceous. *Zoophycos* is common and conspicuous; associated trace fossils are most closely allied with *Thalassinoides*, *Planolites*, and *Taenidium*.

#### Subunit IIF

Interval: 174A-1073A-70X-1, 0 cm, to 71X-CC, 37 cm  
Depth: 635.8–654.1 mbsf

Subunit IIF, apparently Oligocene in age (see “Biostratigraphy” section, this chapter), is dominated by interbedded or admixed silty

clay and sandy mud, and it is lithologically similar to Subunit IID. Both of these lithologic components are generally dark to very dark grayish brown (10YR4/2; 10YR3/2), glauconitic, and bioturbated. Trace fossils tentatively identified include *Chondrites*, *Planolites*, *Taenidium*, *Teichichnus*, *Thalassinoides*, and *Zoophycos* (Fig. 9). The base of the subunit is marked by a somewhat coarser, very glauconitic muddy sand. The distribution of muddy sand, sandy mud, and silty clay defines two fining-upward successions (intervals 174A-1073A-70X-1, 0 cm, to 70X-CC, 42 cm; and 174A-1073A-71X-1, 0 cm, to 71X-CC, 50 cm).

#### Unit III

Interval: 174A-1073A-71X-CC, 37 cm, to 72X-CC, 48 cm (TD)  
Age: late Eocene

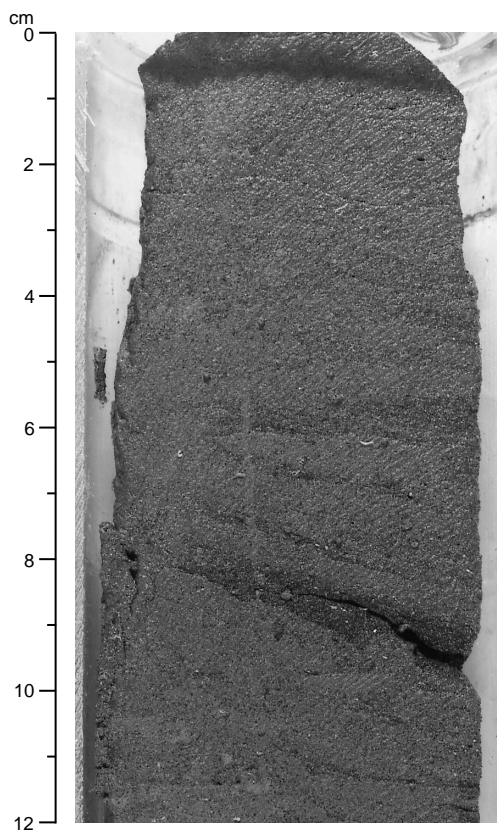


Figure 8. Cross-lamination within very fine-grained sandy mud, Subunit IID (interval 174A-1073A-68X-1, 0–12 cm).

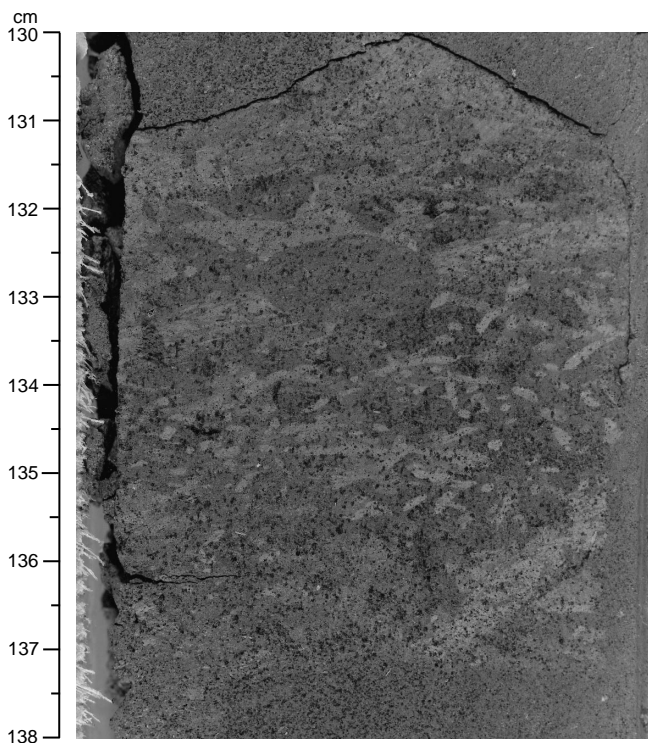


Figure 9. Trace fossils found in Oligocene sediments of Subunit IIF include *Chondrites*, *Planolites*, and *Zoophycos* (interval 174A-1073A-71X-1, 130–138 cm).

Depth: 654.1–663.6 mbsf

Unit III consists of light olive gray (5Y4/2), diatom- and clay-rich nannofossil chalk and olive gray diatom-rich nannofossil clay. The unit is strongly bioturbated, and recognizable trace fossils include *Zoophycos*, *Taenidium*, *Planolites*, *Chondrites*, and *Thalassinoides* (Fig. 10). Sand-sized glauconite is present as a minor component (<10%), and a single lamina that is rich in terrestrial plant debris was observed in Sample 174A-1073A-72X-5, 2–3 cm. Small irregular microfaults are common features through the recovered interval. The upper boundary of the subunit is extremely sharp, but is penetrated by burrows that apparently reflect firmground conditions. These burrows are sharp walled and filled with glauconitic muddy sand derived from Subunit IIF.

**Mineralogy**

The X-ray diffraction (XRD) analyses show variations of abundance with depth of quartz, feldspar, amphibole, calcite, dolomite, siderite, pyrite, and clays in Pleistocene sediments of Unit I (Fig. 11; Table 3). As at Sites 1071 and 1072, quartz, feldspars, amphibole, and clays are clearly detrital in origin. Quartz and feldspar show a good correlation downhole but without any overall trend. The quartz content does not show any clear relationship with grain size, except

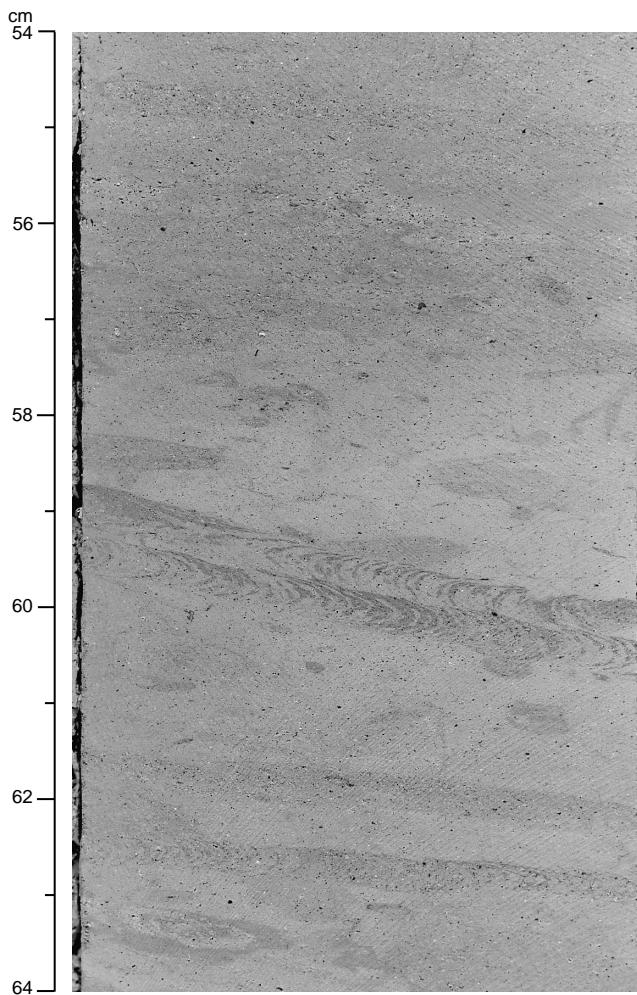


Figure 10. Trace fossils in Eocene sediments of Unit III include *Chondrites*, *Planolites*, *Taenidium*, and *Zoophycos* (interval 174A-1073A-72X-5, 54–64 cm).

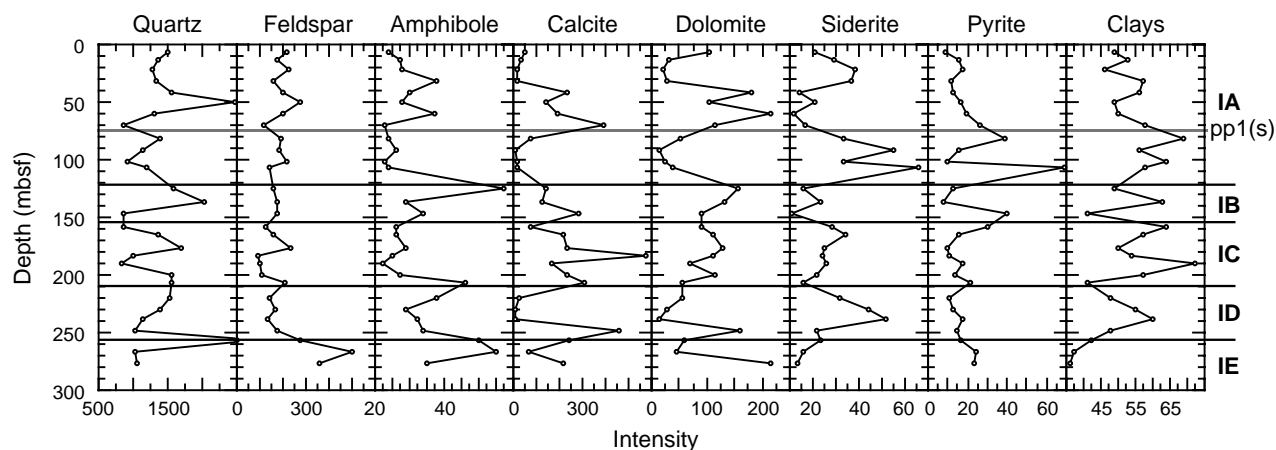


Figure 11. Relative intensity in XRD analyses vs. depth of common minerals in Pleistocene–Holocene(?) sediments from Hole 1073A. Lithostratigraphic Subunits IA through IE and seismic surface pp1(s) are noted on the right.

**Table 3. Relative intensity of main X-ray diffraction peaks for minerals in representative samples from Hole 1073A.**

Depth (mbsf)	Quartz	Feldspar	Amphibole	Calcite	Dolomite	Siderite	Pyrite	Clays
6.45	1493	213	24	49	104	21	9	49
13.40	1371	179	27	30	32	29	16	53
22.40	1269	222	28	18	22	38	18	46
32.10	1348	160	38	13	28	37	12	57
41.80	1543	201	30	236	179	14	13	56
50.58	2479	273	28	140	106	21	17	49
60.85	1310	200	37	189	216	12	19	50
70.34	860	114	23	391	113	17	26	58
81.58	1382	194	24	77	51	33	39	69
91.40	1127	181	26	11	14	55	16	56
100.89	923	221	23	21	25	33	10	64
107.29	1188	144	24	17	40	66	69	58
125.84	1597	160	57	146	158	16	13	49
136.90	2016	178	29	124	131	23	8	63
146.86	866	179	34	286	92	11	40	41
157.84	850	127	26	79	89	28	30	64
165.75	1357	161	26	221	112	34	16	57
176.85	1698	233	29	230	129	25	10	50
182.75	999	93	25	577	112	24	11	54
189.95	823	97	22	168	70	26	18	72
199.99	1558	111	27	237	115	22	14	57
206.50	1549	210	46	310	56	16	21	41
219.50	1537	143	38	25	54	32	11	48
229.60	1396	169	29	6	27	44	13	55
239.10	1152	134	32	12	15	52	18	60
248.69	1024	175	34	457	161	22	15	48
256.80	2497	279	50	239	60	23	17	42
266.26	1033	504	55	71	46	16	24	37
275.97	1057	360	35	214	214	13	23	36

Note: See Figure 11.

near the boundary between Subunits ID and IE (256.80 mbsf), where quartz is abundant in a sandy mud. Calcite and dolomite are present throughout the Pleistocene, in contrast to observations made at Sites 1071 and 1072. In Subunit IA, calcite and siderite show an inverse relationship.

Components observed in smear slides from Site 1073A include quartz, feldspar, glauconite, mica (muscovite, biotite, and chlorite), clays, carbonate, opaque minerals, Fe-oxide, accessory minerals (e.g., amphibole, rutile), and, at the base of the hole, grains of biogenic origin (Fig. 12; see smear slides in Section 4 on CD-ROM, back pocket, this volume). The mica content decreases from the top to the bottom of the hole. From the seafloor to ~72–75 mbsf (approximate depth of seismic surface pp1[s]), the percentage of carbonate increases. Below this level to the base of Subunit IA, carbonate content decreases, whereas the percentage of quartz + feldspar increases. The clay content shows the same trend as the carbonate content. The clay percentage decreases from the depth of seismic surface pp1(s) to the base of Subunit IC; the calcareous fossils show an inverse trend. The

clay content increases at the top of Subunit ID and stays relatively high to the base of Subunit IE. From the top of Unit II to the bottom of the hole, the percentages of the main detrital components, quartz + feldspar and clay, decrease. Glauconite content is variable but significantly higher than in Unit I. The content of the calcareous biogenic component increases concomitantly over this interval. The curve of the siliceous fossils shows the same trend as the calcareous fossils down to the base of Subunit IIB. Below Subunit IIB to the bottom of the hole, there is a decrease in biogenic silica. Overall, these trends in Unit II are consistent with a high degree of condensation at and below the level of surface pp4(s) (Fig. 12).

## BIOSTRATIGRAPHY

Biostratigraphic resolution at Site 1073 is excellent throughout most of the Pleistocene through upper Eocene section. Calcareous nannofossils provide detailed zonations for the stratigraphic interval

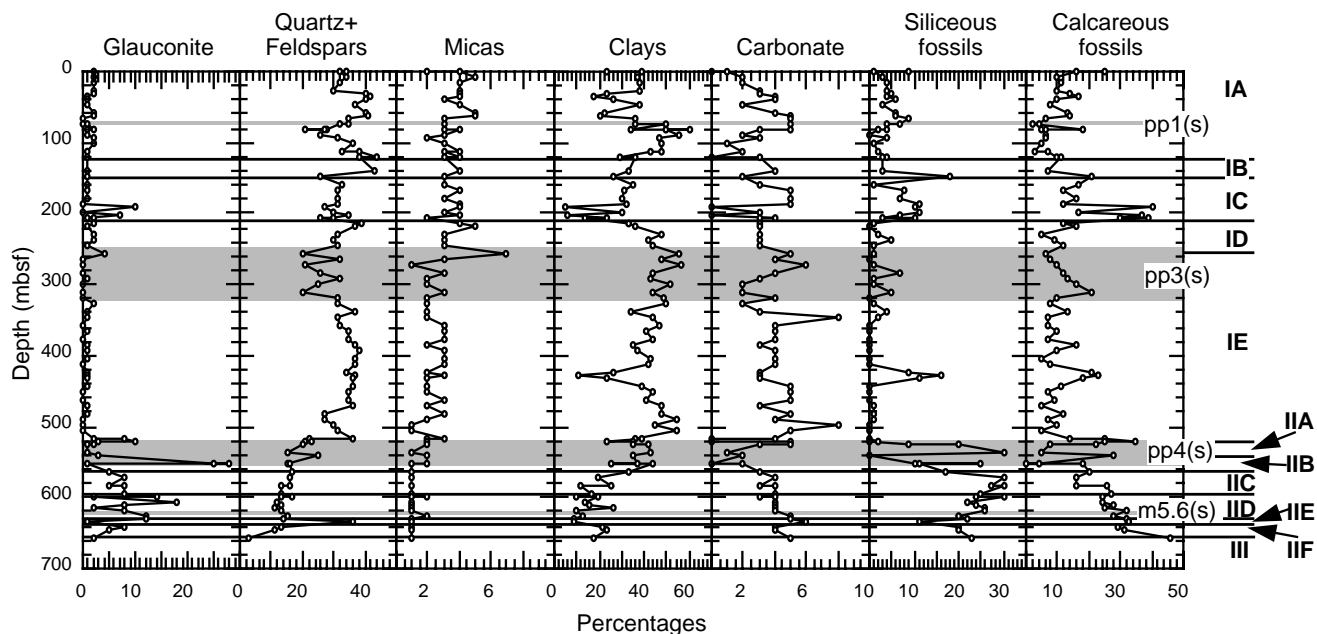


Figure 12. Percentages of glauconite, quartz + feldspars, micas, clays, carbonates, siliceous fossils, and calcareous fossils vs. depth from smear slides of Hole 1073A. Lithostratigraphic subunits are noted on the right vertical axis. Gray shaded areas show depth ranges of seismic surfaces pp1(s), pp3(s), pp4(s), and m5.6(s) derived from checkshot survey in Hole 1073A (see “Seismic Stratigraphy” section, this chapter).

Table 4. Summary of nannofossil datums for Hole 1073A.

Datum	Age (Ma)	Between samples	Depths* (mbsf)
		174A-1073A-	
FO <i>Emiliana huxleyi</i>	0.25	11H-CC/12H-CC	102.36/109.82
LO <i>Pseudoemiliana lacunosa</i>	0.46	36H-CC/37H-CC	324.86/333.63
FO <i>Gephyrocapsa parallela</i>	0.9	56X-CC/57X-CC	515.88/524.13
LO <i>Calcidiscus macintyreii</i>	1.7	56X-CC/57X-CC	515.88/524.13
LO <i>Discoaster tamalis</i>	2.8	57X-CC/59X-3, 68 cm	524.13/537.98
LO <i>Reticulofenestra pseudoubilicus</i>	3.8	59X-3, 68 cm/59X-CC	537.98/544.09
FO <i>Amaurolithus</i> spp.	4.5	59X-CC/62X-CC	544.09/569.91
LO <i>Cyclicargolithus floridanus</i>	12.5	59X-CC/62X-CC	544.09/569.91
LO <i>Sphenolithus heteromorphus</i>	13.5	64X-CC/65X-CC	588.51/597.95
FO <i>Sphenolithus heteromorphus</i>	18.2	67X-CC/69X-CC	616.89/635.90
FO <i>Sphenolithus belemnus</i>	19.2	67X-CC/69X-CC	616.89/635.90
LO <i>Reticulofenestra bisecta</i>	23.9	69X-CC/70X-CC	635.90/645.55
LO <i>Discoaster saipanensis</i>	34.2	70X-CC/71X-CC	645.55/654.46
LO <i>Reticulofenestra reticulata</i>	35	71X-CC/72X-CC	654.46/663.91
FO <i>Isthmolithus recurvus</i>	36	>72X-CC	>663.91

Note: \* = curated depths quoted for biostratigraphic datums are typically greater than drilling depths in intervals with >100% recovery.

cored, and highlight the various stratigraphic discontinuities at the base of the cored interval (latest Pliocene through late Eocene in age). Dinocysts are useful for biostratigraphic zonation for the latest Pleistocene through early Miocene interval. Planktonic foraminifers add to the confidence level of biostratigraphic zonation. Where age calibration is possible using planktonic foraminifers, they are compatible with the nannofossil zonation. Useful nannofossil biostratigraphic datums are summarized in Table 4, and an age-depth plot based on calcareous nannofossil, dinocyst, and planktonic foraminifer data is presented in Figure 13.

Provenance changes indicated by changes in the benthic foraminifer faunas from Site 1073 may be associated with changes in water depth in the Pleistocene. When sea level was relatively low, the source area for inner neritic benthic foraminifers was closest to Site 1073, facilitating transport of the shallow-water specimens to this location. When sea level was relatively high, these shallow species migrated landward and may not have been transported across the shelf to the slope. Lower Pleistocene to lower Pliocene benthic foraminifer faunas are dominated by *Uvigerina* spp.; these are analogous to present-day faunas from the northeast U.S. continental margin, where

the highest abundances of *Uvigerina peregrina* coincide with maxima of organic carbon and silt within slope sediments. The lower Miocene section yields a diverse, in situ bathyal benthic foraminifer assemblage, which indicates that the paleodepth may have been comparable to the present water depth (~600 m). Late Eocene assemblages at Site 1073 are comparable to late Eocene faunas from lower upper to middle bathyal paleodepths (~500–1000 m) reported from the Leg 150 New Jersey slope sites.

### Calcareous Nanofossils

All core-catcher samples, plus additional samples from within several cores, were examined for nannofossils. Nanofossils are generally common to abundant and relatively diverse at this site. They allow a fairly detailed biostratigraphy for the entire sequence, which spans from Pleistocene through upper Eocene. The question of whether or not Holocene sediments are present at the top of Hole 1073A will be addressed by postcruise studies. Nanofossil datums that were recognized are listed in Table 4. A brief description of the nannofossil biostratigraphic results is presented below.

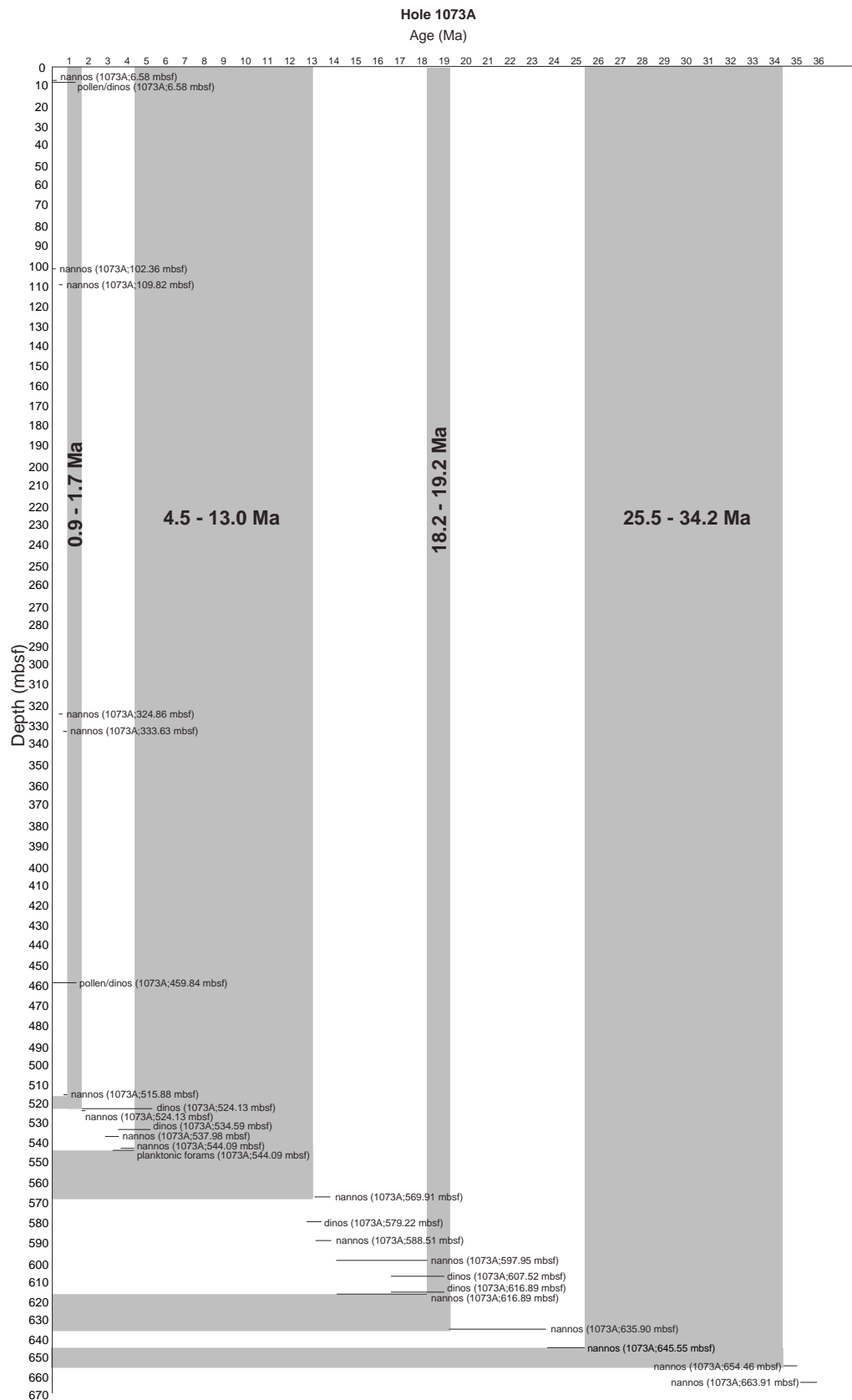


Figure 13. Age-depth plot for Hole 1073A based on calcareous nannofossils (nannos), dinocysts (dinos), and planktonic foraminifers (forams). Vertical shaded areas represent minimum possible intervals of missing time, and horizontal shaded depth intervals represent maximum possible depth ranges encompassing interpreted stratigraphic discontinuities.

Samples 174A-1073A-1H-CC (6.58 mbsf) through 11H-CC (102.36 mbsf) contain *Emiliania huxleyi*, and these samples are placed in Zone CN15 (0–0.25 Ma). The interval between Samples 174A-1073A-12H-CC (109.82 mbsf) and 36X-CC (324.86 mbsf) yields *Gephyrocapsa parallela*, but not *Emiliania huxleyi* or *Pseudoemiliania lacunosa*, and thus belongs to Subzone CN14b (0.25–0.46 Ma). Samples 174A-1073A-37X-CC (333.63 mbsf) through 56X-CC (515.88 mbsf) contain *Pseudoemiliania lacunosa* and *Gephyrocapsa parallela*, and these two taxa constrain the samples to be Subzone CN14a (0.46–0.9 Ma). *Calcidiscus macintyreii* is present in Sample 174A-1073A-57X-CC (524.13 mbsf), whereas discoasters are absent. This suggests an age between 1.7 and 1.9 Ma, which encompasses the Pleistocene/Pliocene boundary. A hiatus is suggested between Samples 174A-1073A-56X-CC and 57X-CC (515.88 and 524.13 mbsf).

Sample 174A-1073A-58X-CC (534.59 mbsf) is barren of nannofossils. Sample 174A-1073A-59X-3, 68 cm (537.98 mbsf), contains *Discoaster tamalis* among several other discoaster species, but no *Sphenolithus* spp.; *Reticulofenestra pseudoumbilicus* is also absent. This assemblage can be assigned an age of 2.8–3.6 Ma. *Reticulofenestra pseudoumbilicus* is present in Sample 174A-1073A-59X-CC (544.09 mbsf), but *Amaurolithus* spp. are absent. This suggests Zone CN11 (3.8–4.5 Ma). Sample 174A-1073A-60X-CC (551.60 mbsf) is barren of nannofossils. Sample 174A-1073A-61X-CC (561.00 mbsf) is rich in siliceous microfossils, but contains only a few specimens of nannofossils; these are not age diagnostic.

The interval between Samples 174A-1073A-62X-CC (569.91 mbsf) and 64X-CC (588.51 mbsf) contains *Cyclicargolithus floridanus*, but no *Sphenolithus heteromorphus*, which suggests an age of 13–14 Ma (middle Miocene). Thus, a major unconformity lies above Sample 174A-1073A-62X-CC (569.91 mbsf). The highest occurrence of *Sphenolithus heteromorphus* is in Sample 174A-1073A-65X-CC (597.95 mbsf), which marks the upper zonal boundary of Zone CN4 (13.5 Ma). This species is present down to Sample 174A-1073A-67X-CC (616.89 mbsf), which is above the lower zonal boundary of Zone CN3 (18.2 Ma). Sample 174A-1073A-68X-CC (626.63 mbsf) is barren of calcareous nannofossils. Sample 174A-1073A-69X-CC (635.90 mbsf) contains a lower Miocene assemblage. In the absence of *Sphenolithus belemnos* and Oligocene species, such as *Reticulofenestra bisecta* and *Zygrhablithus bijugatus*, this sample can be placed in Zone CN1 (19.2–23.9 Ma) in the lower Miocene.

Sample 174A-1073A-70X-CC (645.55 mbsf) yields *Reticulofenestra bisecta* and *Zygrhablithus bijugatus*, but no *Sphenolithus ciproensis* or *Chiasmolithus altus*, and can be assigned an age of 23.9–25.5 Ma (latest Oligocene).

Eocene species were found in Sample 174A-1073A-71X-CC (654.46 mbsf), which includes *Discoaster saipanensis* and *Isthmolithus recurvus*. *Reticulofenestra reticulata* is absent. This suggests a latest Eocene age (34.2–35.0 Ma). A major disconformity is thus revealed between the Eocene and Oligocene. Sample 174A-1073A-72X-CC (663.91 mbsf) contains *Isthmolithus recurvus* and *Reticulofenestra reticulata* among other Eocene species and can easily be an age of 35.0–36.0 Ma, within Zone CP15.

### Planktonic Foraminifers

Sediments from Site 1073 contain abundant to common planktonic foraminifers through most of the cored section (Holocene[?]-late Eocene in age). Pleistocene sediments from 6.58 to 515.88 mbsf (Samples 174A-1073A-1H-CC through 56X-CC) contain a fauna with common to frequent *Globigerina bulloides*, *Globigerina quinqueloba*, *Neogloboquadrina dutertrei*, and *Orbulina universa*. *Globorotalia inflata* and both left- and right-coiling *Neogloboquadrina pachyderma* vary in their abundances from dominant to rare throughout the Pleistocene section (Fig. 14). *Globorotalia inflata* and both left- and right-coiling *Neogloboquadrina pachyderma* are abundant at 6.58 mbsf (Sample 174A-1073A-1H-CC). Left-coiling *Neogloboquadrina pachyderma* is the dominant species of the three previously mentioned forms at 26.4, 92.91, and 515.88 mbsf (Samples 174A-1073A-3H-CC, 10H-CC, and 56X-CC). Right-coiling *Neogloboquadrina pachyderma* is the most abundant of the three forms at 131.38, 159.33, 289.13, 317.14, and 506.59 mbsf (Samples 174A-1073A-14H-CC, 17H-CC, 32X-CC, 35X-CC, and 55X-CC). Both right-coiling *Neogloboquadrina pachyderma* and *Globorotalia inflata* are the dominant forms at 64.32, 364.38, 400.48 and 487.55 mbsf (Samples 174A-1073A-7H-CC, 40X-CC, 44X-CC and 53X-CC). *Globorotalia inflata* is the dominant form at 45.39, 184.69, 324.86, 333.63, 384.65, 421.23, and 459.84 mbsf (Samples 174A-1073A-5H-CC, 20H-CC, 36X-CC, 38X-CC, 42X-CC, 46X-CC, and 50X-CC). Relative dominance of these three foraminifers is illustrated in Figure 14. Although this is not a detailed study, a cursory investigation of the core-catcher samples suggests that there is an important signal in the variation of these foraminifers in the Pleistocene section. These variations may be related to climatic oscillations and associated sea-level changes. Further work on these cores is needed to understand these patterns within the context of climate change.

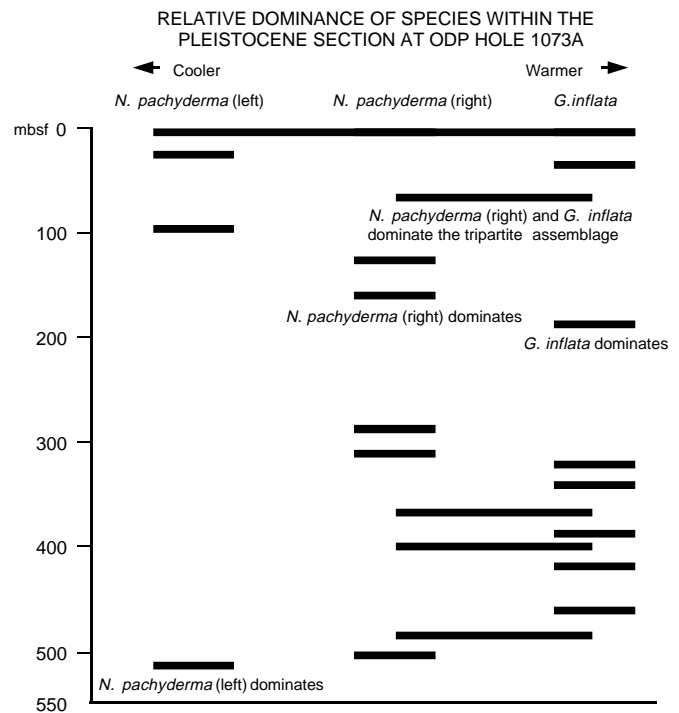


Figure 14. Relative dominance of species within the *Globorotalia inflata*, *Neogloboquadrina pachyderma* (right-coiling), and *Neogloboquadrina pachyderma* (left-coiling) assemblages of the Pleistocene section of Hole 1073A.

*Neogloboquadrina pachyderma* is the dominant species of the three previously mentioned forms at 26.4, 92.91, and 515.88 mbsf (Samples 174A-1073A-3H-CC, 10H-CC, and 56X-CC). Right-coiling *Neogloboquadrina pachyderma* is the most abundant of the three forms at 131.38, 159.33, 289.13, 317.14, and 506.59 mbsf (Samples 174A-1073A-14H-CC, 17H-CC, 32X-CC, 35X-CC, and 55X-CC). Both right-coiling *Neogloboquadrina pachyderma* and *Globorotalia inflata* are the dominant forms at 64.32, 364.38, 400.48 and 487.55 mbsf (Samples 174A-1073A-7H-CC, 40X-CC, 44X-CC and 53X-CC). *Globorotalia inflata* is the dominant form at 45.39, 184.69, 324.86, 333.63, 384.65, 421.23, and 459.84 mbsf (Samples 174A-1073A-5H-CC, 20H-CC, 36X-CC, 38X-CC, 42X-CC, 46X-CC, and 50X-CC). Relative dominance of these three foraminifers is illustrated in Figure 14. Although this is not a detailed study, a cursory investigation of the core-catcher samples suggests that there is an important signal in the variation of these foraminifers in the Pleistocene section. These variations may be related to climatic oscillations and associated sea-level changes. Further work on these cores is needed to understand these patterns within the context of climate change.

Lowermost Pleistocene to upper Pliocene sediments (Sample 174A-1073A-57X-CC; 524.13 mbsf) contain specimens of *Globorotalia inflata*, consistent with the nannofossil ages of 1.7–1.9 Ma in this part of the section. Lower Pliocene sediments (Sample 174A-1073A-59X-CC; 544.09 mbsf) are dominated by *Globorotalia crassaformis* (first appearance datum [FAD] = 4.5 Ma; Berggren et al., 1995) and contain rare specimens of *Sphaeroidinellopsis seminulina* (last appearance datum [LAD] = 3.12 Ma; Berggren et al., 1995). These data are consistent with an early Pliocene nannofossil assemblage. The presence of *Globorotalia praescitula* in Sample 174A-1073A-67X-CC (616.89 mbsf) suggests an early to middle Miocene age. Samples 1074A-1073A-71X-CC and 72X-CC (654.46 and 663.91 mbsf) contain *Catapsydrax dissimilis*, *Subbotina eocaena*, *Subbotina venezuelana*, and *Turborotalia cerroazulensis*. This planktonic foraminiferal assemblage suggests a late Eocene age, also consistent with nannofossil assemblages at these depths.

Abundant to frequent diatoms, together with common to rare radiolarians, are present in Samples 174A-1073A-58X-CC (534.59 mbsf), 61X-CC (561.00 mbsf), 63X-CC (579.22 mbsf) and 67X-CC (616.89 mbsf). In addition, glauconite is abundant in the latter sample and in Samples 174A-1073A-59X-CC (544.09 mbsf), 60X-CC (551.60 mbsf) and 68X-CC (626.63 mbsf). In the Pleistocene interval (6.58–515.88 mbsf), the percentage of planktonic foraminifers relative to total foraminifers is 15%–95%, but is typically >60%. In the core-catcher samples studied from 524.13 (Sample 174A-1073A-57X-CC) to 663.91 mbsf (Sample 174A-1073A-72X-CC), the percentage of planktonic foraminifers is 0%–50%.

### Benthic Foraminifers

Benthic foraminifers are rare to abundant in Pleistocene core-catcher samples examined from Site 1073. Samples yield species that are characteristic of different depth habitats; some samples contain assemblages that indicate a single depth zone, whereas other samples contain species mixed together that are typical of different depth zones. Tracing the origin(s) of the benthic foraminiferal faunas provides information on sediment provenance. For example, samples dominated by *Elphidium excavatum forma clavatum* indicate that sediments were transported from the inner neritic zone (0–50 m). In contrast, some samples yield species typically restricted to inner neritic depths mixed in with species that indicate outer neritic or deeper depths; still other samples lack the shallowest water indicators altogether. There are faunal components present in Pleistocene samples from Site 1073 (including *Cibicides* spp., *Gyroidinoides* spp., *Melonis barleeanum*, *Oridorsalis umbonatus*, *Stainforthia complanata*, and *Valvulinera laevigata*) that are absent or rare in the inner to middle neritic assemblages found at shelf Sites 1071 and 1072, indicating that source areas probably included outer shelf and upper slope sediments. Alternatively, it is possible that these deeper water faunas are in situ. However, no sample above Sample 174A-1073A-57X-CC (524.13 mbsf) yields benthic foraminifers that specifically indicate paleodepths as deep as the present water depth of ~600 m at Site 1073 (e.g., *Anomalinoidea globulosus*, *Cibicides robertsonianus*, and *Planulina wuellerstorfi* are absent). It is possible that most (or even all) of the benthic foraminifers in the Pleistocene section at Site 1073 are a result of downslope transport; further study will resolve this issue.

Provenance changes indicated by changes in the benthic foraminiferal faunas may be associated with changes in water depth. For example, when sea level was relatively low, the source area of the inner neritic benthic foraminifers was closest to Site 1073, facilitating transport of the shallow-water specimens to this location. As sea level rose, the inner neritic species migrated landward and hence farther away from Site 1073. When sea level was relatively high, these shallow specimens may not have been transported across the shelf to the depth of this location. The high sedimentation rates (up to ~80 cm/k.y.) support the likelihood that there was a high rate of downslope transport in the late Pleistocene at Site 1073. A high-resolution study of the benthic foraminiferal faunal changes and inferred provenance changes should provide a detailed record of changes in water depth in the late Pleistocene recorded in Site 1073 sediments.

Lowermost Pleistocene to upper Pliocene Samples 174A-1073A-57X-CC and 58X-CC (524.13–534.59 mbsf) contain abundant *Uvigerina* spp. Lower Pliocene Sample 174A-1073A-59X-CC (544.09 mbsf) yields a diverse, in situ benthic foraminiferal assemblage dominated by high abundances of *Uvigerina peregrina*. This assemblage is analogous to present-day faunas from the northeast U.S. continental margin, where the highest abundances of *Uvigerina peregrina* coincide with maxima of organic carbon and silt within the slope sediments (Miller and Lohmann, 1982). Other taxa that characterize Sample 174A-1073A-59X-CC include *Bulimina mexicana*, *Cibicides* spp., *Laticarinina pauperata*, *Melonis barleeanum*, *Planulina* cf. *wuellerstorfi*, *Plectofrondicularia vaughani*, *Sigmoilopsis schlumbergeri*, *Stilostomella* spp., and *Vulvulina spinosa*.

Samples 174A-1073A-61X-CC through 68X-CC (561.00–626.63 mbsf) are barren or yield rare benthic foraminifers. This interval contains abundant diatoms and glauconite. Lower Miocene Sample 174A-1073A-69X-CC (635.90 mbsf) yields a diverse, in situ bathyal benthic foraminiferal assemblage characterized by *Globocassidulina subglobosa*, *Gyroidinoides* spp., *Hoeglundina elegans*, *Lenticulina* spp., *M. barleeanum*, polymorphinids, and *Stilostomella* sp. A lower depth limit of ~1000 m is indicated by *Melonis pompilioides* and *Siphonina tenuicarinata*, and an upper depth limit of ~200 m is indicated by *Cibicides mundulus*. The presence of several specimens of *Cibicides robertsonianus* indicates that the paleodepth may have been comparable to the present water depth (~600 m).

Upper Eocene Samples 174A-1073A-71X-CC and 72X-CC (654.46–663.91 mbsf) yield diverse, in situ bathyal benthic foraminiferal faunas characterized by *Bulimina subtruncana*, *Bulimina macilenta*, *Bulimina tuxpamensis*, *Cibicides alazanensis*, *Cibicides dickersoni*, *Cibicides micrus*, *Cibicides praemundulus*, *Cibicides eocaenus*, *Cibicides subspiratus*, *Cibicides truncana*, *Globocassidulina subglobosa*, *Gyroidinoides* spp., *Lenticulina* spp., *Martinotiella* sp., *Osangularia* sp., *Pullenia bulloides*, *Stilostomella* spp., *Uvigerina auberiana*, *Uvigerina havanensis*, *Uvigerina semivestita*, and *Vulvulina mexicana*. These assemblages are comparable to late Eocene faunas from lower upper to middle bathyal paleodepths (~500–1000 m) reported from the Leg 150 New Jersey slope sites (Katz and Miller, 1996). For instance, *Bulimina subtruncana*, *Stilostomella paucistriata*, and *Uvigerina semivestita* were common to abundant in the late Eocene at lower upper to middle bathyal depths, but rare to absent at lower bathyal to abyssal depths and during other time periods on the New Jersey margin (Legs 93, 95, and 150; Miller and Katz, 1987; Katz and Miller, 1996). Species found at lower bathyal to abyssal depths (>1000 m) in the Eocene on the New Jersey margin are absent at Site 1073, supporting the shallower paleobathymetric estimate for this site.

### Palynomorphs

Samples 174A-1073A-1H-CC through 50X-CC (6.58–459.84 mbsf) are assigned a Pleistocene age, on the basis of the presence of the dinocyst *Ataxiodinium choanum* (upper lower Pleistocene–Holocene) in some samples and the absence of diagnostic Pliocene or older dinocysts. Because no Pleistocene samples containing common *Operculodinium israelianum* or *Bitectatodinium tepikiense* were found, all samples are assumed to be <1.37 Ma (McCarthy, 1995). Glacial-interglacial fluctuations are evident, with glacial conditions recorded by sparse *Brigantedinium*-dominated dinocyst assemblages with minor *Operculodinium centrocarpum*, *Nematosphaeropsis labyrinthus*, and *Spiniferites* spp., as in Sample 174A-1073A-15X-CC (140.15 mbsf). Pollen assemblages in these glacial samples are dominated by Picea. In contrast, interglacial conditions are clearly recorded by the rich dinocyst assemblage containing *Tectatodinium pellitum*, which has a modern south-temperate to subtropical distribution in the North Atlantic (Harland, 1983), together with *Lingulodinium machaerophorum*, *Achomosphaera andalusiensis*, *Selenopemphix nephroides*, and various *Brigantedinium* spp. and *Spiniferites* spp. in Sample 174A-1073A-21X-CC (193.30 mbsf).

Sample 174A-1073A-57X-CC (524.13 mbsf) is tentatively assigned to the Pliocene, on the basis of the presence of *Operculodinium janduchenei* and *Habibacysta tectata* in a rich dinocyst assemblage dominated by *Operculodinium israelianum* and *Tectatodinium pellitum*, together with *Spiniferites* spp., *Brigantedinium* spp., *Operculodinium centrocarpum*, *Polysphaeridium zoharyi*, and *Achomosphaera ramulifera*. Minor reworking is evident, however, from the presence of *Batiacasphaera sphaerica*, making the age assignment uncertain.

Sample 174A-1073A-58X-CC (534.59 mbsf) is tentatively assigned to the lower Pliocene on the basis of the presence of *Selenopemphix brevispinosa*, which has its LAD in the early Pliocene, and the absence of cysts with LADs in the Miocene. *Tectatodinium*

*pellitum*, *Achomosphaera andalusiensis*, *Spiniferites* spp., and *Brigantedinium* spp. are also found.

Sample 174A-1073A-60X-CC (551.60 mbsf) is assigned a late Miocene age, although the presence of both *Cerebrocysta poulsenii* (Zone DN3–DN8) and *Operculodinium? eirikianum* (FAD in Zone DN9) either suggests that the datums of de Verteuil and Norris (1996) must be revised or that *Cerebrocysta poulsenii* is reworked into sediments younger than ~8.6 Ma. The presence of *Selenopemphix brevispinosa* and *Reticulosphaera actinocoronata* constrain the age to early Pliocene or older. Also present are *Habibacysta tectata*, *Polysphaeridium zoharyi*, *Brigantedinium* spp., *Lejeunecysta* spp., and *Spiniferites* spp.

Sample 174A-1073A-63X-CC (579.22 mbsf) contains *Dapsilodinium pseudocolligerum*, *Cerebrocysta poulsenii*, *Habibacysta tectata*, *Batiacasphaera sphaerica*, *Polysphaeridium zoharyi*, *Labyrinthodinium truncatum*, *Operculodinium centrocarpum*, *Operculodinium placitum*, and *Paleocystodinium golzowense*. The FAD of *Habibacysta tectata* and the LADs of *Cerebrocysta poulsenii* and *Operculodinium placitum* constrain the age of this sample to between ~14.2 and 11.2 Ma. The absence of *Cannosphaeropsis passio* and *Systematophora placantha* from this sample, however, probably further constrains the age to Zone DN6, ~13.2–12.8 Ma, according to the definition of this zone by de Verteuil and Norris (1996).

The presence of *Cousteaudinium aubryae*, *Sumatradinium soucouyantiae*, and *Pyxidinosphaera fairhavenensis*, all of which have FADs in Zone DN2, gives a maximum age of 22 Ma to Sample 174A-1073A-66X-CC (607.52 mbsf), whereas the presence of *Lingulodinium multivirgatum* (LAD top of Zone DN3) gives it a minimum age of 16.7 Ma. Also present, and consistent with an early Miocene age, are *Systematophora placantha*, *Pentadinium laticinctum*, *Reticulosphaera actinocoronata*, *Polysphaeridium zoharyi*, *Lingulodinium machaerophorum*, *Operculodinium centrocarpum*, *Lejeunecysta* spp., and various *Spiniferites* spp., including *Spiniferites pseudofurcatus*. It is possible to constrain the age of Sample 174A-1073A-67X-CC (616.89 mbsf) to early Miocene Zone DN3 (~19–16.7 Ma), on the basis of the presence of *Lingulodinium multivirgatum* (LAD top of Zone DN3), *Sumatradinium druggii* (Zones DN3–DN8), *Apteodinium tectatum* (LAD within Zone DN5, ~14.2 Ma), and *Cousteaudinium aubryae* (Zones DN2–DN4). Also present are *Operculodinium placitum*, *Batiacasphaera sphaerica*, *Operculodinium centrocarpum*, *Polysphaeridium zoharyi*, *Spiniferites* spp., and *Brigantedinium* spp. Sample 174A-1073A-66X-CC (607.52 mbsf) must also, therefore, belong to Zone DN3, and not Zone DN2. In contrast to this relatively thick record of the upper lower Miocene Zone DN3, the record of Zones DN2 and DN1 must be relatively thin, if present, because the next sample analyzed, Sample 174A-1073A-70X-CC (645.55 mbsf), appears to be pre-Miocene on the basis of the presence of a large number of Paleogene cysts, which are not identified.

Amorphous organic matter of marine origin is abundant in Samples 174A-1073A-58X-CC through 70X-CC (534.59–645.55 mbsf), as are foraminiferal linings and lattices of diatoms and radiolarians. This contrasts with the greater abundance of terrigenous organic matter (phytodebris) in the upper ~50 cores, with Sample 174A-1073A-57X-CC (524.13 mbsf) being intermediate in character. The ratio of pollen and terrestrial spores to dinoflagellate cysts mirrors this change, and the implication is that planktonic productivity decreased and/or terrigenous influx increased between the early Pliocene and middle Pleistocene at Site 1073.

### Biostratigraphic Age Control of Stratigraphic Discontinuities

Biostratigraphic control at Site 1073 indicates at least four stratigraphic discontinuities between the latest Pleistocene and the latest Eocene (Fig. 13). Whether Holocene sediments were recovered from Hole 1073A was not resolved on the ship. Postcruise investigations

of calcareous nannofossils, as well as stable carbon and oxygen isotopic analyses, will help determine more accurately the ages of sediments at the top of Hole 1073A.

The first downhole stratigraphic discontinuity encountered has a maximum age range of 0.46–1.9 Ma and a minimum range of 0.9–1.7 Ma. Both calcareous nannofossils and dinocysts help constrain the age of this early Pleistocene discontinuity, which is located in Hole 1073A between 515.88 and 524.13 mbsf.

The age range of the second downhole stratigraphic discontinuity is constrained by calcareous nannofossils, planktonic foraminifers, and dinocysts. This earliest Pliocene to middle Miocene discontinuity is located between 544.09 and 569.91 mbsf, and has an age range of 3.8–13.5 Ma (maximum) to 4.5–13.0 Ma (minimum).

A third stratigraphic discontinuity well constrained by calcareous nannofossils is present in the lower Miocene section, between 616.89 and 635.90 mbsf, and exhibits an age range of 16.7–23.9 (maximum) to 18.2–19.2 Ma (minimum).

The fourth discontinuity is located between 645.55 and 654.46 mbsf. Calcareous nannofossils constrain the age of this latest Oligocene to latest Eocene unconformity between 23.9–35.0 Ma (maximum) and 25.5–34.2 Ma (minimum).

Age ranges quoted are both the narrowest and widest possible for the discontinuity. Uncertainties in the age ranges for stratigraphic discontinuities reflect uncertainties in the ages of bounding intervals. For example, the upper age limit of the early Pleistocene discontinuity is defined on the basis of a calcareous nannofossil sample reported as 0.46–0.9 Ma. The lower limit of the early Pleistocene discontinuity is defined on the basis of a calcareous nannofossil sample reported as 1.7–1.9 Ma. Similarly, depths quoted above reflect the broadest ranges possible to encompass the discontinuity surface. Additional postcruise sampling between these data points should refine the interval/location of these discontinuity surfaces.

### PALEOMAGNETISM

All archive-half sections from Hole 1073A (APC and XCB cores) were subjected to routine pass-through measurements (Tables 5–10 on CD-ROM, back pocket, this volume). Typically, the natural remanent magnetization (NRM) was measured using the pass-through cryogenic magnetometer at intervals of 3 or 5 cm. After measuring the NRM, sections were partially demagnetized, mostly at 20 mT to remove overprints, and were remeasured.

Discrete-cube samples were taken at a rate of one per several cores and were alternating-field (AF) demagnetized at seven steps up to 30 mT. Results from discrete-cube samples are shown in Table 11. To prevent spurious anhysteretic remanent magnetization because of residual magnetic fields in the AF demagnetizer (see “Paleomagnetism” section, “Site 1071” chapter, this volume), demagnetizations of >30 mT were not conducted. Typical examples of demagnetization plots for discrete-cube samples are presented in Figure 15. Drill string overprints with steep positive inclinations were typically removed by demagnetization up to 10 mT. The paleomagnetic direction of discrete-cube samples and archive samples of corresponding horizons agreed well for most samples.

The Tensor tool was used to orient the APC cores from Hole 1073A, starting with the third core (Table 12). Because archive-half Sections 174A-1073A-4H-2 and 4H-3 were actually working halves (erroneously marked as archive halves), 180° was added to the declination values of these sections. Figure 16 shows the paleomagnetic results for APC core samples from Hole 1073A after demagnetization at 20 mT. Declinations after correction using the Tensor tool readings average near zero; however, some of the cores deviate substantially from zero. This may be attributed to the offset of the Tensor tool reading (offset by an external magnetic field, noise from the drill string, or offset of the flux-gate sensor), error during core splitting,

**Table 11. Paleomagnetic and rock magnetic parameters of discrete samples for Hole 1073A.**

Core, section, interval (cm)	Depth (mbsf)	NRM		NRM at 20 mT		MDF (mT)	Susceptibility (SI)
		Intensity (A/m)	Declination (°)	Inclination (°)	Intensity (A/m)		
174A-1073A-							
2H-4, 67-69	11.77	1.32E-02	154.3	44.0	3.56E-03	5	2.54E-04
2H-5, 61-63	13.21	1.91E-02	234.9	58.9	1.80E-03	3	3.82E-04
2H-5, 129-131	13.89	1.90E-02	155.7	60.8	3.61E-03	3	3.48E-04
2H-6, 59-61	14.69	1.21E-02	169.3	41.2	3.29E-03	4	2.78E-04
3H-1, 59-61	16.69	4.04E-02	216.8	63.9	1.50E-02	8	2.91E-04
16H-1, 59-61	140.19	1.32E-02	72.7	56.5	5.35E-03	9	1.82E-04
23H-1, 59-61	203.39	8.48E-03	222.9	45.1	1.88E-03	5	1.43E-04
28X-3, 46-48	246.96	2.20E-02	356.3	55.8	9.99E-03	15	1.85E-04
31X-1, 82-84	272.82	3.98E-02	83.8	74.6	1.25E-02	12	1.81E-04
35X-1, 134-136	310.84	2.79E-02	-5.2	46.9	1.15E-02	10	3.68E-04
37X-1, 61-63	329.91	7.12E-03	-0.2	63.2	1.50E-03	4	2.04E-04
40X-1, 59-61	356.59	4.00E-02	-63.0	83.2	5.70E-03	4	7.58E-04
43X-5, 61-63	390.91	8.42E-03	-17.2	50.1	5.82E-03		1.62E-04
45X-5, 75-77	409.25	2.35E-02	-139.0	57.1	8.82E-03	8	3.04E-04
48X-5, 59-61	437.49	9.49E-04	250.3	59.5	3.62E-04	14	9.05E-05
52X-5, 60-62	474.80	2.34E-02	296.9	54.6	8.33E-03	8	4.07E-04
56X-6, 63-65	514.08	1.26E-01	83.9	61.2	1.53E-02	5	1.32E-03
59X-4, 81-83	539.61	2.85E-03	231.5	58.9	7.55E-04	9	8.11E-05
61X-7, 62-64	559.54	4.81E-04	130.9	-12.4	2.87E-05	5	1.20E-04
63X-6, 62-64	577.52	4.14E-04	201.0	29.5	2.87E-04	30	1.18E-04
69X-2, 60-62	628.40	3.21E-04	175.8	42.0	9.38E-05	5	1.15E-04

Note: MDF = median destructive field.

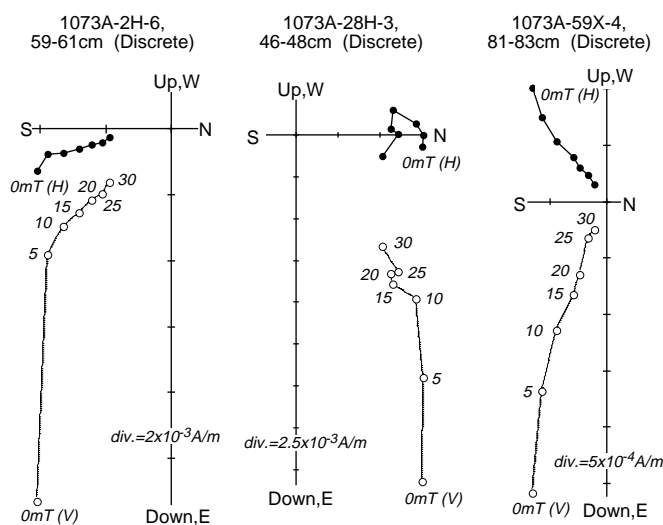


Figure 15. Typical examples of vector endpoint diagrams for discrete samples. Solid circles and open circles represent projections of magnetization vectors onto a horizontal plane and a vertical plane, respectively. Numbers denote demagnetization levels in milliteslas (mT).

and/or an error during measurement (rolling or tilting of sample boat). Because the tool is attached rigidly to the top of the core barrel, it is unlikely that movement of the tool relative to the core barrel could have caused an angular error. Another possible explanation is that the offset, produced by drilling-induced remanence with circular components at the margin of the core, appeared on the archive-half measurements as a sum of total magnetization. Alternatively, the offset geometry of half-core measurements produced the difference in the shape and peak intensity of sensor-response curves with those measured at the center (used for the automatic calculation by the magnetometer software). This would produce a difference in the ratio of X-axis to Y-axis, and thus distort the declination (Oda and Shibuya, 1996). However, an offset of  $>10^\circ$  is difficult to explain by sensor response.

**Table 12. Azimuthal orientation of APC cores from Hole 1073A using the Tensor tool data.**

Core	MTF (°)
174A-1073A-	
1H	NM
2H	NM
3H	254
4H	138
5H	234
6H	354
7H	95
8H	224
9H	182
10H	308
11H	342
12H	241
13H	58
14H	183
15H	66
16H	97
17H	276
18H	44
19H	356
20H	54
21H	160
22H	138
23H	229
24H	196

Notes: MTF = magnetic toolface. The orientation parameter (MTF) is an angle between true north and X-axis of the core coordinate. NM = not measured.

## Magnetostratigraphy

Despite many voids caused by gas expansion of the cores, high-resolution continuous records of inclination and magnetization intensity variations were collected for Pleistocene sediments (Figs. 16, 17). Two possible short polarity reversal events were found within the Brunhes Chron at 15 and 351 mbsf. Magnetic polarity was normal down to 515 mbsf (~pp4[s]; see "Seismic Stratigraphy" section, this chapter), with magnetization intensity fluctuations between 0.1 and 20 mA/m. The B/M boundary (0.78 Ma) was not found above 515 mbsf. Between 515 and 524 mbsf, the polarity of magnetic inclination shows unstable fluctuations that flip between positive and negative. Below 519 mbsf, magnetization intensity is generally low, ranging between 0.05 and 1 mA/m, making it difficult to identify mag-

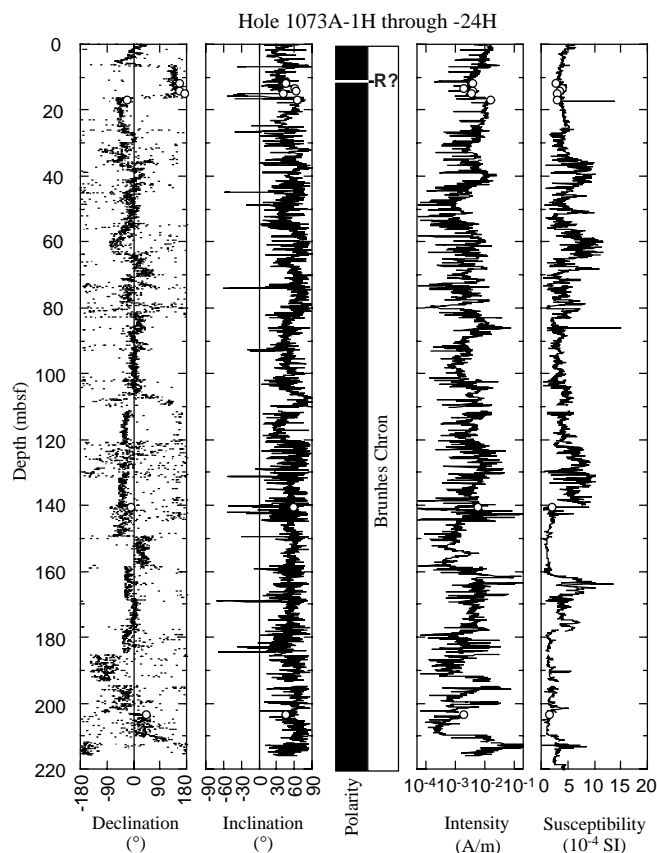


Figure 16. Declination, inclination, magnetic polarity zones, magnetization intensity, and volume magnetic susceptibility for APC core samples from Holes 1073A. Directions and intensity of magnetization are after 20-mT AF demagnetization. Declination of Cores 174A-1073A-3H through 24H were corrected using the Tensor tool (magnetic tool face) angles. Solid lines and open circles indicate pass-through data and discrete data, respectively. In the polarity column, black = normal polarity, white = reversed polarity, and cross-hatched = uninterpretable.

netic polarity zones by pass-through measurements on biscuited XCB archive sections. Shore-based study of discrete-cube samples taken from each biscuit will make it possible to obtain a more reliable magnetostratigraphic record.

### Short Reversals Within the Brunhes Chron

Two possible short reversal events were found in Pleistocene sediments of Hole 1073A. Figure 18 shows a reversal found at 14.8–15.7 mbsf from Core 174A-1073A-2H. The youngest shipboard biostratigraphic datum is 0.25 Ma (calcareous nannofossils), and was found between Samples 174A-1073A-11H-CC and 12H-CC (102.36–109.82 mbsf; see “Biostratigraphy” section, this chapter). Therefore, the reversal centered at ~15 mbsf could be one of several identified reversal events <0.25 Ma (e.g., Laschamp and Blake Events; Worm, 1997; Zhu et al., 1994). More detailed age control from shore-based biostratigraphic and/or oxygen isotopic stratigraphy may provide additional constraints to aid in the identification of this reversal.

Another short reversal was observed in Core 174A-1073A-39X at 350.0–351.8 mbsf (Fig. 19). Declination shows larger fluctuations, which may be caused by biscuiting of the XCB samples. However, the record of inclination seems continuous, with a sharp polarity boundary at the bottom (351.8 mbsf) and a more gradual change at the top (~350.0 mbsf). According to the biostratigraphic constraints (calcareous nannofossils) for Samples 174A-1073A-36X-CC

(324.86 mbsf; 0.25–0.46 Ma; see “Biostratigraphy” section, this chapter) and 37X-CC (333.63 mbsf; 0.46–0.9 Ma), this short polarity reversal event may well be correlated with the Emperor Event (417–490 ka; Worm, 1997).

Neither of the aforementioned reversal events corresponds to lithologic boundaries (see “Lithostratigraphy” section, this chapter), and both are also observed on the continuous magnetic susceptibility records. Although both of the short-reversal intervals appear undisturbed by drilling, except for gas expansion, careful shore-based measurements of discrete samples taken from the centers of the cores are required. During Leg 172, several geomagnetic excursions/reversals were found during the Brunhes Chron that can be correlated to oxygen-isotope Stages 3, 4, 5 (Blake Event?), 7, 9, 11, and 15 (Keigwin, Rio, Acton, et al., 1998; Sites 1060, 1061, 1062). The geographic proximity between Site 1073 and Sites 1060, 1061, and 1062 will make it possible to correlate the excursions through comparison of inclination and intensity variations.

## INORGANIC GEOCHEMISTRY

Eighty-three interstitial water samples were collected from Hole 1073A to examine potential high-resolution variability. Every other section was sampled for the first three cores, then every core thereafter to the bottom of the hole. Exceptions are Core 174A-1073A-22H, where three sections were sampled, and Core 174A-1073A-57X, where whole rounds from two sections were collected.

Downhole profiles of alkalinity,  $\text{HPO}_4^{2-}$ , and  $\text{H}_4\text{SiO}_4$  show four distinct maxima in the upper 300 mbsf, centered around 10, 50, 150, and 260 mbsf (Fig. 20; Table 13). Two additional alkalinity and  $\text{H}_4\text{SiO}_4$  maxima are observed downhole at ~420 and ~565 mbsf. From a maximum of 36.9  $\mu\text{M}$  at 260 mbsf,  $\text{HPO}_4^{2-}$  concentrations decrease abruptly to 4.3  $\mu\text{M}$  at ~323 mbsf, below which concentrations remain uniform and low. In contrast,  $\text{NH}_4^+$  gradually increases with depth to ~150 mbsf, creating a broad subsurface maximum with two, less distinct, local maxima located at 50 and 150 mbsf;  $\text{NH}_4^+$  then decreases downhole. Sulfate reduction rapidly decreases  $\text{SO}_4^{2-}$  concentration to zero by 9.5 mbsf. Sulfate remains low, near zero, to ~550 mbsf, then gradually increases to 10.07 mM near the bottom of the hole (661.5 mbsf). The slight increase in  $\text{SO}_4^{2-}$  concentrations (maximum of 3.84 mM) centered around 300 mbsf may be the result of minor contamination with drilling fluid; such contamination has previously been observed with XCB coring (e.g., Taira, Hill, Firth, et al., 1991; Westbrook, Carson, Musgrave, et al., 1994). However, the steady increase of  $\text{SO}_4^{2-}$  observed to the base of the hole (35% of seawater concentration) is unlikely to be the result of contamination, because it is accompanied by a substantial decrease in methane concentrations (see “Organic Geochemistry” section, this chapter).

Calcium ( $\text{Ca}^{2+}$ ),  $\text{Mg}^{2+}$ , and  $\text{Sr}^{2+}$  decrease between the seafloor and 32 mbsf by 72%, 38%, and 34%, respectively (Figs. 20, 21). Below 32 mbsf,  $\text{Ca}^{2+}$  gradually increases downhole to 600 mbsf, and then increases more abruptly to a maximum of 20.08 mM at the bottom of the hole. In the upper 350 mbsf, profiles of  $\text{Mg}^{2+}$  and  $\text{Sr}^{2+}$  show several distinct maxima and minima (Fig. 21). Corresponding  $\text{Mg}^{2+}$  and  $\text{Sr}^{2+}$  minima are located at 32, 108, 213, and 322 mbsf. A notable exception is observed at ~200 mbsf, where  $\text{Sr}^{2+}$  increases, but  $\text{Mg}^{2+}$  does not show a corresponding maximum. Below 322 mbsf,  $\text{Mg}^{2+}$  increases from 27.31 to 41.18 mM at ~517 mbsf, which is near the lithostratigraphic boundary between Units I and II (see “Lithostratigraphy” section, this chapter); concentrations then remain uniform to the base of the hole.  $\text{Sr}^{2+}$  steadily increases below 322 mbsf, reaching a maximum value of 834  $\mu\text{M}$  at 661.5 mbsf.

The downhole profile of  $\text{Cl}^-$  shows high-frequency variability in the upper 300 mbsf;  $\text{Cl}^-$  maxima are located at 20 (566 mM), 158 (563 mM), and 268 mbsf (563 mM; Fig. 20). Below 300 mbsf,  $\text{Cl}^-$  increases to a maximum of 577 mM at 495 mbsf, decreases across the Unit I/II boundary to a downhole minimum of 566 mM at 530 mbsf, and then increases again to 582 mM near the bottom of the hole.

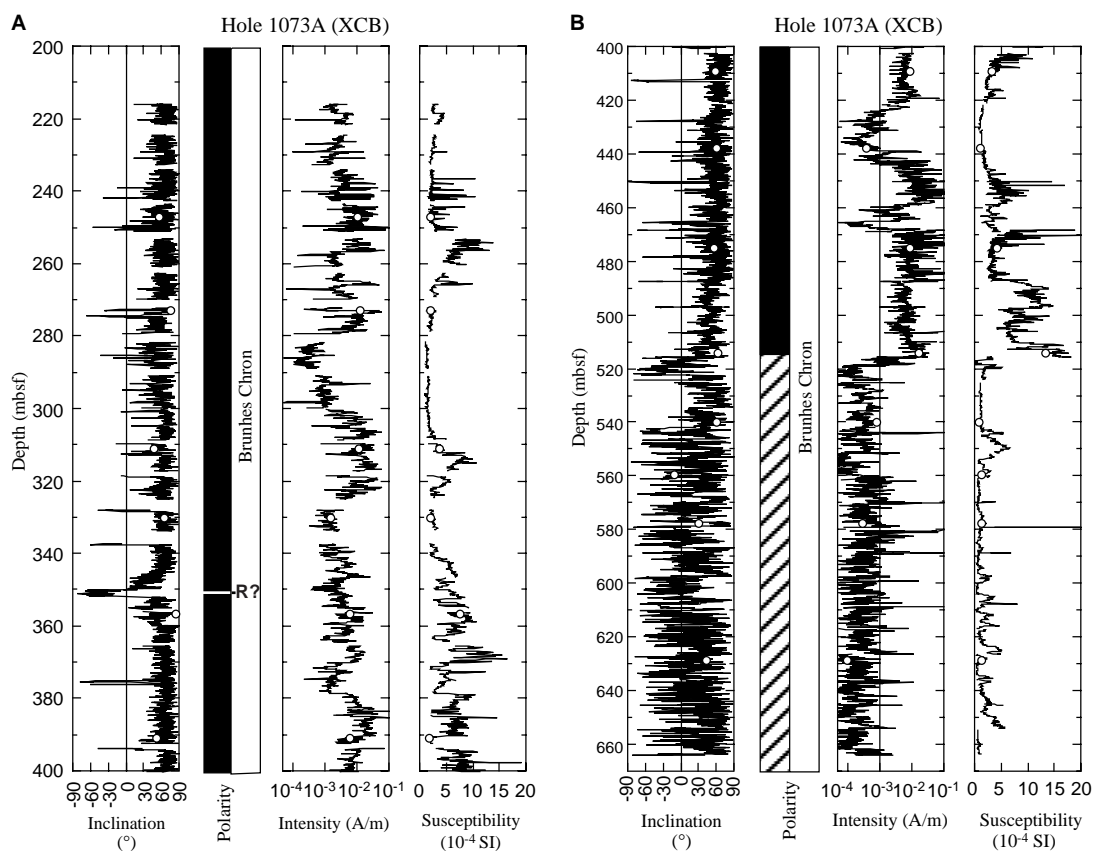


Figure 17. Inclination, magnetic polarity zones, magnetization intensity, and volume magnetic susceptibility of XCB core samples for Hole 1073A from (A) 200 to 400 mbsf and (B) 400 to 670 mbsf. Inclination and intensity of magnetization are after 20-mT AF demagnetization. Solid lines and open circles indicate pass-through data and discrete data, respectively. In the polarity column, black = normal polarity, white = reversed polarity, and cross-hatched = uninterpretable.

Potassium ( $K^+$ ) concentrations gradually decrease downhole to a pronounced minimum interval between 345 and 495 mbsf (mean = 2.80 mM; Fig. 20). Below this minimum zone, near the Unit I/II boundary,  $K^+$  concentrations increase abruptly to an interval of maximum values from 549 to 652 mbsf (mean = 11.78 mM).

### Preliminary Interpretations

Interstitial waters of marine sedimentary sequences are often characterized by broad subsurface maxima in alkalinity,  $NH_4^+$  and  $HPO_4^{2-}$ , which result from bacterial decomposition of organic matter and subsequent diffusion of ions. However, previous work on the New Jersey slope (Leg 150; Mountain, Miller, Blum, et al., 1994) noted an unusual (if not unique) observation in scientific ocean drilling: at least four peaks in downhole profiles of  $HPO_4^{2-}$  and alkalinity. Multiple maxima of these ions are rare, except in cases where advection of fluids is prominent (e.g., Westbrook, Carson, Musgrave, et al., 1994); however, fluid advection cannot be invoked at Site 1073. Limited sampling of interstitial water at Site 903 to the southwest precluded a detailed investigation of the observation (see "Introduction" chapter, this volume). At Site 1073, four well-defined  $HPO_4^{2-}$  and five alkalinity and  $H_4SiO_4$  maxima are observed in interstitial water profiles in the upper 500 mbsf (Pleistocene-Holocene[?]). The distinct maxima of alkalinity and  $HPO_4^{2-}$  suggest production from local organic-matter degradation and that rates of bacterial decomposition of organic matter on the New Jersey slope are highly heterogeneous in time and/or space. High concentrations of  $H_4SiO_4$  correspond to increased abundance of siliceous microfossils observed in smear-slide analyses (see "Lithostratigraphy" section, this chapter), presumably highly soluble amorphous silica. The maxima likely are preserved because the extreme sedimentation rates (up to ~80–90 cm/k.y.; see

"Biostratigraphy" section, this chapter) on the New Jersey slope prevent diffusive homogenization of interstitial water chemistry.

The decrease of  $Ca^{2+}$ ,  $Mg^{2+}$ , and  $Sr^{2+}$  in the upper 100 mbsf (Fig. 21) is consistent with the precipitation of diagenetic carbonates (Baker and Burns, 1985; Compton, 1988). An unusual correspondence between  $Mg^{2+}$  and  $Sr^{2+}$  in the upper 300 mbsf is also observed at Site 903 (Mountain, Miller, Blum, et al., 1994). The minima in this interval may indicate local zones of more intense diagenetic carbonate precipitation. The  $Sr^{2+}$  profile near the bottom of the hole is typical of the release of dissolved  $Sr^{2+}$  during the recrystallization of biogenic carbonate (e.g., Baker et al., 1982). Calcium increases to almost double seawater values at the bottom of the hole; its trend is similar to the general increase of  $Sr^{2+}$ . Dissolution of biogenic  $CaCO_3$ , without substantial reprecipitation of diagenetic carbonates, should lead to an increase in  $Ca^{2+}$  and  $Sr^{2+}$ . However, we would not expect an increase in the  $Sr^{2+}/Ca^{2+}$  value if dissolution of  $CaCO_3$  was the primary cause of the increase in  $Ca^{2+}$  (Fig. 21). The  $Sr^{2+}/Ca^{2+}$  value increases abruptly in the lower part of the hole, which is consistent with dissolution and reprecipitation (recrystallization) of carbonate minerals, not solely carbonate dissolution (Fig. 20). An alternative explanation for the increase in  $Ca^{2+}$  with depth is diffusional communication with a deep-seated,  $Cl^-$ -rich brine, as previously observed on Leg 150 (Mountain, Miller, Blum, et al., 1994). The corresponding reappearance of  $SO_4^{2-}$  in this same interval is consistent with this interpretation; however,  $Cl^-$  does not increase by the amount that would be expected if there was substantial diffusional exchange with a  $Cl^-$ -rich brine.

Potassium ( $K^+$ ) decreases to an interval of minimum values (mean = 2.80 mM; a 73% decrease) between 345 and 495 mbsf, indicating that substantial uptake of  $K^+$  is occurring. A similar, although not nearly as significant, decrease (33%) was observed at Site 903

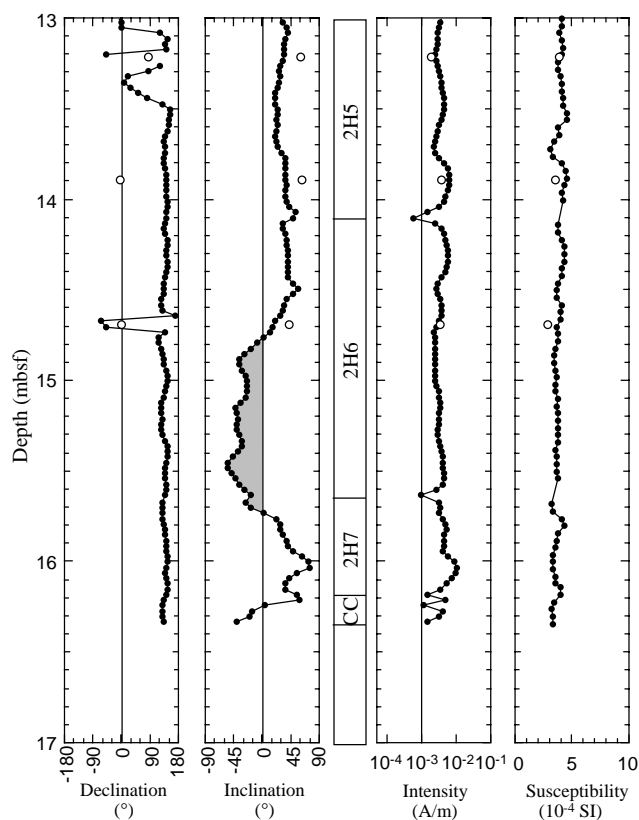


Figure 18. Declination, inclination, magnetization intensity, and magnetic susceptibility for a short polarity reversal event (shaded) from Core 174A-1073A-2H.

(Mountain, Miller, Blum, et al., 1994). Precipitation of glauconite seems a likely  $K^+$  sink; however, the interval is devoid of glauconite (see “Lithostratigraphy” section, this chapter).  $K^+$  uptake in deep-sea sediments normally is associated with the formation of authigenic silicates, resulting from the alteration of volcanic material and/or basalt (e.g., Kastner and Gieskes, 1976). However, no volcanic material or basalt has been observed on the New Jersey slope (see other sections, this chapter; Mountain, Miller, Blum, et al., 1994). At present, the origin of the interval of  $K^+$  depletion is unclear. Below ~505 mbsf (approximately at the Unit I/II boundary),  $K^+$  increases abruptly to values slightly more enriched than seawater. The high  $K^+$  values are associated with an interval of glauconite-rich sediments, which suggests that dissolution of glauconite (perhaps recrystallization) is the source of  $K^+$ .

## ORGANIC GEOCHEMISTRY

Shipboard organic geochemical studies of cores from Hole 1073A included monitoring of hydrocarbon gases, carbonate carbon and total organic carbon, total sulfur, and total nitrogen contents. Procedures are summarized in the “Explanatory Notes” chapter (this volume).

### Volatile Gases

All cores recovered from Hole 1073A were monitored for gaseous hydrocarbons by the headspace gas technique, and where possible by analysis of gas voids by the syringe technique. The rapidly deposited sediments at Site 1073 on the continental slope are similar in many respects to sediments cored on Leg 150 (Mountain, Miller, Blum, et

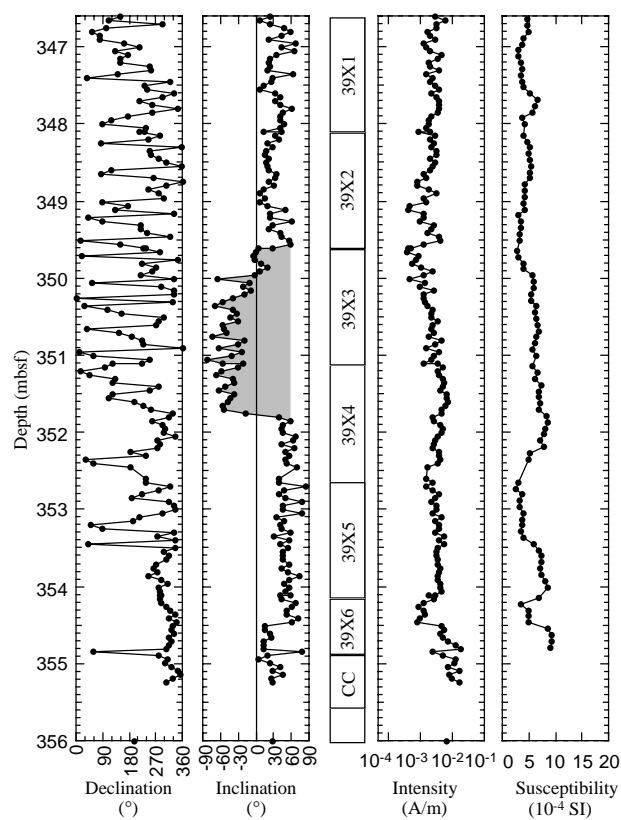


Figure 19. Declination, inclination, magnetization intensity, and magnetic susceptibility for a short polarity reversal event (shaded) from Core 174A-1073A-39X.

al., 1994). Sediments contained abundant methane below 10 mbsf, and gas voids appeared below 34 mbsf. Cores 174A-1073A-5H through 23H (34–206 mbsf) contained sufficient gas to require that cores be allowed to outgas on the catwalk before being cut into sections. Below 215 mbsf, gas content of the cores diminished, as indicated by less vigorous core expansion and outgassing. This decrease in apparent gas content was probably associated with the switch from APC to XCB coring, because the APC cores provide a tighter seal and retain more of the gas when cores are retrieved from the subsurface (see Paull, Matsumoto, Wallace, et al., 1997, p. 114–116). The gas content as measured by core expansion continued to decrease with increasing depth, resulting in scarce gas pockets in cores over the depth interval 312–420 mbsf and none below ~450 mbsf. Gas was essentially absent below 600 mbsf.

### Headspace Gas

Headspace gas results are reported in Table 14. Data reported are in parts per million by volume (ppmv) of methane ( $C_1$ ), ethane ( $C_2$ ), ethene ( $C_2^=$ ), and propane ( $C_3$ ) in the air headspace of a 20-cm<sup>3</sup> vial containing a nominal 5 cm<sup>3</sup> plug of freshly cored sediment. Results are plotted as ppmv methane vs. depth in Figure 22, and as the  $C_1/C_2$  value of headspace gas vs. depth in Figure 23. Methane content increases in cores deeper than 10 mbsf, and the highest observed headspace gas content is present in Section 174A-1073A-3H-6 at a depth of 20.6 mbsf. The dissolved sulfate gradient projects to 0 mM concentration at a depth of ~6 mbsf, which invariably results in the presence of abundant methane in deeper cores. The headspace methane content of the cores (Fig. 22) shows an overall slight decrease with increasing depth over the 20–600 mbsf depth interval. Superimposed on this overall decreasing trend are apparent subtrends of fluctuating

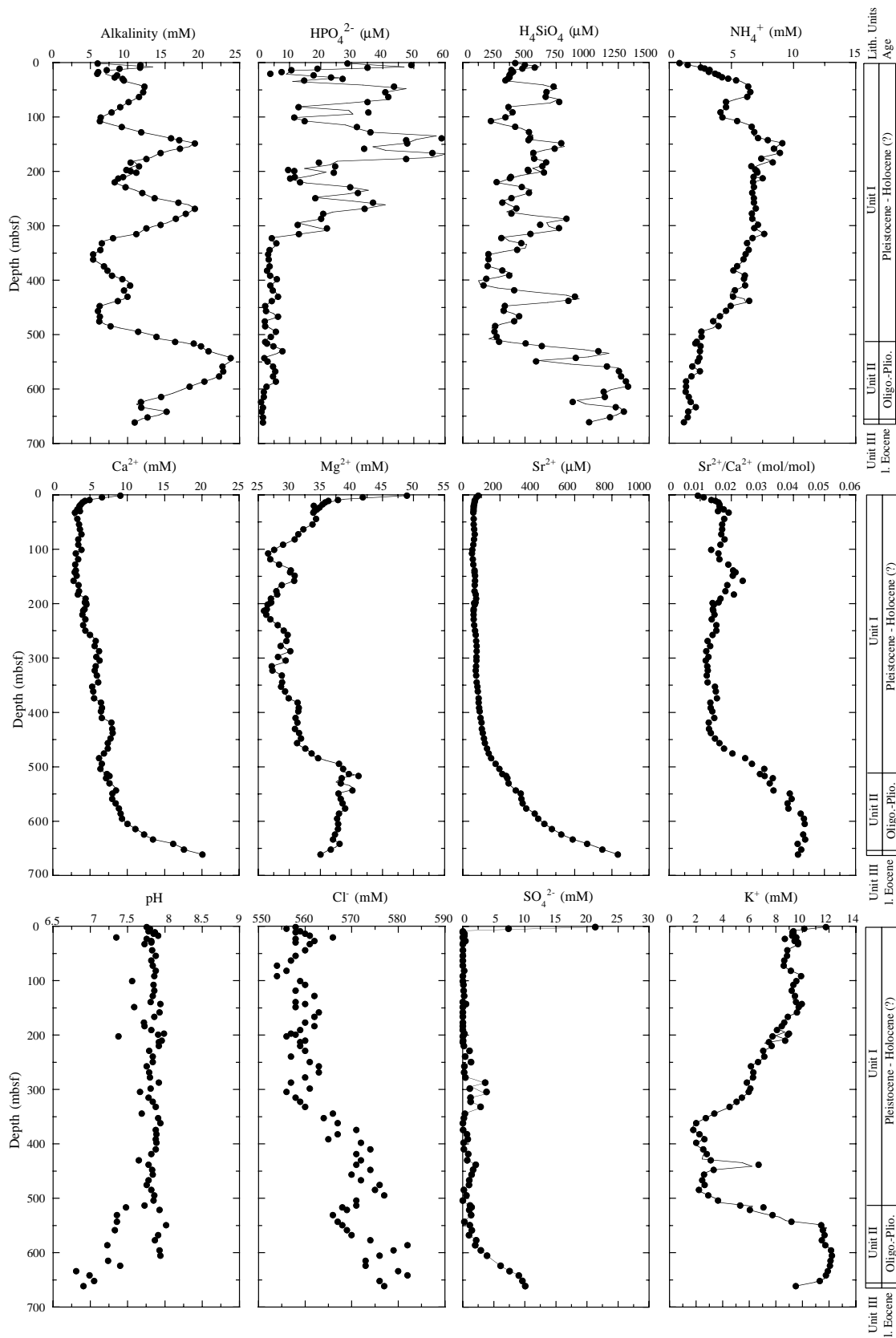


Figure 20. Concentration-depth profiles of interstitial water at Site 1073 with approximate lithostratigraphic boundaries and corresponding ages (see “Lithostratigraphy” and “Biostratigraphy” sections, this chapter).

Table 13. Interstitial water data, Site 1073.

Core, section, interval (cm)	Depth (mbsf)	Alkalinity		Cl <sup>-</sup> (mM)	SO <sub>4</sub> <sup>2-</sup> (mM)	Mg <sup>2+</sup> (mM)	Ca <sup>2+</sup> (mM)	K <sup>+</sup> (mM)	H <sub>4</sub> SiO <sub>4</sub> (μM)	NH <sub>4</sub> <sup>+</sup> (mM)	HPO <sub>4</sub> <sup>2-</sup> (μM)	Sr <sup>2+</sup> (μM)	Sr <sup>2+</sup> /Ca <sup>2+</sup> (mol/mol)	
		pH	Salinity											
174A-1073A-														
1H-1, 140-150	1.4	7.76	5.96	34.5	558	21.31	48.98	9.09	11.78	421	0.84	28.7	84	0.00927
1H-3, 140-150	4.4	7.8	11.74	33.0	556	7.34	41.88	6.63	10.13	501	1.49	49.2	74	0.01112
2H-2, 140-150	9.5	7.78	11.67	32.0	559	0.04	37.85	4.92	9.32	580	2.55	35.1	67	0.01363
2H-3, 140-150	11.0	7.87	8.91	32.0	558	0.00	36.35	4.35	9.25	480	2.87	19.0	65	0.01492
2H-5, 140-150	14.0	7.85	7.20	32.0	560	0.26	35.78	4.03	9.33	390	3.25	10.6	64	0.01590
3H-1, 130-140	17.4	7.91	6.08	32.0	561	0.25	35.35	3.80	9.23	404	3.19	7.5	62	0.01617
3H-3, 130-140	20.2	7.35	5.96	32.0	566	0.00	33.98	3.61	9.54	385	3.70	3.8	59	0.01627
3H-5, 130-140	23.0	7.76	8.59	32.0	558	0.15	34.89	3.58	8.69	377	3.95	17.8	59	0.01639
4H-1, 130-140	26.9	7.82	8.29	32.0	562	0.42	34.45	3.31	9.42	377	4.26	23.4	58	0.01762
4H-3, 130-140	29.8	7.82	9.36	32.0	558	0.12	34.06	3.66	9.66	364	4.75	27.1	58	0.01575
4H-5, 130-140	32.7	7.73	9.52	32.0	561	0.00	33.87	2.98	9.67	345	5.39	14.7	57	0.01914
5H-6, 140-150	44.1	7.83	12.28	32.0	560	0.02	34.34	3.32	8.86	731	6.35	43.7	59	0.01776
6H-7, 130-150	54.1	7.88	12.12	32.0	558	0.00	33.76	3.53	8.84	674	6.54	40.9	60	0.01714
7H-6, 140-150	63.0	7.82	11.55	32.0	557	0.00	32.27	3.68	8.64	667	6.29	41.8	63	0.01710
8H-6, 140-150	72.5	7.84	10.17	32.0	554	0.00	31.48	3.86	8.60	776	4.58	35.1	65	0.01686
9H-6, 140-150	82.0	7.88	9.00	32.0	556	0.23	30.87	3.42	9.12	368	4.56	12.9	61	0.01786
10H-6, 140-150	91.5	7.86	7.86	32.0	554	0.00	29.00	3.45	9.91	400	4.12	35.4	57	0.01650
11H-6, 140-150	101.0	7.56	6.40	32.0	559	0.04	27.57	3.86	9.53	343	4.27	11.5	52	0.01359
12H-4, 140-150	107.5	7.85	6.30	32.0	560	0.10	26.58	3.10	9.32	225	5.46	14.9	49	0.01592
13H-5, 140-150	118.5	7.86	9.22	32.0	558	0.16	26.93	3.41	9.20	421	6.64	31.7	55	0.01615
14H-5, 140-150	128.0	7.84	11.83	32.0	562	0.22	28.40	3.01	9.43	532	6.85	36.0	57	0.01905
15H-6, 140-150	139.0	7.81	15.81	32.0	558	0.00	30.24	3.11	9.52	542	7.16	58.9	64	0.02064
16H-2, 140-150	142.5	7.94	16.92	32.0	560	0.54	30.15	2.97	9.96	529	7.94	47.6	64	0.02143
16H-6, 140-150	148.5	7.59	19.06	32.0	558	0.00	30.87	3.22	9.73	791	9.11	47.9	66	0.02050
17H-6, 140-150	158.0	7.93	17.04	32.0	563	0.00	30.81	2.80	9.60	740	8.43	34.0	67	0.02379
18H-5, 140-150	166.0	7.86	14.44	32.0	562	0.00	28.81	3.46	8.91	567	8.91	56.0	65	0.01876
19H-6, 140-150	176.9	7.72	12.53	32.0	560	0.04	27.92	3.54	8.63	575	7.41	47.6	64	0.01812
20H-4, 140-150	183.4	7.73	10.43	32.0	562	0.00	28.07	3.38	8.46	672	8.33	19.5	70	0.02084
21H-4, 140-150	190.9	7.82	11.55	32.0	559	0.00	27.08	4.42	8.09	641	6.61	24.7	73	0.01656
22H-2, 140-150	197.5	7.99	9.81	32.0	557	0.28	27.11	4.31	8.99	523	6.92	9.6	69	0.01596
22H-3, 140-150	199.0	7.91	10.40	32.0	558	0.20	26.93	4.46	8.90	529	7.05	11.5	63	0.01404
22H-5, 140-150	202.1	7.38	11.22	32.0	556	0.01	26.51	4.50	7.76	653	7.09	24.2	65	0.01441
23H-5, 140-150	210.2	7.96	9.42	32.0	560	0.06	26.38	4.28	8.71	387	6.79	11.7	60	0.01409
24H-1, 134-146	213.1	7.92	8.78	32.0	559	0.00	25.93	4.10	7.49	379	7.52	10.2	58	0.01426
25X-3, 135-150	220.1	7.92	8.29	32.0	559	0.19	26.34	3.99	7.69	273	6.76	13.4	58	0.01461
26X-3, 140-150	228.8	7.79	9.72	32.0	560	1.08	26.97	4.37	7.05	474	6.83	29.5	60	0.01373
27X-4, 135-150	239.8	7.84	11.98	32.0	557	0.40	28.15	4.10	7.13	533	6.68	32.0	62	0.01519
28X-4, 135-150	249.4	7.84	13.61	32.0	561	1.31	29.13	4.37	6.66	390	6.80	18.3	66	0.01515
29X-3, 135-150	257.4	7.76	16.85	32.5	563	0.27	29.76	4.99	6.14	319	6.83	36.9	70	0.01399
30X-3, 135-150	268.4	7.79	19.03	32.0	563	0.23	29.56	5.78	6.30	432	6.97	34.2	72	0.01240
31X-4, 135-150	277.9	7.8	17.82	32.5	560	0.41	28.63	5.63	6.29	390	6.66	20.9	75	0.01323
32X-4, 135-150	287.2	7.92	16.47	32.5	557	3.61	30.17	6.22	5.84	834	6.69	20.2	75	0.01200
33X-5, 135-150	298.0	7.81	14.46	32.5	561	1.13	28.19	5.88	6.08	622	7.14	12.6	74	0.01265
34X-3, 135-150	304.5	7.67	12.54	32.5	556	3.84	29.43	6.29	5.96	774	6.84	22.0	74	0.01182
35X-4, 135-150	315.4	7.78	11.18	32.5	558	1.23	27.20	5.76	5.45	544	7.64	13.0	71	0.01230
36X-3, 135-150	322.8	7.84	8.05	32.0	559	1.29	27.31	5.64	5.05	311	6.72	4.3	70	0.01243
37X-3, 135-150	332.2	7.88	6.57	32.0	560	2.90	28.80	5.92	4.53	471	6.26	5.8	72	0.01218
38X-5, 135-150	344.6	7.69	6.38	32.5	566	0.35	28.87	6.10	3.38	437	6.39	3.6	76	0.01241
39X-4, 135-150	352.5	7.91	5.38	32.0	564	0.19	28.69	5.30	2.75	206	6.14	3.1	79	0.01485
40X-4, 135-150	361.9	7.94	5.39	32.0	567	0.03	29.34	5.44	2.01	208	5.97	3.3	82	0.01504
41X-6, 135-150	374.3	7.88	6.86	32.5	571	0.09	29.92	5.56	1.80	201	5.47	3.6	86	0.01543
42X-5, 135-150	382.2	7.89	7.32	32.0	567	0.68	31.36	6.49	2.26	319	5.17	2.7	86	0.01332
43X-5, 135-150	391.7	7.88	7.92	32.5	565	0.82	31.53	6.63	2.64	373	6.09	3.7	89	0.01342
44X-3, 135-150	398.0	7.89	9.31	32.5	572	0.15	31.45	6.49	2.01	189	6.00	5.9	91	0.01396
45X-5, 135-150	409.9	7.88	10.36	33.0	574	0.20	31.02	6.58	2.54	167	6.11	3.8	96	0.01455
46X-5, 135-150	418.7	7.82	9.55	33.0	571	0.90	31.31	7.88	2.81	414	5.28	4.6	101	0.01277
47X-6, 135-150	430.4	7.65	9.97	32.5	572	0.72	30.93	7.98	3.11	902	5.14	6.3	103	0.01287
48X-5, 135-150	438.3	7.78	8.71	32.5	571	2.11	31.59	8.03	6.70	850	6.44	4.3	108	0.01343
49X-5, 135-150	447.8	7.83	6.26	32.5	574	1.66	31.90	7.77	3.33	339	4.93	2.2	115	0.01482
50X-5, 135-150	456.5	7.84	6.05	32.5	570	1.45	31.29	7.38	2.60	328	4.56	2.4	119	0.01619
51X-5, 135-150	466.7	7.78	6.30	32.5	572	1.06	32.61	7.40	2.47	454	4.08	6.3	131	0.01767
52X-5, 135-150	475.6	7.76	6.21	32.5	576	1.00	33.60	6.87	2.65	414	3.55	2.0	140	0.02041
53X-5, 135-150	484.3	7.82	7.72	33.0	575	0.18	34.64	6.22	2.22	260	3.96	2.2	153	0.02458
54X-5, 135-150	494.6	7.86	11.42	33.0	577	0.57	37.99	6.59	2.92	255	2.59	5.6	176	0.02668
55X-5, 135-150	504.0	7.85	13.90	33.0	571	0.00	38.67	6.41	3.65	273	2.60	4.0	197	0.03066
56X-5, 135-150	513.3	7.73	16.39	33.5	571	1.20	39.62	7.26	5.32	292	2.22	2.2	213	0.02930
57X-1, 135-150	516.7	7.48	18.89	33.5	568	1.43	41.18	7.61	7.07	506	2.10	2.7	234	0.03078
57X-4, 135-150	521.2	7.93	19.87	33.5	569	1.06	38.48	7.18	6.04	636	2.53	4.8	240	0.03343
58X-4, 135-150	530.7	7.36	20.86	33.5	566	1.36	38.31	7.62	7.76	1092	2.46	7.7	247	0.03239
59X-6, 135-150	543.2	7.36	23.86	34.0	567	0.29	40.21	8.49	9.17	910	2.43	1.9	285	0.03360
60X-5, 135-150	549.2	8.02	NM	34.0	568	1.13	37.93	8.01	11.41	589	2.29	2.9	311	0.03885
61X-6, 135-150	558.8	7.33	22.74	34.0	569	1.47	38.30	7.99	11.54	1158	1.87	4.7	316	0.03949
62X-5, 135-150	567.5	7.91	22.83	34.0	570	1.02	38.60	8.43	11.67	1257	2.48	5.4	322	0.03819
63X-5, 135-150	576.8	7.87	22.29	34.0	574	2.18	39.03	8.88	11.46	1274	1.78	4.7	342	0.03846
64X-5, 135-150	586.2	7.23	20.30	34.0	582	2.04	38.02	9.12	11.72	1312	1.36	5.6	387	0.04241
65X-5, 135-150	595.6	7.93	18.34	34.0	579	2.92	37.74	9.31	12.15	1330	1.36	2.6	405	0.04345
66X-5, 135-150	605.2	7.94	NM	34.0	576	3.92	37.88	10.04	12.22	1133	1.32	1.7	439	0.04372
67X-5, 135-150	614.6	7.24	14.50	34.0	573	NM	37.87	11.10	12.11	1143	1.58	1.7	479	NM
68X-5, 135-150	624.2	7.40	11.81	34.0	573	6.12	37.37	12.25	12.06	885	1.72	0.9		

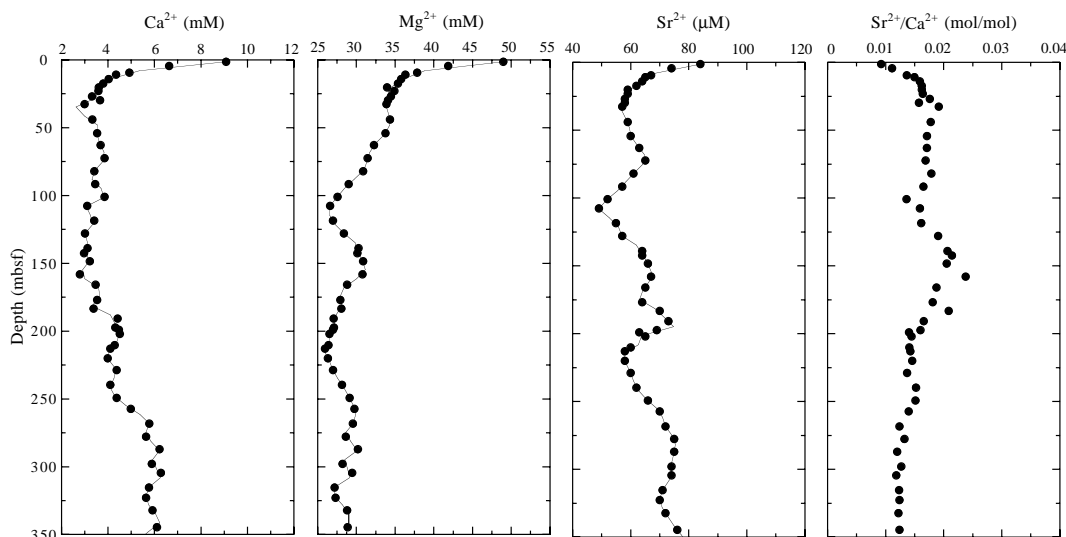


Figure 21. Detail of the concentration-depth profiles of  $\text{Ca}^{2+}$ ,  $\text{Mg}^{2+}$ ,  $\text{Sr}^{2+}$ , and  $\text{Sr}^{2+}/\text{Ca}^{2+}$  (0–350 mbsf).

methane content over periods of ~100 m. Gas measured by the headspace technique is only that retained by the sediment after outgassing has taken place during core retrieval to the surface. The composition of the gas, as expressed by the  $C_1/C_2$  value (Fig. 23), shows the expected gradual increase in the relative ethane content with increasing depth and temperature (given the prevailing sedimentation rate and geothermal gradient). Below 600 mbsf, where the methane contents drop from 5000 to 10 ppmv, the  $C_1/C_2$  value (Fig. 23) also decreases abruptly; this is caused by the decrease in methane rather than an increase in ethane.

### Syringe Gas

Syringe gas results are reported in Table 15. Data reported are ppmv of methane ( $C_1$ ), ethane ( $C_2$ ), and ethene ( $C_2^=$ ) in the syringe sample taken from the gas voids that form in the core liners when cores are brought up to the rig floor. The gases are believed to be essentially pure methane in the subsurface. Hydrocarbon abundances significantly <100% likely are contaminated with air. Nonhydrocarbon gases were monitored by the thermal conductivity detector but are not reported, showing only variable dilution of the methane by air. Carbon dioxide contents are less than a few hundred ppmv, or <0.1%. The  $C_1/C_2$  value of the vacutainer gases (Fig. 24) generally parallels that of the headspace gas data (Fig. 23).

### Carbon and Elemental Analyses

Twenty-nine (about one per core) sediment samples were analyzed for carbonate carbon, total carbon (TC), total organic carbon (TOC, by difference), total nitrogen (TN), and total sulfur (TS) from 0 to 276 mbsf at Site 1073 and are reported in Table 16. Organic carbon and carbonate carbon (as  $\text{CaCO}_3$ ) contents are plotted against depth of burial in Figure 25. Carbonate content fluctuates between 1.9 and 25.8 wt%, with peaks at approximate depths of 42, 70, 147, 183, 249, and 276 mbsf (Table 16). TOC fluctuates between 0.21 and 0.67 wt%, with peaks at approximate depths of 70, 147, 190, and 239 mbsf. These peaks are sufficiently coincident to suggest that productivity variations are recorded in the sediments. TN contents are generally between 0.05 and 0.07 wt%, but with values as low as 0.03 and as high as 0.1 wt%. C/N values fluctuate between 2 and 12, but generally average ~7, and appear to decrease from 8 to 6 over the interval 30–200 mbsf, rising to ~8 at 270 mbsf. TS content is generally low (0–0.3 wt%), with a single sample (157.8 mbsf) at 1.15 wt%. The

peaks in the fluctuations in sulfur content broadly correlate with the peaks in TOC.

## PHYSICAL PROPERTIES

### Introduction

Physical properties data collected at Site 1073 are based on measurements and procedures discussed in the “Explanatory Notes” chapter (this volume). In this section, results of physical properties measurements are presented, trends in the data are discussed, and preliminary correlations are made between physical properties and other shipboard measurements.

### Density and Porosity

At Site 1073, we used the gamma-ray attenuation porosity evaluator (GRAPE) component of the MST to estimate whole-core density at a sample spacing of 4 cm (Fig. 26; Table 17 on CD-ROM). Outliers were removed from the recorded data by visual inspection. Because the most common cause of such outliers is gaps in cores, densities <~1 g/cm<sup>3</sup> were removed. Filtering resulted in removal of ~3% of observed data. Index properties density measurements were generally acquired at a resolution of two to three per core. Index properties samples were used to calculate wet, dry, and grain density; porosity; water content; and void ratio (Fig. 26; Table 18 on CD-ROM).

GRAPE density estimates (Fig. 26) are commonly more variable and lower in value than index properties bulk density measurements in gassy intervals (e.g., 106–135 mbsf and other intervals in Fig. 26). Despite this, the overall trends shown in GRAPE data are validated by index properties measurements, and agreement between index properties and GRAPE density measurements is generally good below ~190 mbsf. This indicates that, with careful filtering, the high-resolution GRAPE data could be a proxy for discrete measurements on sediment samples at Site 1073.

The overall trend of GRAPE and index properties density measurements to ~250 mbsf is that of a slight increase with depth, which is almost certainly linked to compaction processes. This depth approximately correlates with the boundary between lithostratigraphic Subunits ID and IE (see “Lithostratigraphy” section, this chapter). A density peak near this boundary correlates with an interval of slumping and high grain density (see “Lithostratigraphy” section, this chapter). Below 260 mbsf, densities decrease to ~280 mbsf and then in-

**Table 14. Headspace gas composition from sediments at Site 1073.**

Core, section, interval (cm)	Depth (mbsf)	C <sub>1</sub> (ppmv)	C <sub>2</sub> (ppmv)	C <sub>2</sub> <sup>=</sup> (ppmv)	C <sub>3</sub> (ppmv)	C <sub>1</sub> /C <sub>2</sub>
174A-1073A-						
1H-2, 0-5	1.5	3	0	0.3	0	
1H-4, 0-5	4.5	5	0	0.4	0	
2H-1, 0-5	6.6	25,935	0.2	0.2	0	129,675
2H-3, 0-5	9.6	6,994	0	0	0	
2H-5, 0-5	12.6	24,848	0.2	0.1	0	124,239
3H-4, 0-5	20.3	29,445	0.2	0.3	0	147,224
3H-5, 0-5	21.7	16,000	0	0.2	0	
3H-6, 0-5	23.1	12,062	0.1	0.1	0	120,624
4H-4, 0-5	29.9	23,791	0.2	0.3	0	118,954
4H-6, 0-5	32.8	18,170	0.2	0.1	0	90,849
5H-6, 0-5	42.7	12,521	0	0.2	0	
6H-8, 0-5	54.3	10,557	0.2	0.1	0	52,786
7H-7, 0-5	63.1	3,841	0.1	0.2	0	38,408
8H-7, 0-5	72.6	25,890	0.7	0.2	0	36,986
9H-7, 0-5	82.1	6,120	0.2	0.1	0	30,602
10H-7, 0-5	91.6	3,614	0	0	0	
11H-7, 0-5	101.1	6,354	0.2	0	0.7	31,772
12H-5, 0-5	107.6	7,643	0.2	0	0	38,215
13H-6, 0-5	118.6	4,081	0.2	0.1	0	20,407
14H-6, 0-5	128.1	4,918	0.3	0	0.3	16,394
17H-7, 0-5	158.1	11,393	1	0.2	0	11,393
18H-6, 0-5	166.1	6,076	0.4	0	0.1	15,190
19H-7, 0-5	177.0	12,391	0.8	0.1	0.1	15,488
20H-5, 0-5	183.5	10,933	0.8	0	0	13,667
21H-5, 0-5	191.0	6,859	0.6	0.2	0	11,431
22H-6, 0-5	202.2	12,354	0.9	0.2	0	13,727
23H-6, 0-5	210.3	12,442	1.1	0.3	0	11,310
24H-2, 0-5	213.3	9,466	0.9	0.2	0.2	10,517
25X-4, 0-5	220.2	2,028	0.2	0	0	10,139
26X-4, 0-5	228.9	2,811	0.3	0	0	9,370
28X-5, 0-5	249.5	3,775	0.4	0	0	9,438
29X-4, 0-5	257.5	6,138	0.5	0.1	0	12,277
31X-5, 0-5	278.0	5,722	0.6	0.1	0	9,537
32X-4, 0-5	285.8	14,952	1.3	0.2	0	11,502
33X-6, 0-5	298.2	6,651	0.5	0.1	0	13,302
35X-5, 0-5	315.5	6,178	0.7	0.3	0	8,826
36X-4, 0-5	322.9	4,343	0.4	0	0	10,857
37X-4, 0-5	332.3	4,049	0.6	0.1	0.3	6,749
38X-6, 0-5	344.7	476	0	0	0	
40X-5, 0-5	362.0	5,662	0.9	0.1	0	6,292
41X-7, 0-5	374.4	4,928	1.3	0.2	0.4	3,791
42X-6, 0-5	382.4	4,342	1.2	0.2	0	3,619
43X-6, 0-5	391.8	4,852	1.2	0.1	0.1	4,043
44X-4, 0-5	398.1	3,363	0.2	0	0	16,815
45X-6, 0-5	410.0	4,161	0.4	0.2	0	10,403
46X-6, 0-5	418.8	4,069	0.4	0.1	0	10,172
47X-7, 0-5	430.5	5,431	0.8	0.6	0	6,788
48X-6, 0-5	438.4	6,044	0.4	0.2	0	15,110
49X-6, 0-5	447.9	7,072	0.9	0.2	0	7,858
50X-6, 0-5	456.6	6,293	0.4	0.1	0.3	15,731
51X-6, 0-5	466.8	15,939	1	0.2	0.4	15,939
52X-6, 0-5	475.7	10,365	0.6	0.5	0	17,275
53X-6, 0-5	484.4	16,472	0.8	0.1	0	20,590
54X-6, 0-5	494.7	7,577	0.3	0.1	0	25,256
55X-6, 0-5	504.1	12,368	0.4	0	0	30,919
56X-6, 0-5	513.5	6,546	0.3	0.1	0	21,819
57X-5, 0-5	521.3	2,916	0.3	0.6	0	9,720
58X-5, 0-5	530.8	15,200	1.3	1	0.2	11,692
59X-7, 0-5	543.3	3,147	0.6	0.6	0	5,245
60X-6, 0-5	549.3	758	0.2	0.3	0	3,788
61X-7, 0-5	558.9	3,569	0.6	0.5	0	5,948
62X-6, 0-5	567.6	4,723	1.3	0.7	0.4	3,633
63X-6, 0-5	576.9	1,186	0.4	0.4	0	2,966
64X-6, 0-5	586.3	926	0.8	0.9	0.5	1,157
65X-6, 0-5	595.7	633	1.4	2.4	1	452
66X-6, 0-5	605.3	13	0.3	0.4	0.2	45
67X-6, 0-5	614.7	5	0.3	0.3	0.2	17
68X-6, 0-5	624.3	4	0.3	0.4	0.1	14
69X-6, 0-5	633.8	3	0.2	0.2	0	16
70X-5, 0-5	641.8	5	0.5	0.7	0	10
71X-6, 0-5	652.2	4	0.2	0.7	0.5	18
72X-6, 0-5	661.6	8	0.4	0.1	0	19

crease slightly to ~519 mbsf; the latter depth marks the boundary between Subunits IE and IIA and may also represent the Pleistocene/Pliocene biostratigraphic boundary. Below ~519 mbsf, cyclical variation of density measurements may reflect the slow deposition that is inferred to have taken place from the late Eocene to the late Pliocene at Site 1073.

Porosity measurements (Fig. 26) show several overall downhole-decreasing trends, from 0 to 140 mbsf, from ~150 to 250 mbsf, and from ~280 to 519 mbsf. These trends may reflect depositional cycles

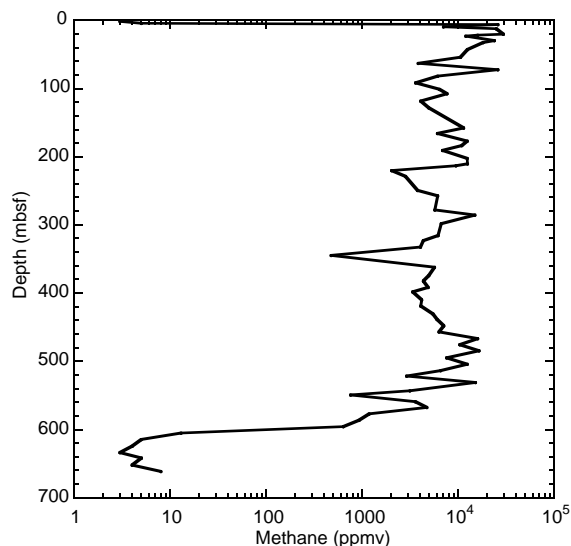


Figure 22. Headspace methane content of sediment vs. depth, Hole 1073A.

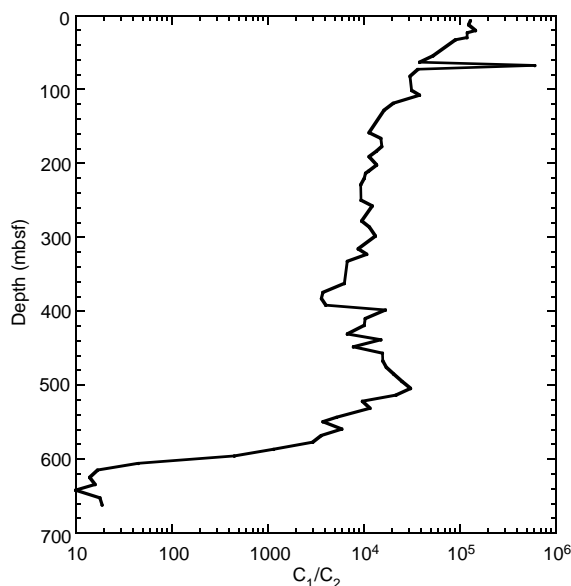


Figure 23. C<sub>1</sub>/C<sub>2</sub> value of headspace gas vs. depth, Hole 1073A.

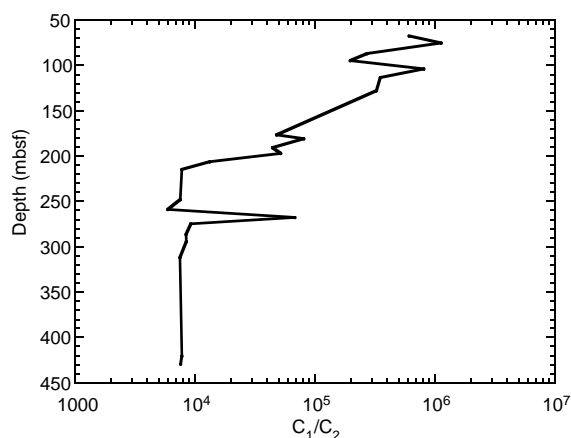
associated with Pleistocene glacial advances and retreats. Smaller scale trends mirror the index properties bulk density fluctuations discussed above.

### Magnetic Susceptibility

Magnetic susceptibility was measured on whole cores at 4-cm intervals on the MST (Fig. 26; Table 19 on CD-ROM). No correction was made to the data to account for incompletely filled cores, but a 5-pt moving-average filter was applied to the raw data to remove points that fell >50% outside of the average; this filtering resulted in removal of ~2.5% of the data. Therefore, susceptibility data are likely to be useful for interpreting overall trends, but not for determining precise values. Susceptibility trends are commonly used to infer changes in depositional environment and/or diagenetic changes. Af-

**Table 15. Syringe gas composition from sediments at Site 1073.**

Core, section, interval (cm)	Depth (mbsf)	C <sub>1</sub> (ppmv)	C <sub>2</sub> (ppmv)	C <sub>2</sub> = (ppmv)	C <sub>1</sub> /C <sub>2</sub>
174A-1073A-					
4H-6, 116-117	34.0	861,310	0	0	
5H-3, 117-118	39.3	882,146	0	0	
6H-4, 107-108	49.4	768,919	0	2.2	
7H-4, 20-21	58.8	716,764	0	0.55	
8H-3, 74-75	67.3	396,481	0.7	0	609,971
9H-2, 65-66	75.3	790,861	0.7	0	1,129,801
10H-3, 120-121	86.8	750,273	2.8	0	272,826
11H-2, 98-99	94.6	825,370	4.2	4.4	196,517
12H-2, 60-61	103.7	687,594	0.9	0	808,934
13H-2, 94-95	113.5	649,378	1.9	0	351,015
14H-5, 125-126	127.8	703,177	2.2	0	327,059
19H-6, 88-89	176.4	851,881	17.7	0	48,129
20H-3, 35-36	180.8	715,525	8.9	0	80,850
21H-4, 111-112	190.6	666,560	15	0	44,437
22H-2, 86-87	197.0	661,132	12.7	0	52,058
23H-3, 44-45	206.2	577,147	43.3	5	13,329
24H-2, 124-125	214.5	621,667	79.8	0	7,790
28X-3, 130-131	247.8	693,279	91.7	0	7,564
29X-4, 111-112	258.6	830,839	139.3	0	5,964
30X-4, 49-50	267.5	955,426	14	0	68,245
31X-2, 98-99	274.5	929,988	100.3	43.2	9,277
32X-4, 44-45	286.3	908,226	107.8	0	8,429
33X-3, 55-56	294.2	919,483	108.3	0	8,490
35X-2, 47-48	311.5	895,091	119.3	0	7,503
46X-6, 137-138	420.2	640,161	82.3	0	7,783
47X-6, 14-15	429.1	683,748	90.1	0	7,593

Figure 24. C<sub>1</sub>/C<sub>2</sub> value of syringe/vacutainer gas vs. depth, Hole 1073A.

ter taking into account the noise content of the data, it is clear that susceptibility data reflect real lithologic changes. For example, within the Pleistocene section, boundaries between lithostratigraphic units (see “Lithostratigraphy” section, this chapter) correspond to changes in susceptibility (compare Figs. 1 and 26). The most dramatic correlation between lithostratigraphy and susceptibility is at ~519 mbsf (the boundary between lithostratigraphic Subunits IE and IIA; Core 174A-1073-57-X), which is tentatively identified as the Pleistocene/Pliocene boundary. This depth is marked by a very abrupt (approximately ten-fold) downward decrease in susceptibility values, from ~250 to ~25 SI, which may represent a marked increase in terrigenous influx associated with Pleistocene climate change.

### Natural Gamma-ray Emission

Natural gamma-ray (NGR) measurements (Fig. 26; Table 20 on CD-ROM) were made using the MST at 20-cm intervals in each section, with a counting period of 30 s. At Site 1073, NGR results are probably influenced by both sand vs. clay and glauconite contents. At the largest scale, there are two distinct groupings of NGR data: values of 40–80 counts above ~569 mbsf, and values of 20–40 counts below

**Table 16. Carbon, nitrogen, and sulfur analyses of sediments from Site 1073.**

Core, section, interval (cm)	Depth (mbsf)	IC (wt%)	CaCO <sub>3</sub> (wt%)	TC (wt%)	OC (wt%)	TN (wt%)	TS (wt%)
174A-1073A-							
1H-5, 45-46	6.45	0.31	2.65	0.77	0.45	0.05	0.33
2H-5, 80-81	13.40	0.36	3.01	0.75	0.39	0.05	0.09
3H-5, 70-71	22.40	0.22	1.85	0.68	0.46	0.04	0.08
4H-5, 70-71	32.10	0.28	2.35	0.71	0.43	0.05	0.10
5H-5, 70-71	41.80	1.63	13.63	2.00	0.36	0.05	0.00
6H-5, 75-76	50.58	0.87	7.31	1.35	0.47	0.06	0.08
7H-5, 75-76	60.85	1.46	12.18	1.85	0.39	0.06	0.09
8H-5, 74-75	70.34	2.28	19.02	2.80	0.51	0.07	0.08
9H-6, 98-99	81.58	0.56	4.68	0.93	0.37	0.06	0.09
10H-6, 129-130	91.39	0.49	4.12	0.95	0.45	0.04	0.07
11H-6, 129-130	100.89	0.22	1.87	0.70	0.48	0.07	0.00
12H-4, 119-120	107.29	0.38	3.20	0.78	0.39	0.05	0.00
14H-4, 76-77	125.86	1.08	9.03	1.45	0.36	0.05	0.00
15H-5, 80-81	136.90	1.25	10.45	1.55	0.30	0.06	0.00
16H-5, 126-127	146.86	1.40	11.67	2.07	0.67	0.09	0.27
17H-6, 124-125	157.84	0.78	6.54	1.38	0.60	0.09	1.15
18H-5, 115-116	165.75	1.31	10.95	1.74	0.42	0.06	0.00
19H-6, 135-136	176.85	1.24	10.40	1.64	0.40	0.06	0.00
20H-4, 79-80	182.75	3.09	25.79	3.37	0.27	0.05	0.00
21H-4, 47-48	189.95	1.19	9.97	1.86	0.66	0.10	0.00
22H-4, 79-80	199.99	1.46	12.21	1.83	0.37	0.06	0.04
23H-3, 70-71	206.50	0.97	8.09	1.43	0.46	0.07	0.08
25X-3, 80-81	219.50	0.29	2.48	0.59	0.29	0.03	0.00
26X-4, 70-71	229.60	0.62	5.16	0.83	0.21	0.07	0.08
27X-4, 70-71	239.10	0.46	3.85	1.13	0.67	0.08	0.22
28X-4, 69-70	248.69	2.25	18.80	2.60	0.34	0.05	0.10
29X-3, 80-81	256.80	1.25	10.43	1.62	0.37	0.04	0.00
30X-3, 76-77	266.26	0.65	5.45	0.91	0.25	0.03	0.00
31X-3, 97-98	275.97	1.85	15.49	2.14	0.28	0.04	0.00

Note: IC = inorganic carbon, CaCO<sub>3</sub> = calcium carbonate, TC = total carbon, OC = organic carbon, TN = total nitrogen, and TS = total sulfur.

~569 mbsf. The ~569 mbsf NGR boundary does not correspond to a lithostratigraphic or biostratigraphic boundary. However, 569 mbsf is close to the level of a prominent biostratigraphic discontinuity or interval of condensation that may coincide with the amalgamation of numerous seismic surfaces (m0.5[s] to m3[s]; see “Biostratigraphy” and “Seismic Stratigraphy” sections, this chapter). The peak value of NGR (93.6 counts) was measured at ~560 mbsf, just above the 569 mbsf discontinuity.

On a finer scale, several cycles of NGR values are observed between 0 and 569 mbsf (i.e., 90–209 mbsf; 209–322 mbsf; 322–440 mbsf; and 440–466 mbsf in Fig. 26). Each of these cycles exhibits low NGR values at the base, succeeded by a gradual upward increase; the beginning of the next cycle is marked by an abrupt upward decrease in NGR value. These cycles are all observed within the Pleistocene part of the section and could be a manifestation of fluctuating rates of terrigenous influx and/or water depth associated with glacial-interglacial cycles.

### Thermal Conductivity

Thermal conductivity was measured once per core (Fig. 26; Table 21 on CD-ROM). The wide sampling interval permits only general observations. Values range between 0.89 and 1.5 W/(m·K) and increase with depth, with the higher values predominantly in coarser grained intervals. The overall trend changes from downhole-increasing to downhole-decreasing close to the presumed Pleistocene/Pliocene boundary (~519 mbsf).

### Compressional Wave Velocity

The PWL on the MST was run only on the first core from Hole 1073A because of gas expansion and resultant cracking of cores (Table 22 on CD-ROM). Only discrete velocity measurements made with the PWS1 transducers and PWS3 frame are shown on Figure 26 (see also Tables 23, 24 on CD-ROM). Gas-expansion cracks also prevented measurement of PWS1 longitudinal (z-direction) velocities

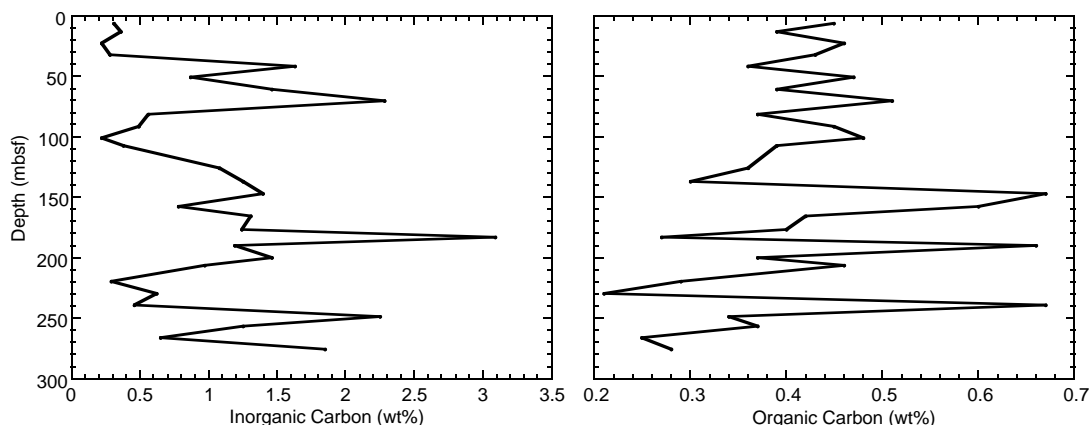


Figure 25. Carbonate carbon and organic-carbon content vs. depth for sediment samples, Hole 1073A.

below Core 174A-1073A-1H (~6 mbsf) and PWS3 frame orthogonal (x-direction) velocities below Core 174A-1073A-2H (~12 mbsf; Fig. 26), although PWS3 measurement became possible again in more lithified sediment beginning in Core 55X (~489 mbsf). The bulk of *P*-wave velocity measurements was therefore in the lower part of Hole 1073A, between ~490 and 663 mbsf. In this interval, measurement frequency was generally two per section (~75 cm spacing), producing a high-resolution velocity record.

*P*-wave velocities predominantly range between 1500 and 2040 m/s (Fig. 26). Velocity increases downhole in Cores 1H and 2H to ~12 mbsf, below which measurements were suspended until ~490 mbsf. Below ~490 mbsf, two broad cycles are observed; smaller scale fluctuations are superimposed on these larger cycles. Velocity increases downhole from ~490 to ~550 mbsf, peaking at 1980 m/s in lithostratigraphic Subunit IIB (composed of sandy mud and silty clay), below the inferred depth of seismic surface pp4(s) (see “Lithostratigraphy” and “Seismic Stratigraphy” sections, this chapter). Velocity values decrease downhole abruptly to ~1700 m/s, and then increase downhole gradually to peak again (maximum of 2040 m/s) between 654 and 658 mbsf in Unit III. This velocity peak is coincident with the top of Eocene chalks. Velocities decrease downhole within the chalks. However, because only one core penetrated the chalk, this lowermost trend is uncertain.

### Shear Strength

Undrained shear strength was measured once or twice per section and more frequently in sections with varying lithology (Fig. 26; Tables 25, 26 on CD-ROM). Presence of gas in the sediment causes expansion, in addition to that resulting from porosity rebound and biscuiting caused by coring; thus, the measured strength is reduced from in situ values. Automated vane shear (AVS) measurements were made from 0 to ~340 mbsf; below this depth the penetrometer was used, either because the vane could not penetrate the core or because the sediment cracked. Strength beyond 220 kPa cannot be measured by the penetrometer; thus, values of 220 kPa commonly represent higher values. Undrained shear strength increases downhole almost linearly with depth throughout Subunit IA, reaching ~50 kPa at ~95 mbsf. Strength increases, following a more variable trend, downhole to ~205 mbsf, reaching ~80 kPa. In the lowermost 20 m of Subunit IC, strength increases abruptly downhole, corresponding with a lithologic change from silty clay to muddy sand. A general downhole decrease in strength from ~110 to 50 kPa is observed in Subunits ID and IE down to ~320 mbsf. Below this depth, strength generally increases downhole. In Subunit IE (~420–440 mbsf), local peaks correspond to sandier sediments, below which a local downhole decrease corresponds to slumping (Core 174A-1073A-50X; 450–460 mbsf; see

“Lithostratigraphy” section, this chapter). Strength values in Unit II generally exceed the penetrometer limit of 220 kPa, except in the sandy mud of Subunit IIB at ~552 mbsf.

### Electrical Resistivity

Longitudinal resistivity measurements were generally made once per section. Resistivity values (Fig. 26; Table 27 on CD-ROM) lie mainly in the range from ~0.6 to 1.4  $\Omega$ m. Grain density is fairly constant, and porosity appears to be the dominant influence on resistivity. Transverse resistivity measurements were made between 182 and 278 mbsf and between 385 and 427 mbsf; these measurements were made at the same locations as the longitudinal measurements in these intervals (Fig. 26; Table 26 on CD-ROM). Transverse resistivities are lower than longitudinal resistivities in the upper part of the 182–278 mbsf interval, but become more similar downhole.

### Summary

As at other Leg 174A sites, several discontinuities and trends in physical properties measurements coincide with observed lithologic changes, unit boundaries, and interpreted seismic discontinuities (see “Lithostratigraphy” and “Seismic Stratigraphy” sections, this chapter). The peak in bulk and grain densities of ~255–260 mbsf may be linked to seismic horizon pp3(s). Natural gamma radiation measurements include a distinct downward decrease within lower–middle Miocene Subunit IIC. The Pleistocene section contains several increasing-upward cycles of natural gamma values, which may reflect glacial-interglacial cyclicality. Velocity measurements increase sharply in the interval from 541 to 561 mbsf; this corresponds to a condensed stratigraphic interval of increasing density (see “Seismic Stratigraphy” section, this chapter). The top of the Eocene chalks is also marked by a downhole velocity increase at ~650–660 mbsf.

Resistivity appears to correlate mainly with porosity, as at other Leg 174A sites. Changes in pore-water chemistry (see “Inorganic Geochemistry” section, this chapter) appear to have little influence on resistivity values. Resistivity, velocity, and density measurements from cores appear to correlate well with those obtained by logging at Site 1073 (see “Downhole Logging” section, this chapter).

## SEISMIC STRATIGRAPHY

### Introduction

In this section, we summarize regional geophysical information available before Leg 174A in the vicinity of Site 1073 (proposed site MAT-13B) and describe in a preliminary fashion its use for decipher-

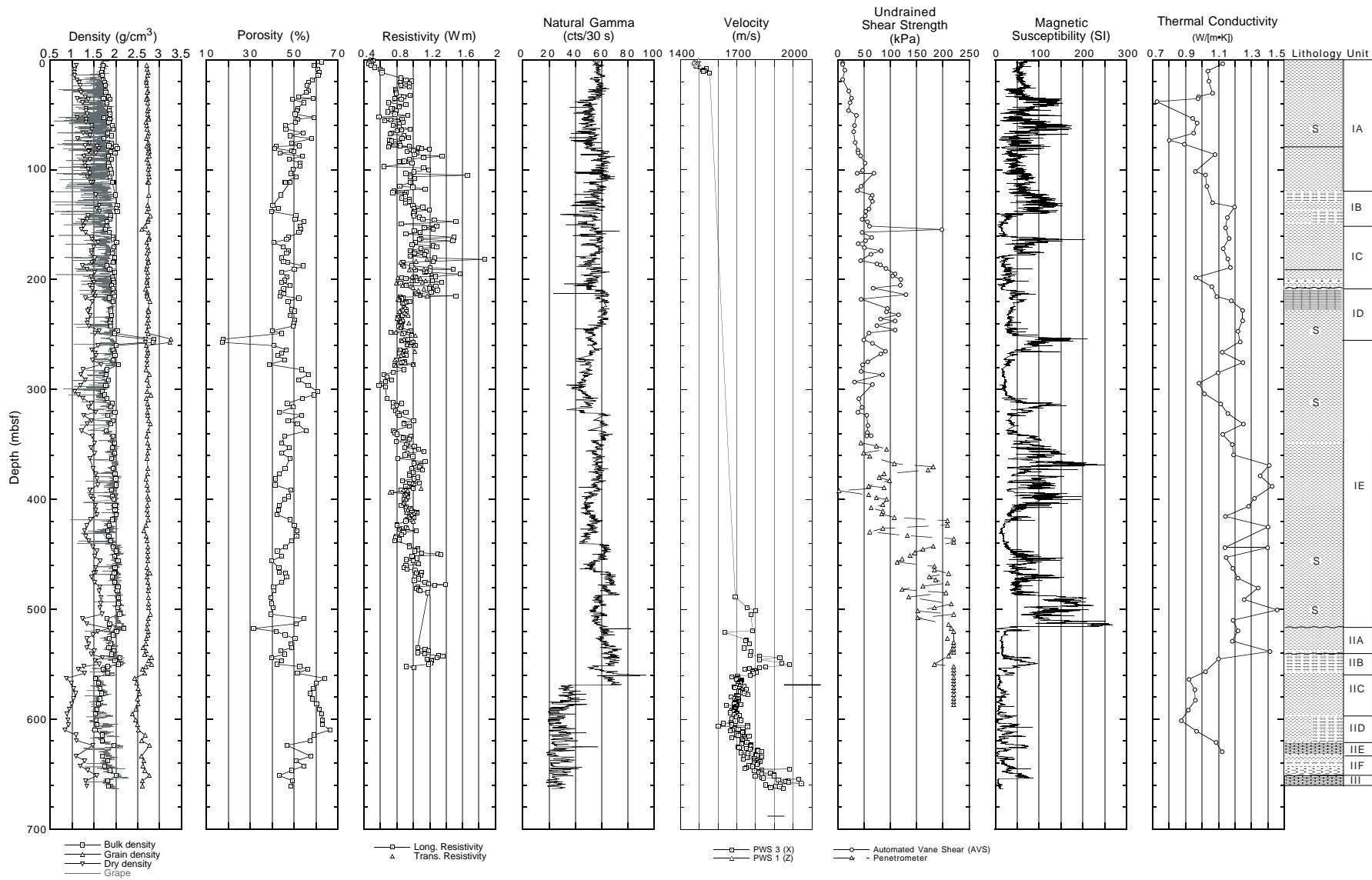


Figure 26. Index properties (IP), multisensor track (MST) GRAPE density, discrete IP porosity, longitudinal and transverse resistivity, natural gamma radiation, PWS-derived *P*-wave velocity, undrained shear strength, MST magnetic susceptibility, and thermal conductivity measurements from Hole 1073A. A summary column showing lithostratigraphic units is also shown (see “Lithostratigraphy” section, this chapter). PWS1 (Z-direction, longitudinal) and PWS3 (X-direction, orthogonal to core axis) *P*-wave velocity measurements are shown. The PWL was run only on the first core. Undrained shear strength measurements were made using the automated vane shear (AVS) and hand-held penetrometer.

ing the relationships between the sampled sections on the shelf at Sites 1071 and 1072, as well as fluctuations of sea level from the latest Paleogene to the present. Site 1073 is located on the uppermost slope within a physiographic province known as the Hudson Apron, and was originally intended as one of four backup sites during Leg 174A (see "Introduction" chapter, this volume; Fig. 27). The site was occupied when difficult drilling conditions precluded further shelf operations. The primary scientific objective at Site 1073 is to relate physical stratigraphy of the uppermost slope, where the section could presumably be well-dated (see "Introduction" chapter, this volume), to sequence boundaries provisionally traced seaward from the shelf. This is consistent with the primary objective of Leg 150 (Mountain, Miller, Blum, et al., 1994), where coeval strata were sampled and logged at sites ~55 km to the southwest (Fig. 27). Site 1073 was chosen to provide absolute-age and deep-water facies controls for correlative seismic surfaces beneath the shelf. Available seismic data suggested that a thick and complete Pleistocene succession would be present at Site 1073; if present, such a section could potentially provide a high-resolution climate record and detailed information concerning slope development during the last 1–2 m.y.

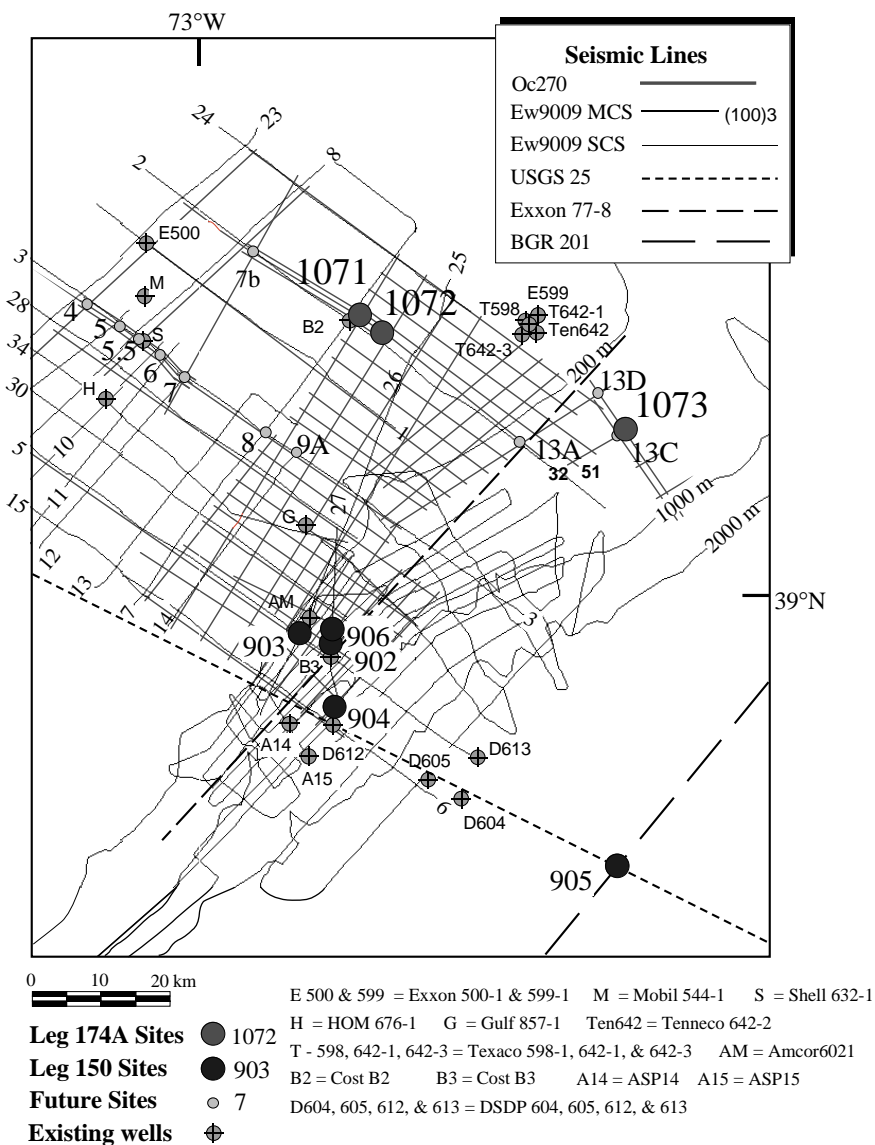
The key data for choosing the location of Site 1073 and developing a scientific rationale for sampling the Hudson Apron are the high-resolution profiles acquired during Oc270 (summer 1995), and par-

ticularly the regional survey stretching from Leg 150 sites on the continental slope to the south to the Hudson Apron to the east (Fig. 27; see "Introduction" chapter, this volume). These data were collected using a 48-channel receiver (6.25 m groups; 22 m offset to the near-trace) and a single generator-injector (GI) air gun towed at 2–3 m below the sea surface. Resolution was estimated to be ~5 m vertically throughout the interval of penetration anticipated for Leg 174A drilling and sampling on the upper slope (to ~1.8 s two-way travelt ime [TWTT]). The Oc270 data build upon another primary geophysical data set, the Ew 9009 profiles (Fig. 27; see "Introduction" chapter, this volume). Site 1073 (MAT-13B) was originally proposed at the intersection of Oc270 Profiles 61 and 32, but concerns expressed by the JOIDES Pollution Prevention and Safety Panel about structural closure and a possible amplitude anomaly led to relocation of the site 900 m southwest along Profile 32, to cdp 1650 (Fig. 28).

### Carrying Seismic Surfaces from the Shelf to the Hudson Apron

In preparation for drilling at Site 1073, surfaces pp3(s) and pp4(s) sampled at Sites 1071 and 1072 were traced seaward along Oc270 Profile 51 (Fig. 27), along with a third, geometrically similar offlap surface (pp1[s]) that rises to the seafloor seaward of Site 1072. These

Figure 27. Map of Leg 174A shelf sites (Sites 1071 and 1072), Site 1073 on the uppermost slope, track lines of profiles collected during Cruises Oc270 (thick solid lines) and Ew 9009 (thin solid lines), other relevant seismic control, and available well information used in assessing the hydrocarbon safety of drilling this part of the New Jersey continental margin. Site 1073 is located on Oc270 strike Profile 32 (indicated); dip Profile 51 (shown), which crosses Profile 32, was chosen to extend outer shelf correlations from the Site 1071/1072 seismic grids to the Hudson Apron (see "Downhole Logging" section, this chapter).



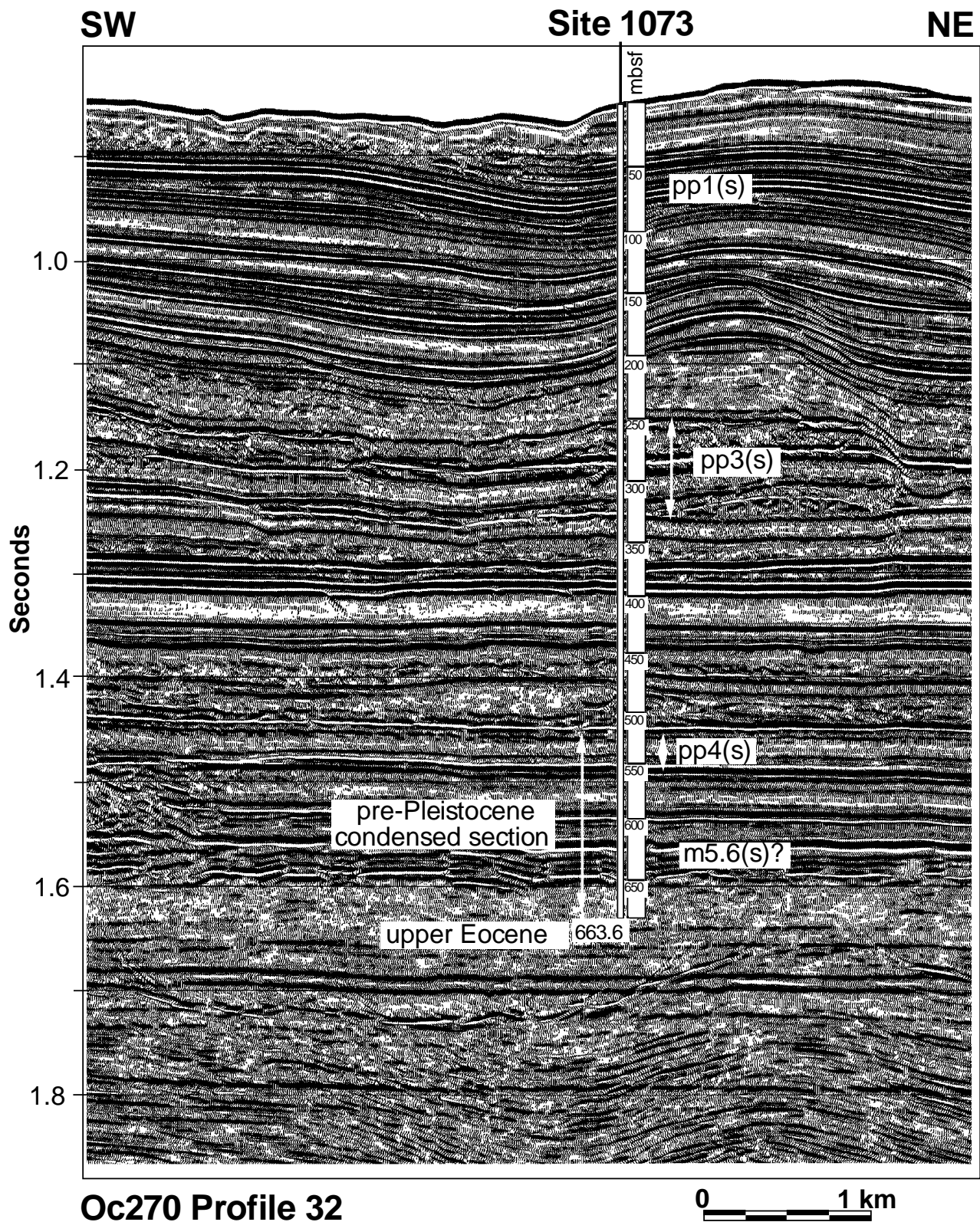


Figure 28. Interpreted version of part of Oc270 Profile 32, an approximate strike section running through Site 1073 (see Fig. 27). The approximate total depth (TD) penetrated in Hole 1073A is indicated (vertical white bar); the approximate depths in meters below seafloor shown on this time section are derived from a velocity function developed from Leg 150, Site 903 (see "Downhole Logging" section, this chapter). The possible locations of some prominent stratigraphic discontinuities/sequence boundaries identified on the outer shelf are shown. Other shelf-slope seismic ties and their log character are detailed in the "Downhole Logging" section (this chapter).

three outer shelf sequence boundaries can be followed along Profile 51 to its intersection with Profile 32, then 9 km northeast along Profile 32 to Site 1073 (Figs. 27, 28). Despite significant hiatuses associated with these surfaces at shelf locations, the Shipboard Scientific Party anticipated that ages could be constrained on the basis of the predrilling assumption that the section at Site 1073 would be thick and relatively complete in the Pliocene–Pleistocene succession, and datable. Surfaces pp5(s) and m0.5(s), also drilled at Site 1072, were suspected to correlate with the succession at Site 1073, but an unambiguous seismic tie could not be made because of condensation (thinning) of the coeval section between the two sites. Sequence boundary m1(s), which was penetrated only at Hole 1071F on the shelf, was also thought to be traceable to the slope; however, the tie of m1(s) from the shelf to Site 1073 is also uncertain as a result of stratigraphic condensation of the Miocene section beneath the outer shelf (Fig. 28).

Profile 32 illustrates some of the sequence-stratigraphic surfaces penetrated and sampled at Site 1073 (Fig. 28). Other seismic features and their log character are discussed in the “Downhole Logging” section (this chapter). Using a velocity function derived at Site 903 during Leg 150 from presumably coeval sediments, a prespud travel-time-depth conversion at the site was calculated (Fig. 28; Table 28). Recovery in Hole 1073A was excellent (105.8% APC, 97.1% XCB; see “Lithostratigraphy” section, this chapter); therefore, tying lithologies sampled to the regional sequence-stratigraphic framework could be accomplished, even where the pre-Pleistocene stratigraphic section was condensed (see below). A full suite of downhole logs (except for Formation MicroScanner [FMS]) was also collected and is critical for tying the interpreted seismic data to the sampled section, and in particular for seismically correlating the condensed, upper Paleogene–Miocene section sampled below ~550 mbsf in Hole 1073A to the expanded, coeval geologic section beneath the shelf to the northwest at Sites 1071 and 1072 (see “Downhole Logging” section, this chapter).

### Calibrating Outer Shelf Sequence Stratigraphy to the Upper Slope

#### Preliminary Lithostratigraphic-Chronostratigraphic Correlations

Figure 28 summarizes tentative ties between upper-slope sequence boundaries identified regionally on Oc270 Profile 32 at Site 1073 and the preliminary lithostratigraphy and chronostratigraphy developed as a result of the virtually complete sampling in Hole 1073A (Table 2). The upper 519.8 m of Hole 1073A is Pleistocene–Holocene(?) (Unit I, see “Lithostratigraphy” section, this chapter). Sequence boundaries pp1(s) and pp3(s) are contained within the Pleistocene section at depths of ~72–75 mbsf and 243–325 mbsf (Fig. 28). Boundary pp4(s) may mark the base of Unit I. Although there is some uncertainty in the tracing of pp4(s) from the outer shelf to Site 1073 (~522–555 mbsf in Fig. 28), biostratigraphic informa-

tion indicates that the base of Unit I is 0.46–1.9 Ma (see “Biostratigraphy” section, this chapter), which is consistent with the age of pp4(s) at Sites 1071 and 1072. A peak in density at ~255–260 mbsf may correspond to pp3(s); correlative peaks in density and velocity at ~540–560 mbsf correspond with stratigraphic condensation at the level of seismic surfaces m0.5(s) to m3(s) (see “Physical Properties” section, this chapter).

Below the base of the Pleistocene, the Neogene section at Site 1073 is highly condensed compared to the shelf section. The entire Miocene interval targeted for drilling on the outer shelf occupies ~75 m at the base of Hole 1073A (Fig. 28). This encompasses surfaces pp5(s), m0.5(s), m1(s), and all of the deeper horizons identified by Greenlee et al. (1992) and calibrated during Leg 150 (Mountain, Miller, Blum, et al., 1994; see “Introduction” chapter, this volume). The Oligocene section is ~20 m thick at Site 1073. Refinement of the core-seismic-log correlations (see “Downhole Logging” section, this chapter) in the deep part of Hole 1073A will only be clarified with shore-based work.

## DOWNHOLE LOGGING

### Introduction

Site 1073 is located above a thick Pleistocene slope section resting unconformably on a comparatively thin interval of Miocene–Oligocene sediments. The entire package is well imaged on Oc270 profiles, on which a number of surfaces can be traced 39 km landward to Site 1072, although shore-based loop correlations across this seismic grid will be required to ensure a detailed set of shelf-to-slope correlations. The goal at Site 1073 was to core and log as deeply as possible into “Icehouse” sediments (Oligocene and younger). This would enable studies to determine the age and deep-water facies of sediments resting on key surfaces that at Site 1071 and 1072 provide paleobathymetry and facies characterization needed to determine the history and geologic impact of glacial-eustatic change. High sedimentation rates, high core recovery, excellent log data quality, and reliable core-log-seismic integration are all crucial elements of this strategy at Site 1073.

### Logging Operations

APC/XCB coring operations at Hole 1073A ended at 663.6 mbsf. A wiper trip was performed to clean the hole for logging, and the BHA was placed at 87.4 mbsf. Six logging runs were performed because of difficulties in lowering the logging tool strings through bridges in the borehole. These logging runs provided sonic, resistivity, and gamma-ray measurements through the full open-hole interval from 88 to 652 mbsf, and partial coverage with the integrated porosity-lithology tool string (IPLT) and the WST. A graphic summary of logging tools deployed and intervals logged is shown in Figure 29.

In the first run, the sonic-resistivity tool string (Natural Gamma-ray Tool [NGT], Long-Spaced Sonic tool [LSS], Dual Induction Tool [DIT-E], and Lamont-Doherty Earth Observatory Temperature-Logging Tool [LDEO-TLT]) could not pass a bridge at 290 mbsf. The upper section of the hole was then logged from 290 mbsf to 88 mbsf. The BHA was lowered past the bridge and placed at 360 mbsf. The second run of the induction-sonic tool string obtained data from 652 to 360 mbsf, with ~11 m of fill preventing the tool from reaching the total depth drilled. In the third run, the WST could not be lowered below 425 mbsf. The tool was clamped at four stations (424, 405, 385, and 370 mbsf) and traveltimes were measured by averaging from five to seven GI air gun shots at each station. The fourth run, using the triple combo tool string (Hostile-environment Natural Gamma-ray Spectrometry tool [HNGS], Accelerator Porosity Sonde [APS], Hostile-environment Litho-Density Tool [HLDT], DIT-E, and LDEO-TLT), logged the interval between 652 and 360 mbsf.

To complete the open-hole coverage in the interval between 290 and 360 mbsf, particularly with sonic velocity data, the BHA was

Table 28. Traveltime and depth to surfaces at Site 1073.

Surface	TWTT (s)	Depth* (mbsf)	Depth** (mbsf [±5%])	Depth*** (mbsf)
seafloor	0.850	0	0	0
A (~pp1[s])	0.943	~72	75 (71–78)	64
B	1.025	136	143 (136–150)	130
C	1.085	184	194 (184–203)	179
D	1.108	204	213 (203–224)	199
E (~pp3[s])	1.153	243	252 (240–265)	238
F (~pp3[s])	1.200	285	293 (279–308)	280
G (~pp3[s])	1.245	325	333 (317–350)	318
H	1.318	392	399 (379–419)	386
I	1.348	420	427 (405–448)	415
J	1.405	~475	479 (455–503)	466
K (~pp4[s])	1.450	~522	522 (495–548)	507
L (~m5.6[s])	1.560	~622	627 (595–658)	604

Notes: \* = time-depth conversion based on Site 1073 checkshot survey; approximate depths are outside the range of the checkshots. \*\* = time-depth conversion based on Leg 150, Site 903 correlations. \*\*\* = time-depth conversion based on sonic log data calibrated to checkshot values within the depth range of the VSP measurements.

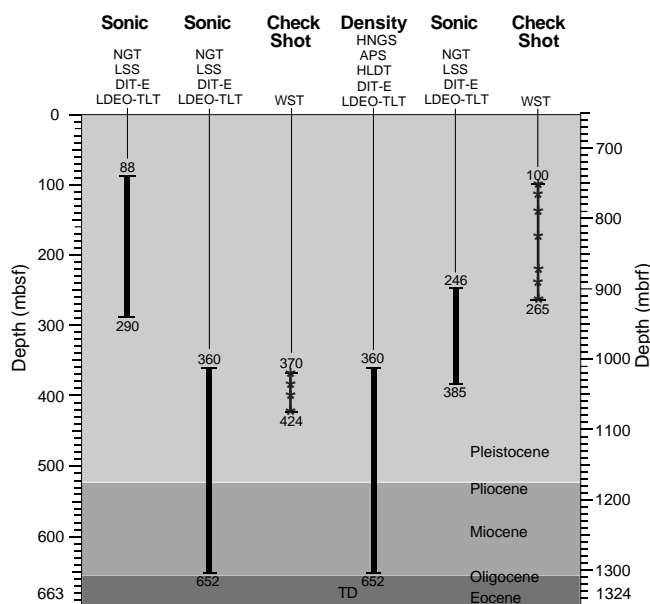


Figure 29. Graphic summary of logging runs in Hole 1073A. NGT = Natural Gamma-ray Tool; LSS = Long-Spaced Sonic tool; HNGS = Hostile-environment Natural Gamma-ray Spectrometry tool; APS = Accelerator Porosity Sonde; HLDT = Hostile-environment Litho-Density Tool; DIT-E = Dual Induction Tool; LDEO-TLT = Lamont-Doherty Earth Observatory Temperature-Logging Tool; WST = Well Seismic Tool; \* = WST geophone clamp depths (i.e., where velocity calculations were actually made).

raised to 246 mbsf. The fifth logging run, using the sonic-resistivity tool string, successfully obtained data between 385 and 246 mbsf, and provided overlap with the sonic/resistivity log data obtained in the upper part (run 1) and lower part (run 2) of the borehole. The BHA was then raised to 87.4 mbsf and checkshots were obtained at a total of seven additional stations (265, 238, 210, 174, 138, 115, 100 mbsf) during the sixth and final logging run.

### Data Quality

The three sonic-resistivity logging runs in the upper, middle, and lower sections of the borehole were spliced into a single profile and are displayed in Figure 30. The corresponding spectral gamma-ray measurements are shown in Figure 31. The IPLT data from the lower part of the borehole are shown in Figure 32. Note that the gamma-ray measurements were not corrected for hole diameter variations and should therefore be interpreted only in a qualitative fashion. Borehole corrections for all logs will be performed at LDEO postcruise after precise depth matching between the different logging runs (see “Shore-based Log Processing” section, CD-ROM, back pocket, this volume). Because borehole diameter was measured only with the IPLT string, gamma-ray corrections will be possible only for the interval between 360 and 652 mbsf.

Variations in borehole diameter affect log quality, particularly for density and porosity measurements that require tool contact with the borehole wall. Data from washed-out intervals between 415 and 460 mbsf are suspect for this reason. Through the remaining lower half of the borehole, the density/porosity data show only small-scale variations that are the result of borehole rugosity. Porosity tool standoff generally is <1 in, well within the acceptable range of maximum standoff for good quality measurements.

Velocity and resistivity measurements are generally less affected by enlarged borehole sections than are other log data, although velocities can be expected to be locally lower in washed-out intervals. Abnormally low sonic velocity values are measured in several intervals, with  $V_p$  as low as 1.5 km/s at 200–210 and 280–315 mbsf, and 1.6–

1.7 km/s at 420–440, 520–532, and 550–570 mbsf (Fig. 30). These abnormal values are probably caused by high porosity and high fluid content, as indicated by the low electrical resistivity within the same intervals. Neutron porosity and density also indicate abnormally high porosity immediately below 518 and 545 mbsf (Fig. 32). A severely washed-out borehole is likely between 420 and 440 mbsf, and possibly between 200 and 210 mbsf (note very low gamma-ray values).

Checkshot traveltimes (Table 29) and integrated sonic-log traveltimes coincide downhole to ~200 mbsf, but begin to diverge from there downward, with the integrated sonic log providing a longer traveltime for the same depth (Fig. 33). There are several reasons for this departure. First, the sonic tool records data from sound traveling through the borehole wall, a path that differs from that followed in the large-scale downhole seismic experiment. Second, the higher frequency content of the sonic tool source (~10,000 Hz) produces a very different waveform than the GI air gun used in the checkshot experiment (~100 Hz). Systematic differences in times measured between signal and first arrival are to be expected because of these contrasting waveforms. Third, borehole fluids invade the formation and can reduce small-scale velocity measurements obtained using the sonic tool. These effects accumulate during the sonic transit time integration and lead to errors in depth-to-traveltime estimates, up to ~20 ms deeper at 420 mbsf in comparison to the checkshot data. The checkshot data, therefore, provide a useful correction to the borehole depths as measured by the sonic log.

## Results

### Log-Core Correlations and Evidence for Cyclicity

Gamma-ray log data show several asymmetric cycles of uphole increases followed by abrupt decreases in natural radioactivity (accented by arrows in Fig. 30). The abrupt decreases typically occur at or near the estimated depths of sequence stratigraphic discontinuities observed in the seismic data (see below). Major cycles occur within the following intervals: 516–465, 418–322, 268–209, 198–152, and 144–105 mbsf. The shallowest cycle probably continues upward above the shallowest depth of open-hole log data. The intervals 465–440 and 320–285 mbsf show variable gamma-ray values, with a suggestion of smaller-scale cycles of increasing-upward values.

Gamma-ray cyclicity is especially prominent in the thorium content displayed in Figure 31. The locally high potassium values at 550–540 mbsf correspond to glauconite concentrated near the base of lithostratigraphic Subunit IIB; elsewhere, thorium and potassium roughly vary in unison, as shown by a fairly steady Th/K value (Fig. 31), suggesting little change in clay mineralogy. Uranium content does not contribute to the total gamma-ray cyclicity in the Pleistocene sediments above 520 mbsf (compare the computed gamma-ray uranium-free [CGR] and spectral gamma-ray [SGR] curves). Furthermore, uranium values suggest three groupings: moderate values from the top of the logged interval to 285 mbsf, low values from 285 to 515 mbsf, and much higher and variable values from 515 mbsf to the bottom of the logged interval. The latter are observed within pre-Pleistocene sediments, where the especially high values (>5 ppm between 560 and 585 mbsf; Fig. 31) correspond to some of the highest total organic carbon values of Hole 1073A. At this depth interval (and only this interval), the locally high uranium values account for the divergence between the CGR and SGR curves. In general, it should be noted that all of these log values represent measurements of bulk sediment; shore-based analyses of clay mineralogy may reveal more detailed patterns.

The abrupt changes in sound velocity, uranium content, and density values at 515–520 mbsf (Figs. 30, 31, and 32, respectively) correspond with an abrupt upward increase in sedimentation rate at the base of the Pleistocene section (lithostratigraphic Unit I; see “Lithostratigraphy” section, this chapter). The lower sound velocity and resistivity values below this depth suggest an undercompacted, possibly overpressured interval, especially between 515 and 530 mbsf. The “normal” compaction revealed by the overall downward increase



1073A Spectral Gamma-ray Summary

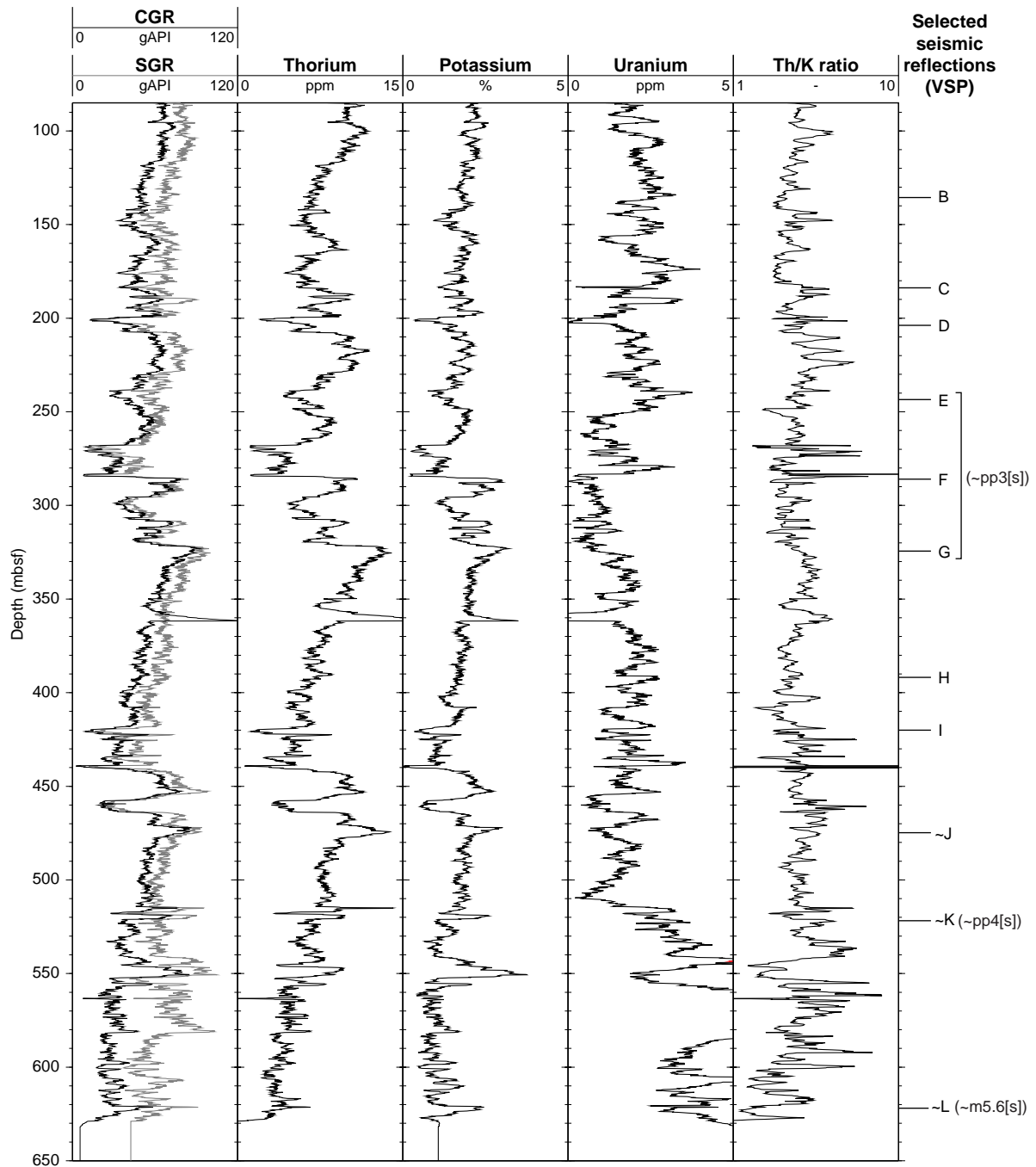


Figure 31. Summary of spectral gamma-ray logs. Gamma-ray measurements are not corrected for hole diameter variations. Depths to locally defined stratal surfaces (see Fig. 36) converted to depth (see text and Table 28) are shown.

sonic data, and the checkshot data (note that the latter extend only to 424 mbsf; Fig. 33). However, throughout most of the depths where all three data types are available, the sonic-log values are the lowest. These low sonic values may have been artificially lowered because of an enlarged borehole; at some depths this can be confidently established only in the upper half of the borehole (e.g., 455–462 mbsf; Fig. 32), where caliper data were collected (see “Logging Operations” section, above). However, it does not appear that the unusually low sonic-log values below 550 mbsf are caused by poor borehole conditions (compare Figs. 30 and 32).

We converted seismic reflection traveltimes to depths below sea-floor using a combination of checkshot data and the Site 903 conver-

sion as follows. Each of the 11 checkshot measurements was plotted as a time-depth pair (Fig. 33), and values were linearly interpolated. Below 424 mbsf (the deepest checkshot measurement point), calculations on the basis of the Site 903 time-depth correlations were used.

We identify 12 seismic surfaces in Oc270 Profile 32 (Figs. 34–36; Table 28), and for clarity they are simply labeled by the letters A (shallowest) through L (deepest). We attach no lithostratigraphic or chronostratigraphic significance to eight of the 12 other than the fact that on Profile 32, the geometry of reflections immediately above and below each surface suggests marked stratal discontinuity on the basis of observed truncation or onlap. Shore-based loop correlations across the grid of Oc270 data are needed to tie most reflections landward to

Hole 1073A IPLT Summary

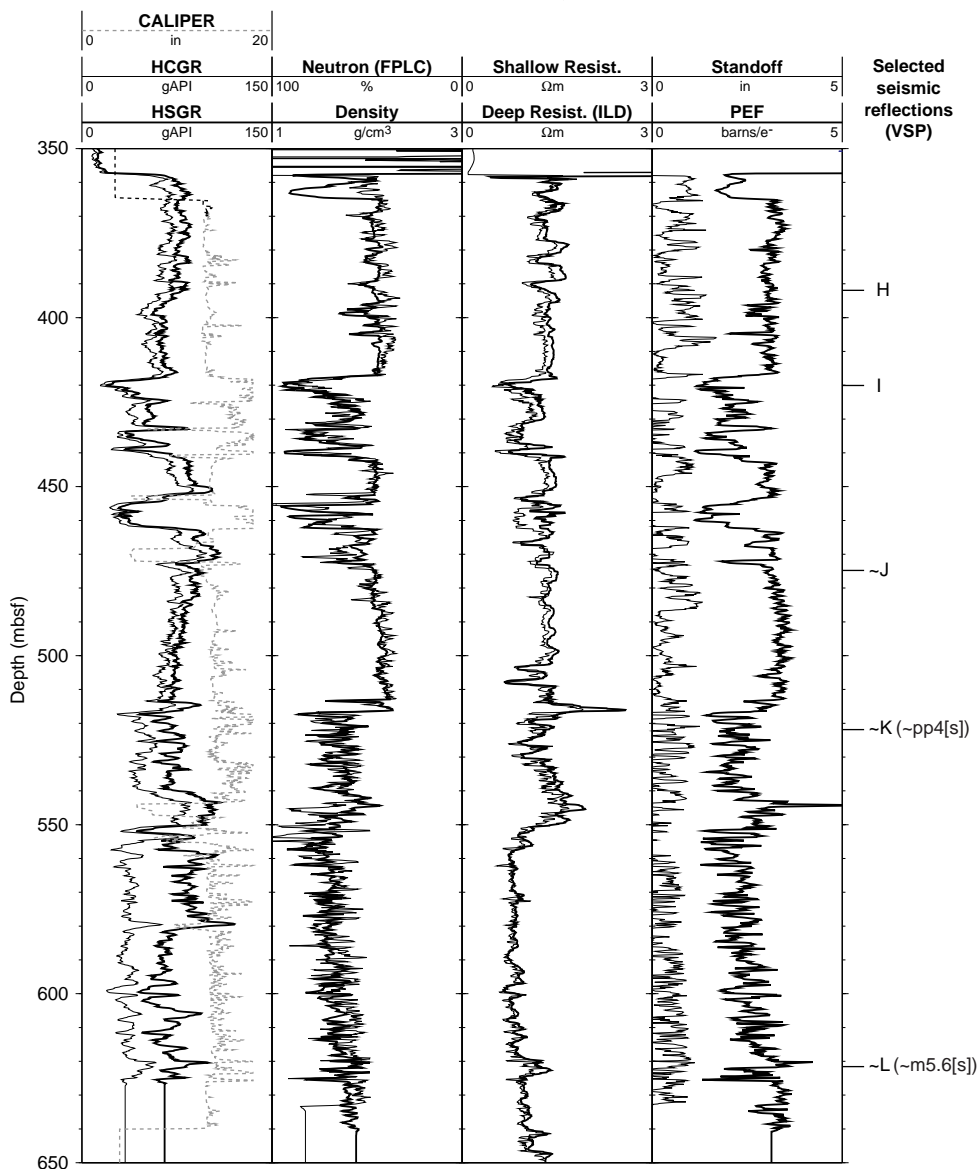


Figure 32. Logging results from the integrated porosity-lithology tool (IPLT) string in the lower part of Hole 1073A. Depths to locally defined stratal surfaces (see Fig. 36) converted to depth (see text and Table 28) are shown.

Table 29. Checkshot data collected at Hole 1073A.

Depth (mbrf)	OWTT (ms)	Depth (mbsf)	TWTT (ms)	Interval velocity (m/s)
650.5	426	0	0	1504
750	493.1	100	133	1710
765	501.85	115	151	1610
788	516.1	138	179	1590
824	538.7	174	224	1769
860	559	210	265	1736
888	575.1	238	297	1750
915	590.5	265	328	1789
1020	649.1	370	446	1920
1035	656.9	385	461	1902
1055	667.4	405	482	1936
1074	677.2	424	502	

Notes: First two columns from the left record the unprocessed checkshot data. Depth is referenced in meters below rig floor (mbrf) and one-way traveltime (OWTT) is referenced from the sea surface. The last three columns record the processed checkshot data. Two-way traveltime (TWTT) is referenced from the seafloor; interval velocities record the average velocity between the depths shown. Water depth at this site is 639 m.

surfaces mapped previously (Greenlee and Moore, 1988; Greenlee et al., 1992; Fulthorpe and Austin, 1998; N. Christie-Blick et al., unpubl. data). Four reflections on Profile 32, however, can be correlated to other surfaces. The shallowest of these is A. On Oc270 Profile 51 across the adjacent outer continental shelf, pp1(s) is a surface characterized by marked offlap and onlap and interpreted as a sequence boundary (see “Introduction” chapter, this volume, and “Seismic Stratigraphy” section, this chapter). Surface A is the interpreted continuation of pp1(s) on the slope. Although a preliminary correlation at present, pp1(s)/A exhibits subtle truncation beneath and high-amplitude reflections immediately above, with small channels cutting into this surface along strike on Profile 32. The Site 903 time-depth conversion predicts A at 75 mbsf (Table 28). Stratal relationships on Oc270 dip Profile 51 show that E is younger than surface pp3(s), which was observed at Sites 1071 and 1072, whereas G is older (see “Seismic Stratigraphy” sections, “Site 1071” and “Site 1072” chapters, this volume, for discussion of pp3[s]). Reflection K is located at or above surface pp4(s) at Sites 1071 and 1072. Finally, reflection L can be traced to the shelf and southwest to Leg 150, Site 903, and

appears to correspond with surface m5.6(s) (Mountain, Miller, Blum, et al., 1994).

The calculated sub-bottom depths to all 12 reflections are shown in Figure 30 (using the 1073 checkshot data), and in Figures 34 and 35 (using the Site 903 time-depth function). The calculated depths to reflections using the checkshot-derived function are 10–25 m shallower than those derived from the time-depth function from Site 903. One correlation in particular casts doubt on the sonic/checkshot depth conversions, and favors the conversion using Site 903 data. Profile 32 (as well as intersecting Oc270 dip Profiles 59 and 61) shows that reflection K (tentatively correlated to pp4[s]) at 600 ms below the seafloor at Site 1073 is an erosional surface overlain by irregular reflections, which suggests slumped sediments. Site 903 velocities place this surface at 522 mbsf, at the depth of the disconformable Pleistocene/Pliocene contact (seen in Core 174A-1073A-57X). The sonic-log data (Fig. 33), by contrast, place this at 495 mbsf, within the Pleistocene sediments of lithologic Subunit IE, which contains exotic clay intraclasts (see “Lithostratigraphy” section, this chapter.) All log parameters measured at Site 1073 show sharp changes at 520 mbsf (and not at 495 mbsf), further supporting the correlation made on the basis of Site 903 velocity data. Additional shore-based integrated analysis of log, core, and seismic data will be needed to characterize these surfaces more precisely.

### Log-Seismic Correlation Using Synthetic Seismograms

A one-dimensional synthetic seismogram was constructed for Site 1073 (Fig. 35) using sonic-log data edited to remove cycle skips and assuming a constant density of 2.0 g/cm<sup>3</sup>. The latter was necessary because a complete density log was not acquired over the sonic-logged interval. The reflection coefficients were then calculated on the basis of the change in impedance with depth. Finally, an 80-Hz, minimum phase, Ricker wavelet (a simple yet accurate approximation of the sea-bottom reflector on the Oc270 data) was convolved with the reflection coefficients. Calculated sub-bottom depths to the 12 reflections identified on Profile 32 at Site 1073 used the Site 903 time-depth function (see also Fig. 34).

Two points should be considered. First, despite a correction for spherical spreading of acoustic energy, amplitudes of reflections in the processed seismic data decay with depth, whereas those of the synthetic seismogram do not. Second, it is important to remember that the log data were spliced together from three different logging runs (see “Logging Operations” section, above). However, no abrupt shifts in the log data are apparent at the splicing depths.

Several similarities are present between the synthetic seismogram and the actual seismic data. At the F surface, there is a very prominent, double-peak/double-trough reflection in both the seismic data and the synthetic seismogram (Fig. 35). This reflection ties to an abrupt, two-step upward increase in the velocity log. Similarly, the I surface (Fig. 35) matches an abrupt velocity contrast that is imaged as a prominent reflection in both the synthetic and seismic data. Sonic-log values, without checkshot corrections, were used below this depth, and the correlation between the seismic data and the synthetic data is not as good.

## SUMMARY AND CONCLUSIONS

Site 1073 on the upper continental slope recovered an extremely thick succession of Pleistocene age (~520 m; Table 2) and a relatively condensed section of Pliocene–upper Eocene sediments that are at least in part coeval with the strata investigated on the shelf at Sites 1071 and 1072. This permits refinement of the ages of pp3(s) and pp4(s), and the dating of a still younger offlap surface (pp1[s]) that rises to the seafloor seaward of Sites 1071 and 1072. Offlap surface pp2(s), mapped in seismic data beneath the outer shelf, merges with pp3(s) both seaward of Sites 1071 and 1072 and landward of Site 1073. Miocene and older sequence boundaries, including m0.5(s) and

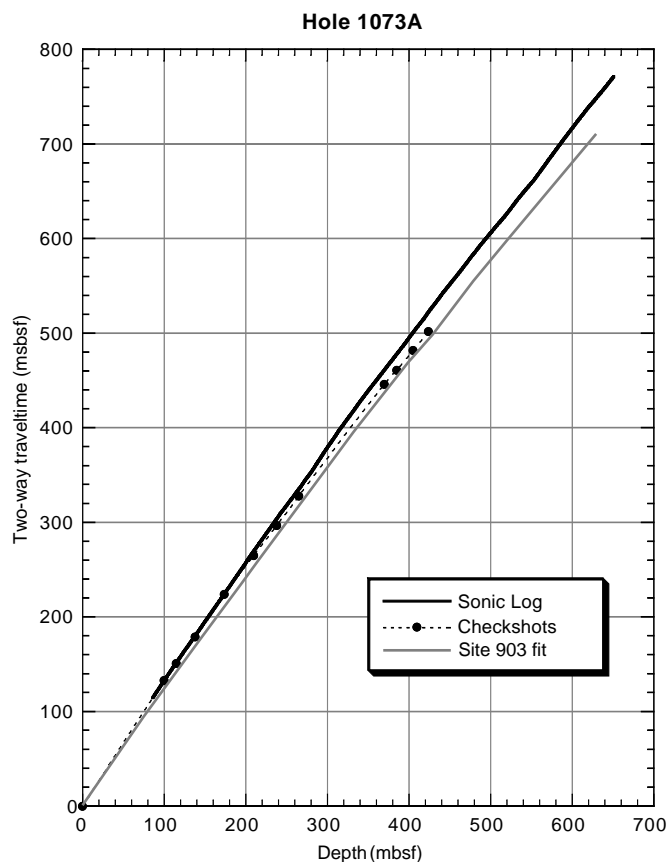


Figure 33. Traveltime-depth conversion curves obtained from Hole 1073A checkshot survey, integrated Hole 1073A sonic log, and best-fit curve from Site 903 (Mountain, Miller, Blum, et al., 1994). The sonic log was spliced from logging runs 1, 2, and 5 and edited for cycle skips. The sonic-log values indicate longer traveltime (slower velocity) than do the checkshot data at the same depth. This is probably because sonic tool measurements are affected by formation invasion and enlarged borehole sections.

m1(s), tend to become amalgamated landward of Site 1073, and cannot be dated with confidence.

The main elements of the succession are as follows. Unit I (Holocene[?]-Pleistocene; 0–519.8 mbsf) consists predominantly of silty clay with minor intervals of sandy mud and rare sand beds and laminae. Unit II (Pliocene–Oligocene; 519.8–654.1 mbsf) consists predominantly of silty clay with thin interbeds of silt and sand. Locally, it is foraminifer rich, glauconitic, diatomaceous, or composed of nanofossil chalk. The degree of bioturbation is variable. Unit III (upper Eocene; 654.1–663.6 mbsf) is a thoroughly bioturbated clay-rich nanofossil chalk and nanofossil clay.

Using a velocity function developed from Leg 150, Site 903, and checkshot data from Site 1073, pp1(s) is located at ~72–75 mbsf, and is dated as <0.25 Ma on the basis of nanofossils. Surface pp3(s) has been traced to 243–325 mbsf, and dated as 0.25–0.46 Ma (nanofossils). If deeper than 324.86 mbsf and shallower than 346.64 mbsf, pp3(s) is 0.46–0.9 Ma (nanofossils). However, we know from Sites 1071 and 1072 that pp3(s) is <0.78 Ma. So a conservative estimate for its age is 0.25–0.78 Ma, and it is most likely <0.46 Ma. Surface pp4(s) is tentatively interpreted at a depth of 519.8 mbsf on the basis of core and log data, and a marked biostratigraphic hiatus between 515.88 and 524.13 mbsf. The contact is characterized by an abrupt upward change from bioturbated clay to pebbly sandy clay with mud clasts up to several centimeters in diameter. It also corresponds with prominent positive excursions in gamma-ray, velocity, and resistivity values, and a prominent upward increase in both density and photoelectric factor. The interpreted depth of 519.8 mbsf is close to that

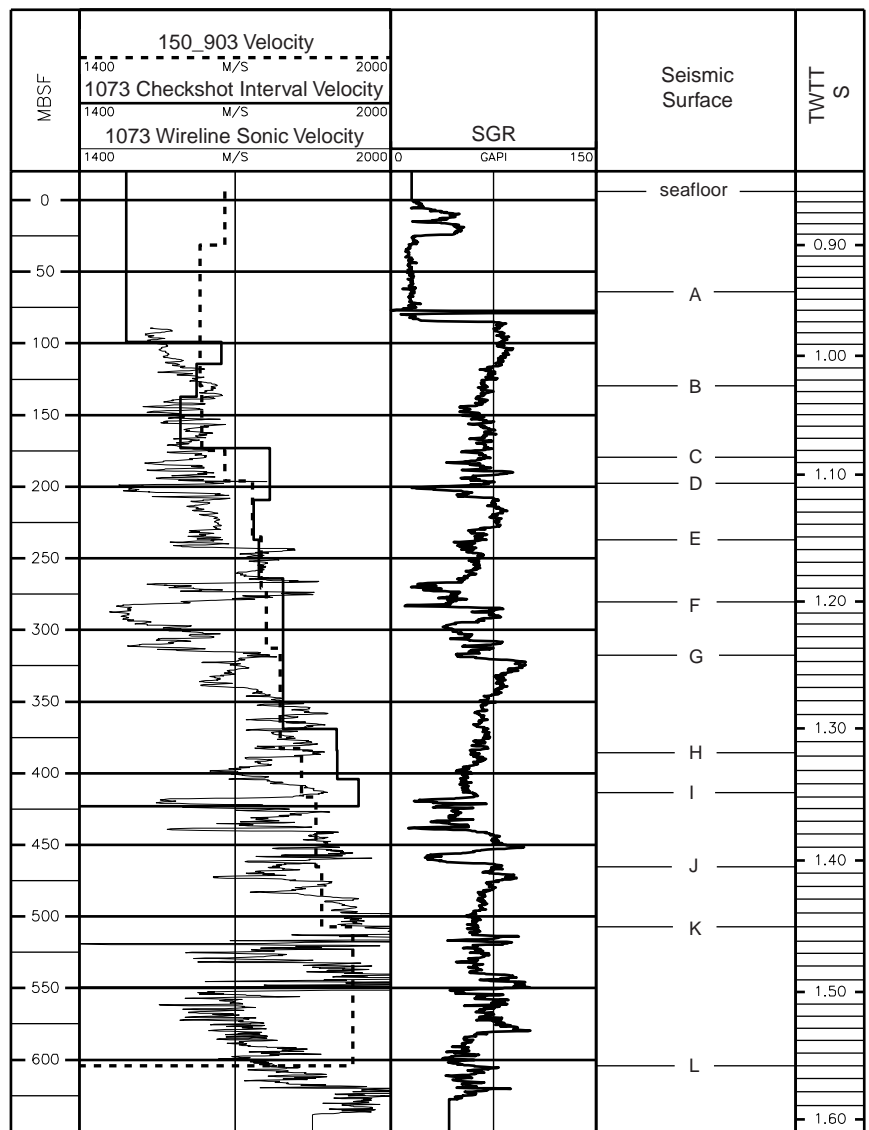


Figure 34. Velocity-depth plot of Hole 1073A (mbsf in column 1 at far left). Two independent velocity data sets derived at Hole 1073A (wireline sonic velocities and interval velocities calculated from the checkshot survey) are shown in column 2. Interval velocities estimated from Leg 150 Site 903 drilling results are shown for comparison. Wireline gamma-ray values at Hole 1073A are shown in column 3. Twelve seismic reflections, A through L (column 4), are positioned at depths calculated from merged sonic log and checkshot measurements (see Table 28). The two-way traveltime to each reflection is listed in column 5.

predicted from checkshot data at Site 1073 (522–555 mbsf), a range that includes uncertainty in the tracing of surface pp4(s) from the shelf. If this interpretation is correct, surface pp4(s) is dated as 0.46–1.9 Ma (nannofossils and dinocysts). If pp4(s) is located shallower than 515.88 mbsf, it is younger than 0.9 Ma; if it is located deeper than 524.14 mbsf, it is older than 1.7 Ma. However, surface pp4(s) is dated at Sites 1071 and 1072 as 1.4–7.4 Ma, implying that it cannot be any shallower than 515.88 mbsf at Site 1073. Taken together, these data imply an age of 1.4–1.9 Ma.

An alternative interpretation is that surface pp4(s) traces to a major biostratigraphic hiatus or interval of condensation between 544.09 and 569.91 mbsf, the approximate depth range of Subunit IIB. This encompasses an upward change from silty clay to glauconitic sandy mud at 560.1 mbsf, and an abrupt upward increase in gamma-ray, velocity, and resistivity values at 552 mbsf. The biostratigraphic hiatus has a maximum range of 3.8–13.5 Ma, and a minimum range of 4.5–13.0 Ma. It, therefore, most likely coincides with an amalgamation of surfaces m0.5(s), m1(s), and four other mapped surfaces down to m3(s). If sequence boundary pp4(s) merges with these other surfaces, its age is poorly constrained at Site 1073. Additional postcruise work is needed to firm up the shelf-to-slope seismic correlation. Assuming existing age control (Miller et al., in press), surfaces m4(s) and m5(s) ought to be located in the interval between 569.91 and 616.89 mbsf,

but they have not been independently traced with confidence in seismic profiles from the inner part of the shelf. Surface m5.6(s) has been tentatively traced from the shelf to Site 1073, where its predicted depth is ~622 mbsf. If that depth is assumed, the age of this surface is 16.7–23.9 Ma (dinocysts and nannofossils), a range that encompasses the existing age control for this surface (Miller et al., in press). A major unconformity is recognized at 654.1 mbsf (Core 174A-1073A-71X) between nannofossil chalk (upper Eocene; 34.2–35.0 Ma) and bioturbated silty clay, sandy mud, and glauconitic muddy sand (uppermost Oligocene; 23.9–25.5 Ma). This presumably includes most or all of the Oligocene sequence boundaries recognized at the New Jersey Coastal Plain.

Interstitial waters of marine sedimentary sequences are often characterized by a broad subsurface maximum in alkalinity and  $\text{HPO}_4^{2-}$ , which results from bacterial decomposition of organic matter and subsequent diffusion of ions. However, high-resolution analyses of interstitial waters at Site 1073 show well-defined alkalinity and  $\text{HPO}_4^{2-}$  maxima in the upper 500 mbsf. Limited sampling of interstitial water at nearby Site 903 (Leg 150; Mountain, Miller, Blum, et al., 1994) also noted peaks in downhole profiles of alkalinity and  $\text{HPO}_4^{2-}$ . The maxima appear to exist in interglacial sediment separated by ~90 m and ~100 k.y. These observations indicate that rates of bacterial decomposition of organic matter on the New Jersey slope

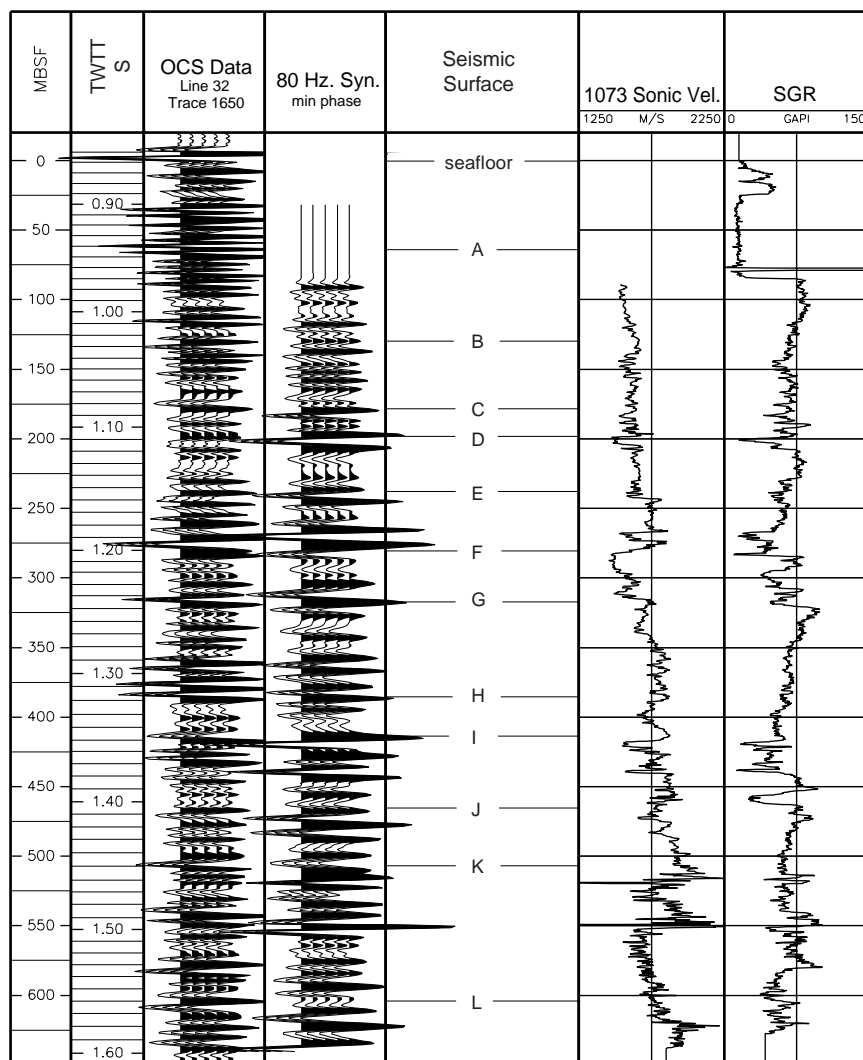


Figure 35. Synthetic seismogram at Site 1073 over the entire drilled interval plotted vs. depth. The correspondence between mbsf and TWTT (columns 1 and 2) is based on sonic log data calibrated to checkshot values within the depth range of the VSP measurements (see Table 28). An 80-Hz, minimum-phase, Ricker wavelet was convolved with the reflection coefficients generated from the sonic log. A constant density of 2.0 g/cm<sup>3</sup> was assumed. The sonic log was despiked to account for cycle skipping caused by poor borehole conditions. Synthetic seismograms and actual data are plotted with positive to the right and peaks (compression) filled black. The actual seismic data is cdp 1650 on Oc270 Profile 32. The velocity log and the gamma-ray log were spliced from three separate logging runs (Fig. 29).

are highly heterogeneous in time and/or space. These maxima are probably preserved because very high sedimentation rates on the New Jersey slope prevent diffusive homogenization of interstitial water chemistry.

#### REFERENCES

- Baker, P.A., and Burns, S.J., 1985. The occurrence and formation of dolomite in organic-rich continental margin sediments. *AAPG Bull.*, 69:1917–1930.
- Baker, P.A., Gieskes, J.M., and Elderfield, H., 1982. Diagenesis of carbonates in deep-sea sediments: evidence from Sr<sup>2+</sup>/Ca<sup>2+</sup> ratios and interstitial dissolved Sr<sup>2+</sup> data. *J. Sediment. Petrol.*, 52:71–82.
- Berggren, W.A., Kent, D.V., Swisher, C.C., III, and Aubry, M.-P., 1995. A revised Cenozoic geochronology and chronostratigraphy. In Berggren, W.A., Kent, D.V., Aubry, M.-P., and Hardenbol, J. (Eds.), *Geochronology, Time Scales and Global Stratigraphic Correlation*. SEPM (Soc. Sediment. Geol.), 54:129–212.
- Compton, J.S., 1988. Degree of supersaturation and precipitation of organogenic dolomite. *Geology*, 16:318–321.
- de Verteuil, L., and Norris, G., 1996. Miocene dinoflagellate stratigraphy and systematics of Maryland and Virginia. *Micropaleontology*, 42 (Suppl.).
- Fulthorpe, C.S., and Austin, J.A., Jr., 1998. Anatomy of rapid margin progradation: three-dimensional geometries of Miocene clinoforms, New Jersey margin. *AAPG Bull.*, 82:251–273.
- Greenlee, S.M., Devlin, W.J., Miller, K.G., Mountain, G.S., and Flemings, P.B., 1992. Integrated sequence stratigraphy of Neogene deposits, New Jersey continental shelf and slope: comparison with the Exxon model. *Geol. Soc. Am. Bull.*, 104:1403–1411.
- Greenlee, S.M., and Moore, T.C., 1988. Recognition and interpretation of depositional sequences and calculation of sea-level changes from stratigraphic data—offshore New Jersey and Alabama Tertiary. In Wilgus, C.K., Hastings, B.S., Kendall, C.G.St.C., Posamentier, H.W., Ross, C.A., and Van Wagoner, J.C. (Eds.), *Sea-Level Changes: An Integrated Approach*. SEPM (Soc. Sediment. Geol.), 42:329–353.
- Harland, R., 1983. Distribution maps of recent dinoflagellate cysts in bottom sediments from the North Atlantic Ocean and adjacent seas. *Palaeontology*, 26:321–387.
- Kastner, M., and Gieskes, J.M., 1976. Interstitial water profiles and sites of diagenetic reactions, Leg 35, DSDP, Bellingshausen Abyssal Plain. *Earth Planet. Sci. Lett.*, 33:11–20.
- Katz, M.E., and Miller, K.G., 1996. Eocene to Miocene oceanographic and provenance changes in a sequence stratigraphic framework: benthic foraminifers of the New Jersey Margin. In Mountain, G.S., Miller, K.G., Blum, P., Poag, C.W., and Twichell, D.C. (Eds.), *Proc. ODP, Sci. Results*, 150: College Station, TX (Ocean Drilling Program), 65–95.
- Keigwin, L.D., Rio, D., Acton, G.D., et al., 1998. *Proc. ODP, Init. Repts*, 172: College Station, TX (Ocean Drilling Program).
- McCarthy, F.M.G., 1995. Major paleoceanographic change in the North Atlantic Ocean 1.4 million years ago: palynological evidence. *Geol. Assoc. Can. Progr. Abstr.*, A67.
- Miller, K.G., and Katz, M.E., 1987. Eocene benthic foraminiferal biofacies of the New Jersey Transect. In Poag, C.W., Watts, A.B., et al., *Init. Repts. DSDP*, 95: Washington (U.S. Govt. Printing Office), 267–298.

- Miller, K.G., and Lohmann, G.P., 1982. Environmental distribution of Recent benthic foraminifera on the northeast United States continental slope. *Geol. Soc. Am. Bull.*, 93:200–206.
- Miller, K.G., Mountain, G.S., Browning, J.V., Kominz, M., Sugarman, P.J., Christie-Blick, N., Katz, M.E., and Wright, J.D., in press. Cenozoic global sea level, sequences, and the New Jersey Transect: results from coastal plain and continental slope drilling. *Rev. Geophys.*
- Mountain, G.S., Miller, K.G., Blum, P., et al., 1994. *Proc. ODP, Init. Repts.*, 150: College Station, TX (Ocean Drilling Program).
- Oda, H., and Shibuya, H., 1996. Deconvolution of long-core paleomagnetic data of Ocean Drilling Program by Akaike's Bayesian Information Criterion minimization. *J. Geophys. Res.*, 101:2815–2834.
- Paull, C.K., Matsumoto, R., Wallace, P.J., et al., 1997. *Proc. ODP, Init. Repts.*, 164: College Station, TX (Ocean Drilling Program).
- Shipboard Scientific Party, 1994. Site 903. *In* Mountain, G.S., Miller, K.G., Blum, P., et al., *Proc. ODP, Init. Repts.*, 150: College Station, TX (Ocean Drilling Program), 129–205.
- Taira, A., Hill, I., Firth, J.V., et al., 1991. *Proc. ODP, Init. Repts.*, 131: College Station, TX (Ocean Drilling Program).
- van Hinte, J.E., Wise, S.W., Jr., et al., 1987. *Init. Repts. DSDP*, 93 (Pts. 1 and 2): Washington (U.S. Govt. Printing Office).
- Westbrook, G.K., Carson, B., Musgrave, R.J., et al., 1994. *Proc. ODP, Init. Repts.*, 146 (Pt. 1): College Station, TX (Ocean Drilling Program).
- Worm, H.-U., 1997. A link between geomagnetic reversals and events and glaciations. *Earth Planet. Sci. Lett.*, 147:55–67.
- Zhu, R.X., Zhou, L.P., Laj, C., Mazaud, A., and Ding, Z.L., 1994. The Blake geomagnetic polarity episode recorded in Chinese loess. *Geophys. Res. Lett.*, 21:697–700.

Ms 174AIR-105

**Note: Core-description forms (“barrel sheets”) and core photographs can be found in Section 3, beginning on page 195. Smear-slide data and shore-based log processing data can be found on CD-ROM (back pocket of this volume). See Table of Contents for material contained on CD-ROM.**

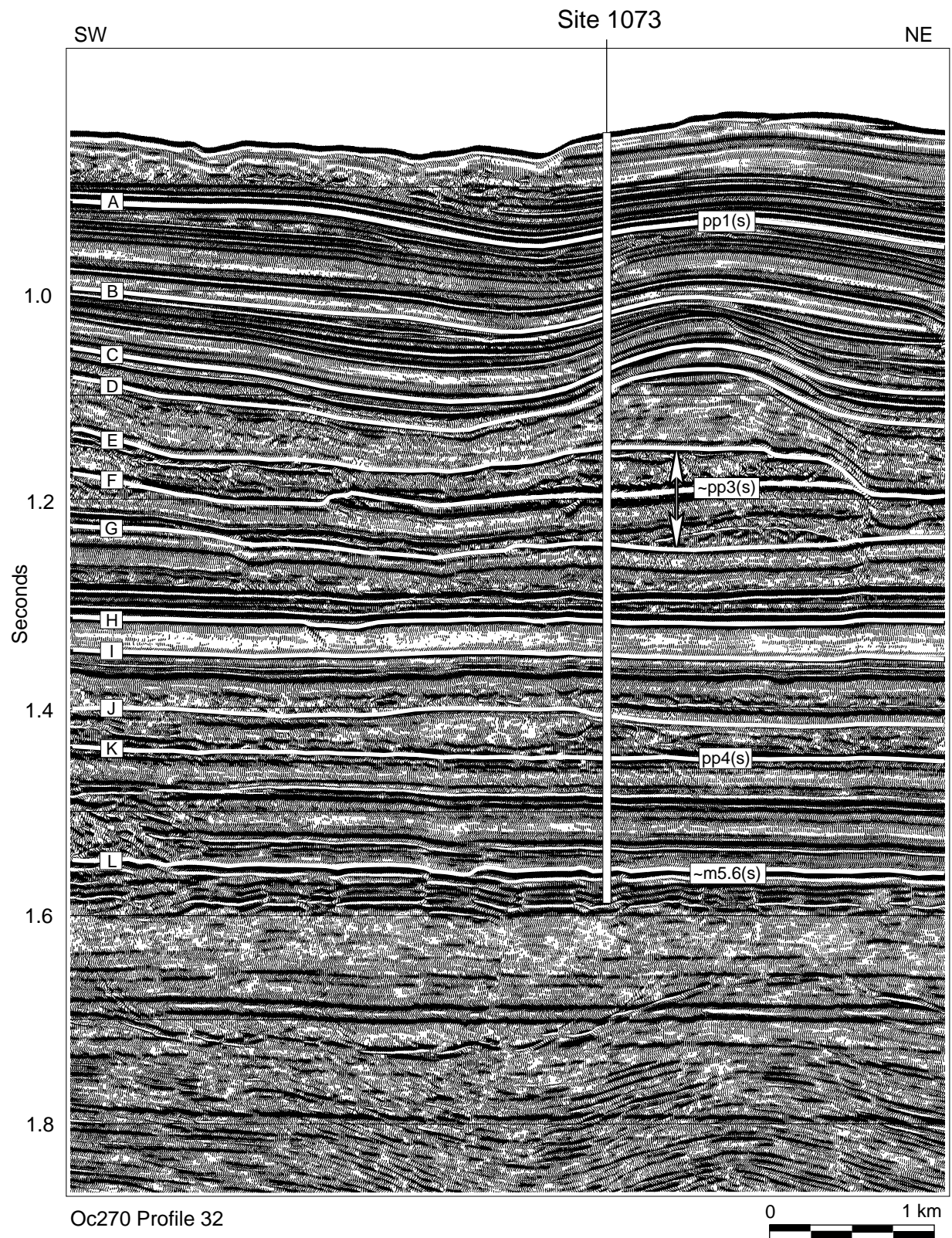


Figure 36. Oc270 Profile 32 showing the 12 surfaces defined locally by stratal geometry (see text and “Seismic Stratigraphy” section, this chapter). Each is matched to the log and synthetic seismogram in Figures 34 and 35. Note that only surfaces A, E/G, K, and L have been tentatively correlated to any stratigraphic hierarchy beyond Site 1073 (to surfaces pp1[s], pp3[s], pp4[s], and m5.6[s], respectively; see text).